# Micro Total Analysis Systems for Coulometric and Volumetric Nanotitrations

Dissertation
submitted to the Faculty of Sciences of the University of Neuchâtel,
in fulfilment of the requirements for the degree of *"Docteur ès Sciences"*

by

**Olivier Thierry Guenat**

Diplômé en électronique-physique
de l'Université de Neuchâtel

Institute of Microtechnology
University of Neuchâtel
Rue Jaquet-Droz 1, CH-2007 Neuchâtel
Switzerland

# IMPRIMATUR POUR LA THÈSE

**Micro Total Analysis Systems for Coulometric and Volumetric Nanotitrations**

de M. Olivier Guenat

---

UNIVERSITÉ DE NEUCHÂTEL

FACULTÉ DES SCIENCES

La Faculté des sciences de l'Université de Neuchâtel sur le rapport des membres du jury,

Mme M. Koudelka-Hep et
MM. N.F. de Rooij (directeur de thèse), W. Morf,
B. van der Schoot (Neuchâtel) et
P. Kirschenbühler (Herisau)

autorise l'impression de la présente thèse.

Neuchâtel, le 18 avril 2000

Le doyen:

J.-P. Derendinger

# Abstract

The present thesis was devoted to the development and applications of microsystems for titrimetric measurements in analytical chemistry. By using microfabrication technologies, microchannels and microelectrodes could be miniaturized to such an extent that the sample volume normally used in conventional batch titrations was reduced by a factor of up to ten million. This tremendous volume reduction led to a 60 to 100-fold decrease of the analysis time.

The first part of this work focuses on the fabrication and on the study of a universal coulometric nanotitrator able to carry out different titration types, such as precipitation, redox, complexometric and acid-base titrations. Two measurement techniques have been applied in order to investigate coulometric titrations in steady and continuous flow conditions, respectively. It could be demonstrated that both methods allowed the linear determination of sample concentrations ranging from about 0.1 up to 10mM by changing the titration conditions such as the applied current and/or the flow rate. Typical titration times around 5 to 10 seconds were found with an excellent reproducibility. Besides, the lifetime of the device revealed to be surprisingly long, so that several thousand measurements could be achieved with the same device and with the same electrode configurations.

In the second part of this thesis, a μTAS for volumetric titrations was developed, and was shown to allow the performance of preliminary continuous flow volumetric titrations. To this end an accurate dosing system, made of electroosmotic nanopumps able to pump almost any kind of liquid, regardless of their conductivity or ionic strength, with the exception of the viscosity, was studied and developed. Continuous and stable flow rates of a few nanoliters per minute up to a few microliters per minute could be achieved. A micromixer and a potentiometric detector were integrated on the same device, together with two nanopumps.

# Résumé

Le sujet de cette thèse est l'étude de microsystèmes destinés à des applications de chimie analytique, plus précisément à des mesures titrimétriques. Ce travail a démontré que la miniaturisation de microcanaux et de microélectrodes engendre une réduction importante (jusqu'à 10 millions de fois) du volume de l'échantillon à titrer. Il en résulte une diminution du temps d'analyse de 60 à 100 fois en comparaison avec des systèmes titrimétriques traditionnels.

La première partie de cette étude présente la fabrication et la caractérisation d'un nanotitrateur coulométrique universel, capable d'effectuer des titrages par précipitation, complexométriques, redox et acide-base. Deux techniques de titrages coulométriques, l'une basée sur un débit nul, la seconde sur un débit constant, ont été utilisées. En ajustant les paramètres de titrages, tels que le courant et/ou le débit, les deux méthodes ont permis la détermination linéaire de la concentration d'échantillons, dans une gamme de concentration de 0.1 à 10 mM. Des temps de titrages de 5 à 10 secondes ont été obtenus de manière très reproductible. La durée de vie de ces microsystèmes s'est révélée beaucoup plus longue qu'espéré, ce qui a permis d'accomplir plusieurs milliers de titrages avec le même dispositif et en utilisant les mêmes électrodes.

Un système miniaturisé d'analyses (μTAS) pour les titrages volumétriques a été réalisé et étudié dans la deuxième partie de la thèse. Composé d'un système de dosage précis, d'un micromélangeur et d'un capteur potentiométrique, ce dispositif a permis d'effectuer des mesures préliminaires de titrages volumétriques à débit constant. Le système de pompage choisi, basé sur l'électroosmose, a permis de pomper des liquides, indépendamment de leur pH et/ou de leur force ionique, à l'exception de leur viscosité, à des débits de quelques nanolitres par minute à quelques microlitres par minute.

# Table of Contents

# 1. Introduction

Titrimetric methods include a large number of procedures, which are among the most widely used analytical techniques. They enable the determination of the concentration of various analytes in aqueous and non-aqueous solutions.

Automated volumetric titrators, which are accurate and give reproducible results, are a familiar tool in routine analysis. However they are not adapted for in situ monitoring because the analysis time required is relatively long. The latter aspect is due to the large volume of analyte routinely employed in conventional batch titrations. This chapter first discusses the reduction of the analyte volume in relation to unique properties intrinsic to microsystems, such as small analyte and titrant consumption, very fast diffusion times, and fast analysis time. It then presents the objectives and the structure of this thesis.

---

## 1.1. Titrations in Analytical Chemistry

### 1.1.1. Definition of the term titration [1, 2]

Titration is a process which involves determining the quantity of an analyte by adding measured increments of substance with which it reacts. This substance is called the titrant and is usually a standardized solution, but it can also be a standardized amount of ions generated at an electrode by an electric current of known magnitude. When the amount of added titrant is chemically equivalent to the amount of analyte in the sample, the equivalence point is reached. The equivalence point of a titration is a theoretical point that cannot be determined experimentally. Instead, its position can be estimated by observing some physical or chemical change associated with the condition of equivalence. This practical estimate is called the titration end-point.

Indicators are often added to the analyte solution in order to provide an observable physico-chemical change (the end-point) at or near the equivalence point. Potentiometric and amperometric methods are examples of other very common procedures used to monitor the titration end-point.

### 1.1.2. Titrimetric methods

Titrimetric methods include a large and powerful group of procedures, which are among the most widely used analytical techniques. They allow convenient, accurate, and relatively fast determinations of the concentration of a large number of analytes. Depending on the chemical reaction in progress, it is possible to identify precipitation, complexometric, redox and neutralisation titrations.

Titrators are sometimes classified as batch or continuous flow titrators [3]. A batch titrator is a titrator that deals with a measured amount of sample and measures the volume of standardized solution required to react with the whole sample. Most of the titrators used in practice are of the batch type. They can be divided in two different groups: volumetric [2, 4, 5] and coulometric titrators [6, 7]. The first reports about volumetric titrations can be traced back to the early 1800s, with the apparition of the first burette [4]. In volumetric titrations (fig.1.1a), increments of the reagent solution - the titrant - are added to the analyte until the reaction is complete.

In coulometric titrations (fig.1.1b) however, the titrant is generated electrochemically between a generator electrode and a counter electrode.

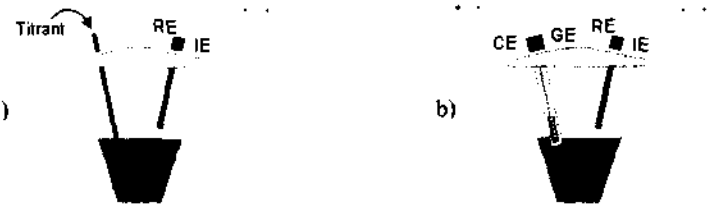


*Fig.1.1. a)Volumetric batch titration, RE and IE stand for reference and indicator electrodes, respectively. b) coulometric batch titration, CE and GE are the counter and the generator electrodes, respectively.*

The direct proportionality between the quantity of electricity and the extent of oxidation and reduction observed upon the passage of current through an electrochemical cell was discovered by Faraday in 1834 [8]. The unit faraday (1F = 96'485 $Cmol^{-1}$) stands for the quantity of electrical charge that corresponds to one mol or $6.022 \times 10^{23}$ electrons.

Two major methods are used in coulometry. The first method, often called *controlled-potential*, involves maintaining the potential of the working electrode at some fixed value until zero current is approached, which signals the completion of the reaction. By selecting the adequate potential, only the electrochemical reaction of the species of interest will proceed.

The second technique makes use of a *constant-current* which is passed in the sample cell until an indicator signals the completion of the reaction. The quantity of electricity required to attain the end-point is then calculated from the magnitude of the current and the time of its passage. This method has a wider variety of applications than the former.

Continuous flow titrators [3, 9-26] are systems in which analyses are performed in streaming solutions. The relevance of this technique, also called gradient technique, can be attributed to two factors: first, the general interest for industrial continuous monitoring of specific chemical reactions, and second, the simplicity of sampling and washing procedures involved in automated continuous-flow analyzing units, which leads to higher sampling rates.

Initiated in the sixties [3], this technique was mainly developed in the seventies by a number of groups active in the field. Pungor's group [10-18] studied theoretically as well as in experiments a series of coulometric titrations in continuously flowing solutions. They initiated the so-called triangle-programmed titration technique, which is a programmed reagent addition. The underlying program of the addition process was an isosceles triangle, with the reagent rate varying as a function of time. Ruzicka and co-workers investigated flow injection titrations with [21] and without [22] gradient chamber, as well as stopped-flow coulometric [23-25] titrations. Flow injection titrations are based on the injection of a small sample volume into a carrier stream, which also acts as the titrant. Both sides of the sample plug react with the titrant, which results in a gradient zone. In contrast, the stopped

flow coulometric methods rely on the means of transport of the reacting mixture. The flow is stopped by bringing the pump to a standstill at an accurately predetermined time, so that the injected sample reaches a gradient chamber where it is titrated coulometrically. All the above-mentioned procedures were reviewed in two monographs [27, 28]. More recently, different groups reported studies based on the triangle-programmed techniques, either in coulometric [19, 20] or in volumetric [29] titrations.

Each method has different capabilities and limitations. When performed under well-defined conditions, the triangle-programmed titration technique offers a linear system response and an analyte determination without calibration. In contrast, the response of the flow injection titration method is logarithmic, but it has the advantage of using a simple single-line system.

Except for the stopped flow method, all these procedures have their intrinsic kinetic feature in common. As a consequence, chemists are still divided as to whether the continuous flow titration method is strictly speaking a titration procedure or not. Pardue and Fields [30] argued that the titrant and the analyte react in non-stochiometric proportions, since the volume of both the titrant and the analyte is not well defined as it is in a batch titration. Furthermore, they stated that similar results could be obtained without a reagent in the flow system. They concluded that gradient titrations should be regarded as a form of classical kinetic method rather than continuous flow titrations. Valcarcel and Luque de Castro [28] agreed with Pardue and Fields' conclusions, especially with regard to the need of a stochiometric ratio at the equivalence point. Nevertheless, they questioned the validity of the second statement by Pardue and Fields concerning the role of the chemical reaction in the flow system. They therefore favoured the use of the terminology dedicated to batch titration for continuous flow titrations.

This controversy about terminology is beyond the scope of this thesis. Although, we do recognize that continuous flow titrations have common features with classical kinetic methods, the terminology employed for conventional titration will be used throughout this work to facilitate comprehension of the subject.

### 1.1.3. Comparison between volumetric and coulometric titrations [2, 4, 6, 7, 31]

Batch volumetric titration analysis is by far the most widely used titrimetric technique. It allows reliable measurements and it can operate as a selective method, depending on the analyte and its titrant. On the other hand, the coulometric titration has several significant advantages – whether batch or continuous – over a volumetric procedure. Of the utmost importance is the elimination of problems associated with the preparation, standardization, and storage of titrant solutions. This advantage is particularly significant when dealing with unstable reagents. Since such titrants are consumed as soon as they are generated at the electrode, their utilization in a coulometric determination is straightforward.

Coulometric methods also excel when small amounts of analyte have to be titrated because, through the proper choice of the electric current, tiny quantities of reagent can be generated with ease and accuracy. For example, a titration with an applied current of 10 μA during 100 seconds is easy and corresponds to about $10^{-8}$ mol (n=1) or only a few micrograms of titratable material. On the other hand, the use of very dilute solutions and the accurate measurement in small volumes are a difficult task.

Coulometric methods have been developed for all types of volumetric reactions. Nevertheless, coulometry is rarely used in routine analysis, except for water determination (Karl-Fischer titration). This may be explained by the greater complexity of the electrochemical reactions and by the limited selectivity.

### 1.1.4. Direct potentiometric end-point detection

End-point detection methods are closely related to titrimetric methods. The physico-chemical change associated with the condition of equivalence is often detected by potentiometric methods, i.e. by measuring the potential of an indicator electrode versus a reference electrode separated by a salt bridge. Direct potentiometric measurements provide a rapid and convenient method for the determination of the activity of a variety of cations and anions in solution.

Potentiometric methods are classified according to the nature of the electrodes. One or both of the electrodes may be non-polarizable or polarizable [2, 31]. Classical

direct potentiometry identifies the method, which makes use of a non-polarizable indicator electrode without any current flowing through the measurement cell.

The reference electrode [2, 32] is usually a half-cell with a stable, well known electrode potential which is independent of the concentration of analyte or any other ions in the solution being studied. The reference electrodes mostly used are silver-silver chloride or calomel reference electrodes. In some cases, and particularly in flow injection analysis systems, a relative differential signal is sufficient to quantify the analysis. Then, pseudo-reference electrodes, such as Pt or Ag wires, can be implemented as well.

On the other hand, most indicator electrodes used in potentiometry are highly selective in their responses. Prominent examples, beside certain metallic electrodes, are ion selective electrodes [33], glass electrodes, or ISFET (ion selective field effect transistor) [34]. Ideally, the indicator electrode immersed in the solution of the analyte develops a potential that selectively depends on the activity of the analyte.

### 1.1.5. Future trends in the titration research field

The measurement and the continuous monitoring of the concentration of chemical species is of increasing importance in various domains, such as environmental analysis, chemical production, medical diagnostics, research, and other fields of routine analysis. In almost all cases, the chemical compound of interest has to be determined in sample matrices that contain a host of other compounds, including possible interferents. Moreover, due to the always-growing number of analyses, the analysis time has become an important issue. Furthermore, in situ analyses will probably be required in specific cases, such as in environmental analysis and in harsh environments [35], and will therefore necessitate robust analytical instruments.

Titrimetric methods are able to meet many of these requirements, because of their excellent reliability and considerable universality. Nevertheless, despite the great importance of these methods in analytical chemistry, very few innovations with regards to sensitivity and analysis time have been introduced in the past years in commercially available titrators. As a matter of fact, depending on the accuracy level desired for the measured concentration, a single titration process takes several minutes, and usually several more in the batch mode.

In such systems, the speed of analysis is fundamentally limited by the large amount of solution to be titrated. In fact, the reaction rate of most titration reactions is essentially correlated with the rate of distribution of the species across the involved volume. Even if mixing is enhanced by stirring, it remains a slow process, as it has to be repeated after each titrant addition. Therefore, reducing the sample volume may open new perspectives for increasing the speed of analysis. The next section focuses on these aspects and summarizes unique and interesting features of miniaturized analysis systems.

## 1.2. Miniaturization of Chemical Analysis Systems

Over the past decades, the design of instrumentation for the measurement of chemical, physical and biomedical parameters has brought analytical chemistry to a highly automated and technologically advanced science [36]. However, if one considers the fundamental chemical and physical phenomena on which these measurement are based, it becomes clear that only a few molecules or ions need to be present for quantitative measurement to occur. In other words, the physics and engineering of measurement science can be considered as oversized when it comes to meet the needs of chemical measurement.

### 1.2.1. The μTAS concept

These reflections have recently led an increasing number of research groups to focus on miniaturized chemical analysis systems, and especially on micro total analysis systems (μTAS) [37-39]. The term μTAS was first used ten years ago at the Transducers '89 conference [40]. μTAS involves the miniaturization of all the functions found in an analytical method such as pumps, valves, mixing and reaction chambers, separation columns, detectors and electronics. One of the more exciting prospects of the μTAS concept is the suggestion that the entire chemical measurement laboratory could be miniaturized onto a device of a few square centimetres (lab-on-chip). This type of miniaturization has become possible largely through the adoption of microfabrication techniques mostly developed by the microelectronics industry. In 1979, Terry et al. [41] were among the first to use integrated circuit technology to fabricate a miniaturized gas chromatograph. Nevertheless, it was not until research aiming at capillary electrophoresis on a chip set off that the μTAS research field drastically built up [42-44].

Due to their small size, μTAS present unique intrinsic characteristics, such as short diffusion times and large surface-volume ratios (see table 1.1). Moreover, the effects of certain physico-chemical phenomena, for instance, surface tension, adsorption and capillary forces become significant in microscale systems. In addition, the very small volumes of sample and reagent solutions required to perform an analysis lead to a drastic reduction of the sample and reagent consumption. This

factor could possibly lower the detection limit and could one day make possible the detection of single molecules in routine analytical determinations.

| *Dimension (mm)* | *Volume* | *Surface-volume ratio* | *Diffusion time (s)* | *Number of molecules conc. of 1 μM* |
|---|---|---|---|---|
| *1* | *1 μL* | *2* | *500* | $6 \times 10^{11}$ |
| *0.46* | *100 nL* | *4* | *107* | $6 \times 10^{10}$ |
| *0.22* | *10 nL* | *9* | *23* | $6 \times 10^{9}$ |
| *0.1* | *1 nL* | *20* | *5* | $6 \times 10^{8}$ |
| *0.05* | *100 pL* | *43* | *1* | $6 \times 10^{7}$ |
| *0.02* | *10 pL* | *93* | *0.2* | $6 \times 10^{6}$ |
| *0.01* | *1 pL* | *200* | *0.05* | $6 \times 10^{5}$ |
| *0.001* | *1 fL* | *2000* | *0.0005* | *602* |

*Table 1.1. Diffusion times as a function of the dimension for a diffusion coefficient of $10^{-9}$ $m^2/s$. Volume was calculated from the third power of the indicated dimension, whereas the surface volume-ratio was calculated for a cylindrical channel whose radius corresponds to the indicated dimension.*

### 1.2.2. Micro- and submicroliter titrations

Several approaches have been proposed by different research groups to detect the end-point of micro- or submicrotitrations.

In 1985, van der Schoot [45] developed an innovative coulometric microtitrator based on diffusional transport in a close microchannel. This microtitrator designed for neutralisation titrations made use of ISFETs to detect the titration end-point. Van der Schoot mainly performed stopped-flow titrations. In addition, some preliminary titrations were carried out in the continuous flow mode [46]. Later, Olthuis and other co-workers of Bergveld [47-49] improved different characteristics of the microtitrator by changing parameters, such as size, material, and type of the coulometric actuator electrodes, and by investigating several mathematical modellings [50-52].

In 1988, Gratzl and co-workers [53, 54] proposed a system for dispensing the titrant by diffusion through a membrane. This method made use of a titrant-filled

microburet, positioned in a microscopic sample. Successful titrations have been carried out for several applications including complexometric, precipitation, and acid-base titrations. Even when the analysis times were sometimes below a minute and despite the extremely small volume being titrated, the fragile glass burettip and its positioning in the sample microdrop makes the practical application of such a device questionable. Litborn et al. [55] reported a similar system using an automated dosing technique based on the use of piezoelectrically driven pipettes.

Other methods based on electrodeposition frequency shift titrimetry [56] were proposed, although they remain limited to very specific applications.

## 1.3. Objectives and Outline of the present Thesis

The objectives of this thesis consist in the development of chemical micro- or nanosystems dedicated to titrations. These systems should permit fast, reliable and universally applicable analyse, such as precipitation, complex-formation, redox and acid-base titrations. In addition, the fabrication costs of these systems should be kept as low as possible, since disposable devices are planned ahead. Therefore, in order to fabricate these devices by means of only a small number of microfabrication processes, their designs will be kept as simple as possible.

The first part of the present study focuses on devices for very fast coulometric nanotitrations. In this first section, coulometry is preferred over volumetry since it allows an easy and accurate dosing of extremely small amounts of electrogenerated species. The concept of these nanotitrators is similar to those studied by Bergveld's group. However, in contrast to the former devices designed for neutralisation titrations, the nanotitrators presented here aim at performing precipitation, complex-formation, redox and acid-base titrations on the basis of the same device. In addition, noble metal indicator electrodes are preferred over the earlier used ISFETs in order to simplify the fabrication process. Stopped-flow coulometric titrations are carried out for the above-mentioned types of titrations by using a constant current source. Chapter 2 shows detailed results and presents a simple mathematical model used for determining the geometrical parameters of the device. In order to limit the diffusion contribution, the nanotitrators are also tested in the continuous flow mode. The triangle-programmed titration technique developed by Pungor's group is used by applying a triangular current profile in the coulometrical cell at different flow rates. Results obtained under these conditions are described in chapter 3.

The second part of this work involves the design and the characterization of a complete μTAS for coulometric and volumetric nanotitrations. This μTAS involves a pump, a mixer and a reaction chamber on a single chip. A pulsation-free pump driven by electroosmosis is developed and characterized. Pulsation-free flows are compulsory for microsystems; unfortunately, adequate pumps are either very expensive or inappropriate for this application. At very low flow rates (<10μL/min), the pulsations generated by conventional peristaltic pumps and piston-pumps influence the analysis and lead to inaccuracy and to measurement errors. Chapter 4

presents the new electroosmotic nanopump that has the ability to pump almost any kind of liquids, irrespective of their pH and/or their conductivity. Theoretical aspects of electroosmosis in microchannels with regards to the pressures arising in the system and the attainable flow rates are also discussed. Chapter 5 describes the design and the fabrication of a static micromixer placed downstream from these electroosmotic nanopumps. This micromixer enables the complete mixing of a sample solution and of a titrant solution. Finally, preliminary results of volumetric nanotitrations performed within the μTAS are described in chapter 6.

**References**


[1] IUPAC, International Union of Pure and Applied Chemistry, Compendium of analytical nomenclature, by Freiser and Nancollas, 1987, p.47.

[2] Skoog D.A., West D.M., Holler F.J., *Analytical Chemistry, an introduction*, Saunders College Publishing, 6th ed., Philadelphia, 1994.

[3] Blaedel W.J., Laessig R.H., *Continuous automated, buretless titrator with direct read-out*, Anal. Chem., vol.36, No.8, 1964, p.1617-23.

[4] Harris D.C., *Quantitative Chemical Analysis*, 4th ed., Freeman and Company, New York, 1995.

[5] Stur J., Bos M., van der Linden W.E., *A generalized approach for the calculation and automation of potentiometric titrations, Part I. Acid-Base titrations*, Anal. Chim. Acta, 158, 1984, p.93-111.

[6] Kies H.L., *Coulometry*, J. of Electroanalytical chemistry, 4, 1962, p.257-86.

[7] Bishop E., *Comprehensive analytical chemistry, volume IID. Coulometric analysis*, ed. Wilson & Wilson, Elsevier, Amsterdam, 1975.

[8] Faraday M., *Experimental researches in electricity, 7th series*, Phil. Trans. Royal Soc. London, Ser. A, 124, 1834, p.77-122.

[9] Fleet B., Ho A.Y.W., *Gradient titration, a novel approach to continuous monitoring using ion-selective electrodes*, Anal. Chem., 46, 1974, p.9-11.

[10] Pungor E., Toth K., Nagy G., *Some aspects of the application of ion selective electrodes in flowing systems*, Ion and enzime electrodes in biology and medicine, Int. Workshop at Schloss Reisensburg near Ulm, Urban & Schwarzenberg, München, 1976, p.56-76.

[11] Pungor E., Toth K., Nagy G., Feher Zs., *Methods for automatic analysis with ion-selective electrodes*, 2nd Symp. on Ion-selective electrodes, Matrafured, Hungary, 1976, p.67-91.

[12] Nagy G., Fehér Zs., Tóth K., Pungor E., *A novel titration technique for the analysis of streamed samples – the triangle-programmed titration technique,Part I. General Considerations*, Anal. Chim. Acta 91, (1977) 87-96.

[13] Nagy G., Fehér Zs., Tóth K., Pungor E., see [12], *Part II. Argentimetric titrations*, Anal. Chim. Acta 91, (1977) 97-106.

[14] Nagy G., Fehér Zs., Tóth K., Pungor E., see [12], *Part III. Titrations with electrically generated bromine*. Anal. Chim. Acta 100, (1978) 181-91.

[15] Nagy G., Fehér Zs., Tóth K., Pungor E., *Evaluation of acid-base titration curves obtained by the triangle-programmed titration technique in flowing solutions*, Talanta, 26, 1979, p.1143-53.

[16] Fehér Zs., Kolbe I., Pungor E., *Iodimetric determination of penicillins by a triangle programmed flow-through titration technique*. Analyst, 113, 1988, p.881-4.

[17] Fehér Zs., Kolbe I., Pungor E., *Determination of the drug content of pharmaceuticals containing phenothiazine compounds by triangle programmed flow titration,* Fresenius Z. Anal. Chem., 332, 1988, p.345-50.

[18] Fehér Zs., Kolbe I., Pungor E., *Application of flow-through techniques to drug dissolution studies,* Analyst, 116, 1991, p.483-7.

[19] Dakashev A.D., Dimitrova V.T., *Pulse coulometric titration in continuous flow,* Analyst, vol.119, 1994, p.1835-8.

[20] Becker M., Fuhrmann, Spohn U., *Selective determination of gas dialysable components in complex sample solutions using triangle programmed coulometric titration in continuous flow systems,* Anal. Chim. Acta, 324, 1996, p.115-23.

[21] Ruzicka J., Hansen E.H., Mosbaeck H., *Flow injection analysis, Part IX. A new approach to continuous flow titrations,* Anal. Chim. Acta, 92, 1977, p.235-49.

[22] Ramsing A.U., Ruzicka J., Hansen E.H., *The principles and theory of high-speed titrations by flow injection analysis,* Anal. Chim. Acta, 129, 1981, p.1-17.

[23] Chen R., Ruzicka J., Christian G.D., *Flow injection titration-linear or logarithmic,* Talanta, vol.41, No.6, 1994, p.949-55.

[24] Taylor R.H., Winbo C., Christian G.D., Ruzicka J., *Bromine number determination by coulometric flow-injection titration,* Talanta, vol. 39, No.7, 1992, p.789-94.

[25] Taylor R.H., Ruzicka J., Christian G.D., *Flow injection coulometric titrations,* Talanta, vol. 39, No.3, 1992, p.285-92.

[26] Simpson S.F., Holler F.J., *Potentiometric detection system for flow injection titrimetry,* Anal. Chem., 54, 1982, p.43-6.

[27] Ruzicka J., Hansen E.H., *Flow injection analysis,* 2nd ed., John Wiley & Sons, New York, 1988, p.56-60, 229-242.

[28] Valcarcel M., Luque de Castro M.D., *Flow injection analysis,* John Wiley & Sons, New York, 1987, chap.8 and 9.

[29] Lopez Garcia I., Vinas P., Campillo N., Hernandez Cordoba M., *Linear flow gradients for automatic titrations,* Anal. Chim. Acta, 308, 1995, p.67-76.

[30] Pardue H.L., Fields B., *Kinetic treatment of unsegmented flow systems, Part 1. Subjective and semiquantitative evaluations of flow-injection systems with gradient chamber.* Anal. Chim. Acta, 124, 1981, p.39-63.

[31] Bard A.J., Faulkner L.R., *Electrochemical methods, Fundamentals and applications,* John Wiley & Sons, New York, 1980, p.390-1.

[32] Ives D.J.G., Janz G.J., *Reference electrodes, theory and practice,* Academic Press, 1961, New York.

[33] Morf W.E., *The principles of ion-selective electrodes and of membrane transport,* Elsevier Scientific Publishing, Amsterdam, 1981.

[34] Janata J., Huber R.J., *Solid state chemical sensors,* Academic Press, Inc., New York, 1985, chap.2.

[35] Campbell J.A., Stromatt R.W., Smith M.R., Koppenaal D.W., Bean R.M., Jones T.E., Strachan D.M., Babad H., *Organic analysis at the Hanford nuclear site*, Anal. Chem., vol. 66, No. 24, 1994, p.1208A-15A.

[36] Haswell S.J., *Development and operating characteristics of micro flow injection analysis systems based on electroosmotic flow, Critical review*, Analyst, vol. 122, p. 1R-10R.

[37] Micro Total Analysis Systems'94, Proc. μTAS'94, Twente, The Netherlands, 1994.

[38] Micro Total Analysis Systems'96, Proc. μTAS'96, Basel, Switzerland, Analytical Methods & Instrumentation, Special Issue, 1996.

[39] Micro Total Analysis Systems'98, Proc. μTAS'98, Banff, Canada, Kluwer Academic Publishers, Dordrecht, 1998.

[40] Manz, A., Graber N., Widmer H.M., *Miniaturized total chemical analysis systems: a novel concept for chemical sensing*, Sensors and Actuators, B1, 1990, p.244-8.

[41] Terry S.C., Jarman J.H., Angell J.B., *A gas chromatograph air analyzer fabricated on a silicon wafer*, IEEE Trans. Electro. Devices, 1979, ED-26, p.1880-6.

[42] Manz A., Harrison D.J., Verpoorte E. M.J., Fettinger J.C., Lüdi H., Widmer H.M., *Miniaturization of chemical analysis systems-A look into next century's technology or just a fashionable craze*, Chimia, 1991, 45, p.103.

[43] Jacobson S.C., Hergenröder R., Koutny L.B., Ramsey J.M., *Open channel electrochromatography on a microchip*, Anal. Chem., 66, 1994, p.2369.

[44] Harrison D.J., Glavina P.G., Manz A., *Towards miniaturized electrophoresis and chemical analysis system on silicon*, Sensors and Actuators, B 10, 1993, p.107.

[45] van der Schoot B. H., *Coulometric sensors*, Ph.D. Thesis, Univ. of Twente, Enschede, The Netherlands, 1986.

[46] van der Schoot B. H., Bergveld P., *An ISFET-based microlitre titrator: integration of a chemical sensor-actuator system*, Sensors and Actuators, 8, 1985, p.11-22.

[47] Olthuis W., van der Schoot B.H., Chavez F., Bergveld P., *A dipstick sensor for coulometric acid-base titrations*, Sensors and Actuators, 17, 1989, p.279-83.

[48] Olthuis W., Bomer J.G., Bergveld P., Bos M., van der Linden W.E., *Iridium oxide as actuator material for the ISFET-based sensor-actuator system*, Sensors and Actuators, B5, 1991, p.47-52.

[49] Olthuis W., Bergveld P., *Integrated coulometric sensor-actuator devices*, Mikrochim. Acta, 121, 1995, p.191-223.

[50] Olthuis W., Luo J., van der Schoot B.H., Bergveld P., *Modelling of non-steady-state concentration profiles at ISFET-based coulometric sensor-actuator systems*, Anal. Chim. Acta, 229, 1990, p.71-81.

[51] Luo J., Olthuis W., Bergveld P., Bos M., van der Linden W.E., *Modelling of coulometric sensor-actuator systems based on ISFETs with a porous actuator covering the gate*, Anal. Chim. Acta, 274 (1993), p.7-23.

[52] Kolev S.D., van der Linden W.E., Olthuis W., Bergveld P., *Mathematical modelling and optimisation of a coulometric sensor-actuator system based on three-dimensional diffusion*, Anal. Chim. Acta, 285, 1994, p.247-63.

[53] Gratzl M., Yi C., *Diffusional microtitration: acid-base titrations in pico- and femtoliter samples*, Anal. Chem., 65, 1993, p.2085-8.

[54] Yi C., Gratzl M., *Diffusional microtitration: reagent delivery by a diffusional microburet into microscopic samples*, Anal. Chem., 66, 1994, p.1976-82.

[55] Litborn E., Stjernström M., Roeraade J., *Nanoliter titration based on piezoelectric drop-on-demand technology and laser-induced fluorescence detection*, Anal. Chem., 70, 1998, p.4847-52.

[56] He F., Shi J., Xie Q., Nie L., Yao S., *A new titration method: electrodeposition frequency shift titrimetry*, Microchemical Journal, 52, 1995, p.325-32.

# 2. Stopped-flow coulometric nanotitrations

If a coulometric titration is carried out in only a portion of a microchannel, the volume of the titrated sample solution is reduced to a few nanoliters. This is why the determination of less than a nanogramm of analyte becomes possible over a very short period of time.

This chapter describes in detail the fabrication of a coulometric nanotitrator equipped with such a microchannel. The characterization of the nanotitrator applied for four different types of titrations – precipitation, complexometric, redox and acid-base titrations – is then discussed. The coulometric titrations are carried out in static sample solutions, which implies that only diffusion processes drive the titration reactions. Finally, the optimisation of some geometrical parameters are commented upon. Parts of this chapter have been published in [1-4].

## 2.1. Introduction

Stopped-flow methods are a particular case of gradient techniques and are often related with FIA systems [5, 6]. These methods are founded on the mean of transport of the reacting mixture. In stopped-flow coulometric titrations, the flow is stopped by bringing the pump to a standstill at an accurately predetermined time, so that the injected sample reaches a gradient chamber where it is coulometrically titrated. In this way, Ruzicka and co-workers investigated acid-base [7] and bromimetric [8] titrations. They reported the titrations of sample solutions with a wide concentration range. This method was also employed to perform Karl-Fischer's coulometric titrations [9]. In most cases, tens of seconds up to several minutes were required to complete the whole titration procedure.

In systems where the sample length does not play a crucial role, the stopped-flow method is even easier to apply, and thus makes the presence of a complex

injection mechanism superfluous. In 1985, van der Schoot and Bergveld [10-12] developed such a system, based on a miniaturized flow-through cell. The use of microfabrication techniques made possible the integration in the miniaturized cell of the coulometric electrodes, made of a structured gold layer, and of a potentiometric sensor. This microtitrator was designed for neutralisation titrations and made use of ISFETs to detect the titration end-points. The amount of electrical charge used for a coulometric titration was found to be linearly proportional to the concentration of the titrated sample for short periods of time. Due to the small volume involved in the titration, short end-point times in the order of 5 to 20 seconds were found.

Later, Olthuis and co-workers [13-17] modified this microtitrator for in situ applications. They removed its cover lid and transformed it in a dipstick sensor. Stricly speaking, this modified device cannot be categorized within the field of flow-through systems. Nevertheless, titration was indeed driven by a diffusion process – semi-infinite in the z direction – and most of the findings of Olthuis et al. are therefore applicable to *stopped-flow systems*.

Considering the problem of redox interference during the titrant generation at a noble metal electrode by the electrolysis of water, Olthuis et al. [15, 16] implemented metal oxide actuator electrodes as an alternative to the noble metal electrodes used by van der Schoot. This option has the advantage of eliminating the use of an additional redox couple, which can be oxidised and reduced at a lower potential than that at which the interfering ions react. The long-term stability of the metal oxide layer is however questionable [18]. Another type of actuator electrode, made of porous gold and closely spaced around and over the gate of the ISFET was also investigated [19] and was shown to allow extremely short analysis times. The sharpness of the titration end-points was, however, less pronounced than in the case of planar actuator electrodes. Furthermore, several modellings of the diffusion and migration processes involved in the reaction were performed [20-23].

The sensor presented in this chapter is an integrated chemical sensor and actuator system that is designed for concentration determinations of specific analytes by means of coulometric titrations under stopped-flow conditions. The sample solution – whose titrated volume is about 15 to 70 nL – is confined to a microchannel where the coulometric reaction takes place only locally. In contrast to the above-mentioned devices, this system can carry out different types of titrations on the basis

of the same device: precipitation, complexometric, redox and acid-base titrations. In addition, this nanotitrator does not require the use of ISFETs, which significantly reduces the complexity of the device. Detection of the titration endpoint is performed by a direct potentiometric method using metallic indicator and reference electrodes. The output signals of the nanotitrator are mainly determined by its dimensions and by the current applied to the cell; they are as a rule not subject to changes of the standard potential of the indicator electrode. Therefore, one can expect that the device will yield stable signals for a long time of application. Hence, a unique calibration fixing the geometrical parameters of the cell is usually sufficient.

In the following paragraphs, basic theoretical aspects of coulometric and potentiometric methods used in this study, as well as of the transport mechanisms involved in the system are described. The design and the fabrication processes of two types of nanotitrators are then presented, followed by the characterization of the devices in different configurations. The final remarks concern the optimisation of different geometrical parameters.

## 2.2. Constant Current Coulometry

Coulometric titrations have been developed for all types of chemical reactions. Coulometric methods are powerful and have some real advantages in comparison with classical volumetric titrations [24]. Principal among these is the avoidance of standard solutions and the absence of problems associated with the preparation, standardization and storage of these solutions.

### 2.2.1. Basic theory

In constant current coulometry, the amount of charge (in coulombs) needed to convert the analyte to a different chemical state is measured. The primary reagent removed or added at the generator electrode consists of electrons. As a result of chemical oxidation or reduction involving these electrons, a chemical reagent, which can be considered as the intrinsic titrant, is generated and reacts quantitatively with the analyte to be determined. Because the current is constant, the total amount of reagent produced is directly related to the reaction time.

One of the fundamental requirements for all coulometric methods is that the species determined should interact with 100% current efficiency. Thus, for a constant current $i$, the number of moles of analyte $n_a$ involved in the reaction is given by the amount of charge $Q$ divided by Faraday's constant $F$ and by the equivalent number $z$ of electrons participating in the reaction. The analyte concentration $c$ is obtained by dividing $n_a$ by the actual volume $V$ of titration:

$$c = \frac{n_a}{V} = \frac{Q}{zFV} = \frac{it}{zFV} \qquad (2.1)$$

where $t$ is the equivalence time.

### 2.2.2. Types of coulometric titrations

Almost all kinds of metals commonly used in electrochemistry, as well as carbon layers [25] can be structured by micromachining techniques. In these respects, there are no limitations for the coulometric titrations that can be carried out in microsystems.

The type of titrations to be carried out determines the choice for the material of the coulometric actuator electrodes. Some of the most frequently used coulometric titrations are defined below, and will be experimentally carried out in section 2.7.

*Argentimetric titrations*

Electrogenerated silver ions are applicable to both precipitation titrations of halide ions, thiocyanate ions, etc. and to the titration of substances, that form strong complexes with silver ions, such as cyanide ions.

When a constant current is applied to a solution containing halide, pseudo-halide or sulphide ions, the silver ions generated at the anode (eq.2.2) form a precipitate (eq.2.3) with the anions $X^{z-}$ ($Cl^-$, $Br^-$, $I^-$, $SCN^-$ or $S^{2-}$). The sparingly soluble silver salt is mainly deposited as a solid film on the silver anode, until the remaining concentration of anions becomes so small that their rate of transfer to the anode is smaller than the rate at which silver ions are generated. Between this point and the equivalence point, the silver ions produced at the anode diffuse into the bulk solution, and precipitation then rather occurs in the solution. Because the potential is sufficiently low, generation of silver ions is 100% efficient up to relatively high current densities [26].

$$Ag \rightarrow Ag^+ + e^- \qquad (2.2)$$

$$zAg^+ + X^{z-} \rightarrow Ag_zX \qquad (2.3)$$

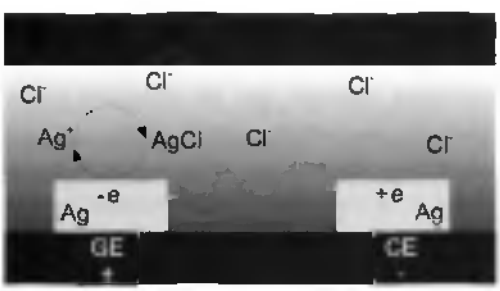


*Fig.2.1. Precipitation reaction process occurring at the silver generator electrode in a KCl sample solution.*

*Stopped-flow coulometric nanotitrations*

The generation processes occurring in complexometric titrations are analogous to those of precipitation reactions and only differ in that all components are soluble. The silver ion is generated by anodic stripping just as for precipitation reactions (eq.2.2), and the ligand species $L^{n-}$ (for example: $CN^-$, $S_2O_3^{2-}$) is generated by reduction of a suitable complex of $L^{n-}$, releasing the ligand species

$$Ag^+ + 2L^{n-} \rightarrow AgL_2^{1-2n} \quad (2.4)$$

*Redox titrations*

Oxidation-reduction reactions are characterized by the transfer of electrons from the substance which is oxidized (the reductant) to the substance which is reduced (the oxidant). During the oxidation of the sample or during the generation of the oxidant from an intermediate, the reaction written according to IUPAC conventions

$$Ox + ne \underset{i_a}{\overset{i_c}{\rightleftharpoons}} Red \quad (2.5)$$

proceeds backwards, and $-i_a$ exceeds $i_c$. During the reverse process, i.e. the reduction of the sample, the forward reaction takes place. The main problems associated with the generation of oxidants and reductants are the prevention of the electrode material from taking part in the reaction, the preservation of electrode activity to the desired reaction, and the minimization of solvent electrolysis [27]. These are the reasons why noble metals are preferred as actuator electrodes for redox titrations. The latter electrodes are commonly made of platinum, which behave like an inert material that usually does not participate in the redox chemistry, except as a conductor of electrons.

Moreover, interfering reactions can be eliminated either directly by the appropriate regulation of the voltage applied to the cell (controlled potential coulometry), or indirectly by adding to the solution a large concentration of another substance which reacts at the electrode and thereby limits the potential drift. For an overall 100% titration efficiency with respect to the substance being determined, the product of the electrode reaction of the added redox buffer must react stochiometrically with the analyte.

For instance (fig.2.2), if *Fe(II)* ions are to be determined by oxidation titration, an excess of *Ce(III)* ions is usually added to the solution as electron-transferring

reagent in order to prevent hydrolysis of water from taking place. The latter ions are oxidized at a lower potential than that for water hydrolysis.

$$Ce(III) \rightarrow Ce(IV) + e \qquad (2.6)$$

At the very beginning of the electrolysis, the predominant anode reaction is direct oxidation of *Fe(II)* ion. However, the potential of the platinum anode soon drifts to a value sufficiently positive, so that the oxidation of *Ce(III)* to *Ce(IV)* ions sets in; then the *Ce(IV)* ion thus produced is transferred in the bulk of the solution where it oxidizes *Fe(II)* ion. The cerium (IV) produced diffuses rapidly from the electrode surface and oxidizes an equivalent amount of iron (II).

$$Fe(II) + Ce(IV) \rightarrow Fe(III) + Ce(III) \qquad (2.7)$$

The overall reaction is finally given by:

$$Fe(II) \rightarrow Fe(III) + e \qquad (2.8)$$

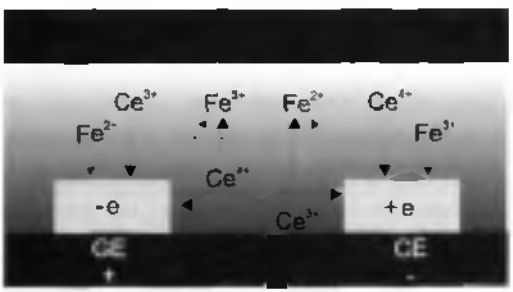


*Fig.2.2. Coulometric redox reactions occurring at the Pt generator and counter electrodes in a Fe(II) sample solution containing an excess of Ce(III). Main and secondary reactions are drawn with solid and dotted lines, respectively.*

*Neutralisation titrations*

In the study of acidobasic coulometric titrations, electrolysis of water is generally used to generate the reagent. The half-reaction occurring at the anode, where protons are generated by oxidation of water, is:

$$2H_2O \rightarrow O_2 + 4H^+ + 4e^- \qquad (2.9)$$

and the half-reaction at the cathode, where hydroxyl ions are produced by reduction of water, is:

$$2H_2O + 2e^- \rightarrow H_2 + 2OH^- \qquad (2.10)$$

At a noble metal electrodes, electrolysis of water occurs at relatively high electrode potentials, which places some restrictions on the composition of the solution in order to prevent side reactions. Furthermore, at high current densities, hydrogen and oxygen gas bubbles may evolve. When an additional redox-couple that can be oxidized and reduced at lower electrode potentials is added to produce the desired pH-changes, the undesired reactions can be suppressed. Quinhydrone is such a redox couple [28], which can simultaneously act as a pH indicator (see §2.3).

### 2.2.3. Secondary reactions occurring in coulometry

To fulfil the 100% current efficiency condition, one must take the side reactions occurring in coulometry into account. Some of them, such as the generation of oxygen and hydrogen in aqueous solutions, were already discussed and are the most important undesired effects. Other secondary effects [29], such as the anodic dissolution of the electrode metal, which also happens to inert electrode material like platinum, can affect the accuracy of the coulometric analysis. Bishop's excellent monograph [27] summarizes various side reactions that may occur for the different type of titrations.

## 2.3. Direct Potentiometric Detection

When the titrant is generated at the coulometric electrode, the analyte is depleted near the indicator electrode, which results in a sudden and sharp change of the potential at the equivalence point. Detection is preferably carried out by a potentiometric method. The potential is measured between the indicator electrode, located where the titration takes place, and the reference electrode, placed in the microchannel far from the titration cell. It can therefore be assumed that the pseudo-reference electrode is not influenced by the titrated solution. The equivalence point lies at the inflexion point of the curve, i.e. at the point of maximum slope, given by the first derivative of the potential vs. the titration time.

As mentioned in the introduction, the use of ISFETs was avoided in order to simplify the technological process and thus to reduce fabrication costs. Therefore, noble metallic electrodes were used both as indicator and as reference electrodes. Strictly speaking, the reference electrode – whose potential can vary – is a pseudo-reference electrode. However, as the information given by the relative potential change at the indicator electrode is sufficient to detect the titration endpoint, this pseudo-reference electrode, made either of Pt or of Ag, serves its purpose very well.

### 2.3.1. Metallic electrodes

Metal-based indicator electrodes can be classified as electrodes of the first kind, electrodes of the second kind, and inert redox electrodes [24]. An electrode of the first kind consists of a pure metal electrode that is in direct equilibrium with its cations in the solution.

Electrodes of the second kind are made of metals that respond to the activities of anions that form sparingly soluble precipitates or stable complexes with the respective cations. A typical example is the potential of a silver electrode that correlates reproducibly with the activity of chloride ion in a solution saturated with silver chloride. Here, the electrode reaction can be written as

$$Ag(s) + Cl^-(aq) \rightarrow AgCl(s) + e^- \qquad (2.12)$$

Silver is a metal that undergoes reversible oxidation and can therefore be used as an indicator electrode for silver ion. The potential E of the electrode is given by the Nernst equation:

$$E = E^{0}_{Ag} + 0.059V \log [Ag^{+}] \quad (2.13)$$

where $E^{0}_{Ag} = 0.799\ V$ and $[Ag^{+}]$ is the activity of excess, uncomplexed silver ions.

Inert conductors such as Pt, Au, Pd and C responds to the potential of redox systems with which they are in contact. Potentiometric electrodes for redox titrations are commonly made from platinum, which generally acts as an indicator of the activity ratio of a redox couple. Platinum does usually not participate in the redox chemistry, except as a conductor of electrons and as a redox indicator. For redox reactions, the potential is generally given by:

$$E = E^{0} - \frac{0.059V}{z} \log \frac{(Red)}{(Ox)} \quad (2.14)$$

where $z$ is the equivalent number of electrons participating in the reaction.

In the case of acid-base titrations, the pH determination was based on the measurement of the redox potential of quinhydrone [28], which acts as a pH indicator. By saturation of the sample with quinhydrone, an equimolar mixture of quinone and hydroquinone is established. The basic equilibrium for the hydroquinone couple is:

$$C_6H_4O_2 + 2H^{+} + 2e^{-} \rightarrow C_6H_4(OH)_2 \quad (2.11)$$

This is a reversible redox process in which hydrogen ions participate. A disadvantage of quinhydrone is that it is a weak acid itself and thus may affect the titration curves at high pH.

### 2.3.2. Detection limit of potentiometry

The detection limits of potentiometric methods are usually situated around $10^{-5}$M, which is sufficient for the present application. These specifications are very interesting for microsystems since they are almost totally insensitive to volume changes or miniaturization [30].

## 2.4. Modelling of Diffusion Processes during Titration in a Microchannel

A series of model assumptions are made with regard to the description of the present system. Migration effects on the flux of the analyte are neglected by assuming a sufficiently large concentration of supporting electrolyte to be present. Convection is considered to be negligible in the quiescent solution. Hence, diffusion is the only source of mass transport to be taken into account.

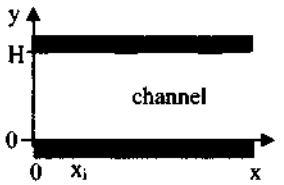


When the titration starts, the zone of analyte near the actuator electrodes is first depleted. By diffusion, this zone grows larger and reaches the indicator electrode ($x_i$). Later, the expansion of the titrated volume by diffusion is stopped in the y-direction by the top of the channel (H), but it still continues laterally in the x-direction. The indicator electrode responds with a diffusion-controlled delay to the actual activity of analyte species.

Since the distance between indicator and actuator electrodes is considerably smaller than the height of the microchannel ($x_i < H$), one can assume a one-dimensional system to obtain an approximate solution of the diffusion problem. The mass transfer in the x-direction, which takes place in the microchannel can be approximated by the model for semi-infinite linear diffusion [31]. When the system consists of an acidic solution with species *HA* that is exposed to a planar actuator electrode at $x=0$, Fick's second law of diffusion becomes:

$$\frac{\partial C_{HA}(x,t)}{\partial t} = D_{HA}\frac{\partial^2 C_{HA}(x,t)}{\partial x^2} \qquad (2.15)$$

where $D_{HA}$ ($m^2/s$) is the diffusion coefficient of the acid *HA*. The following initial and boundary conditions apply:

$$C_{HA}(x,0) = C_{HA}^{*} \qquad (2.16)$$

$$\lim_{x\to\infty} C_{HA}(x,t) = C_{HA}^{*} \qquad (2.17)$$

where $C_{HA}$* (M) is the initially present analyte concentration. These relationships express on one hand the homogeneity of the solution at $t=0$ (eq.2.16), and on the other hand the semi-infinity condition (eq.2.17) which states that regions sufficiently distant from the electrode are unperturbed by the experiment. At $t=0$, the current $i$ (A) is switched on, which results in the generation of $OH^-$ ions according to equation (2.10). The local titration reaction with the acid $HA$ is assumed to be instantaneous, so that Fick's first law of diffusion applies for $x=0$ and $t\geq 0$ in the form:

$$D_{HA}\left(\frac{\partial C_{HA}(x,t)}{\partial x}\right)_{x=0} = \frac{i}{FA} \qquad (2.18)$$

where $F$ (C/mol) is the Faraday constant and $A$ ($m^2$) the surface of the actuator electrode.

Using Laplace transforms, equations (2.15) to (2.18) lead to the following solution [31]:

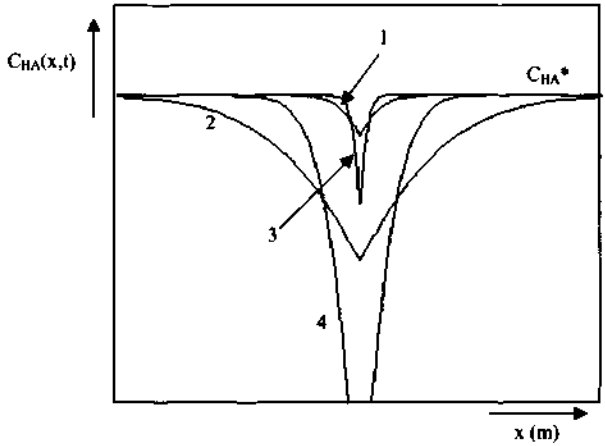


*Fig.2.3. Concentration profiles at the actuator electrode (located at the center) during a constant current electrolysis at two different times and for two different diffusion coefficients. Curves 1 and 2 represent the concentration profiles of $H_3O^+$ ions at $t_1$ and $t_2$, curves 3 and 4 the concentration profiles of HAc at $t_1$ and $t_2$.*

$$C_{HA}(x,t) = C_{HA}^{*} - \frac{i}{FAD_{HA}}\left\{2\sqrt{\frac{D_{HA}t}{\pi}}\exp\left(\frac{-x^2}{4D_{HA}t}\right) - x\,\mathrm{erfc}\left(\frac{x}{2\sqrt{D_{HA}t}}\right)\right\} \qquad (2.19)$$

which reduces to equation (2.20) for $x=0$:

$$C_{HA}(0,t) = C_{HA}^{*} - 2\frac{i}{FA}\sqrt{\frac{t}{D_{HA}\pi}} \qquad (2.20)$$

Figure 2.3 shows typical concentration profiles $C_{HA}(x,t)$ around the actuator electrode at two different times and for two different diffusion coefficients. Evidently, the coulometric generation of $OH^-$ ions results in the neutralization of the analyte in a zone near the electrode and in a concomitant drop of the acid concentration. Curves 1 and 2 represent the concentration profiles for $H_3O^+$ ions in a strong acid sample ($D_H=9.33x10^{-9}m^2/s$), whereas curves 3 and 4 show the concentration profiles for the weak acid $HAc$ ($D_{HAc}=1.21x10^{-9}m^2/s$) at $t_1$ and $t_2$, respectively. The results clearly show that at the time $t_2$, the concentration of acetic acid near the actuator electrode is zero, whereas the strong acid solution is only partially depleted. Accordingly, when an equivalent amount of acid is initially present in the immediate proximity of the actuator electrode, acetic acid is titrated faster than a strong acid such as nitric acid. This surprising fact is explained by the slower supply of the weak acid by diffusion from the bulk solution. After the titration end-point is reached, the continuous generation of hydroxide ions at the actuator electrode produces an excess concentration $C_{OH}(x,t)$ into the sample solution.

In this case, the present simple model is no longer valid and has to be replaced by a complex-moving boundary approach [32], involving the mass fluxes coupled to the neutralization reaction for all participating species.

Another complication arises when the titrated volume finally reaches the top of the channel. Nevertheless, the results derived in this section offer a qualitatively correct interpretation of experimental observations (see paragraph 2.7.7).

## 2.5. Design and Fabrication of the Coulometric Nanotitrator

Over the past decade, microfabrication techniques have been employed by a growing number of research groups, and publications reporting advances in this field have exponentially increased. Recently, two monographs [33, 34] reviewing standard microfabrication techniques have been published. As a consequence, this paragraph gives only a brief description of the techniques used for the fabrication of the coulometric nanotitrators.

One of the goals of this work was to obtain a disposable device by realizing an inexpensive coulometric nanotitrator. Therefore, the technological strategies chosen for all the devices fabricated had the same target: the use of a simple technology that requires a minimum of masks and of technological processes.

Two generations of coulometric nanotitrators were fabricated. Their design and their fabrication are basically identical, except for their lid.

### 2.5.1. Design and equivalent electrical circuit

The coulometric nanotitrator is made of a microchannel in which planar coulometric and potentiometric microelectrodes are deposited (fig.2.4). The coulometric electrodes – two generator electrodes and a counter electrode, and the potentiometric electrodes – an indicator and a reference electrode – are distributed along the microchannel. In contrast to conventional batch titrators, the counter

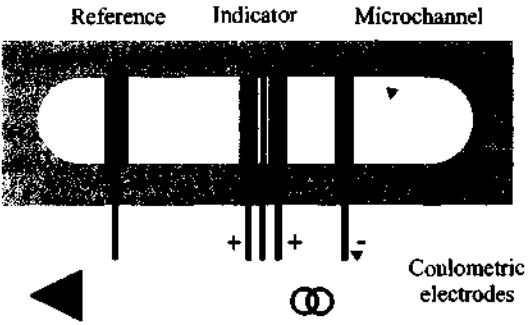


*Fig.2.4. Schematic view of the coulometric nanotitrator.*

electrode does not need to be insulated; indeed, it is situated far from the titration place and thus does not distort the detected signal. Besides, as already pointed out in §2.3, the reference electrode is a pseudo-reference electrode made of a simple metallic layer.

*Equivalent electrical circuit*

The electrical behaviour of the sensor and actuator device can be explained by considering its equivalent electrical circuit (fig.2.5). Depending on their geometrical parameters, the electrical resistances of the planar electrodes are small – in the order of 15 to 50 Ohms. Due to the presence of a strong electrolyte, the electrical resistances of the solution sections are also kept low. Due to the high input impedance of the amplification stage, the potentiometric detection circuit does not interfere in the coulometric circuit. Nevertheless, the detected signal is slightly shifted by the voltage drop on resistance $R_{LGen1}$. Since this iR drop remains constant during the whole titration, it does not perturb the determination of the titration end-point.

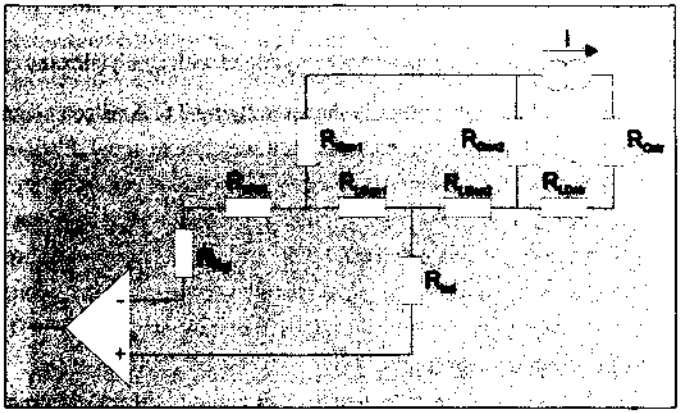

*Fig.2.5. Equivalent electrical circuit of the nanotitrator. $R_{Ref}$, $R_{Ind}$, $R_{Gen1}$, $R_{Gen2}$, $R_{Cntr}$, denote the electrical resistance of the reference, the indicator, the generator and the counter electrode, respectively. The subscript L designates the electrical resistances of the solution between the electrodes.*

*Design features*

The microchannel has a length of 18mm, a width of 1mm, and a variable height. The width of the generator electrodes is 250µm. They are separated from the 30µm wide indicator electrode by 20µm. The reference electrode (400µm wide) is situated at the beginning of the channel far from the titration place, so as to prevent interference from the coulometric reaction.

Different channel heights were tested, namely 100µm and 25µm. Therefore, the total volume of the channel is 2 µL and 0.5 µL respectively. However, since the titration occurs locally, the effective sample volume involved in the intrinsic titration cell – which includes the generator electrodes and the indicator electrode – consists of only about 68 nL and 15nL of analyte solution, respectively.

The first design of the coulometric nanotitrator was designed in a way similar to the bloodgas sensor developed by Arquint [35] for the monitoring of $pO_2$, $pCO_2$ and pH of the blood. The idea was to profit from the technology developed for the bloodgas sensor, especially by adapting the formation of polysiloxane ring that defines a reaction chamber for the sample solution.

### 2.5.2. Fabrication process for the nanotitrator equipped with a polysiloxane ring

A cross section of the nanotitrator is shown in figure 2.6. A silicon wafer, coated with a 500nm thermal dioxide layer, was used as a substrate material. Platinum planar electrodes of different sizes were deposited on the silicon substrate by using a standard evaporation process, followed by a lift-off technique. The adhesion of the Pt layer (150nm) on the oxide was enhanced by the use of an intermediate layer of Ta (10nm), which chemically binds to the passivation layer by oxide formation. Finally, a 200nm thick insulation layer of silicon nitride was deposited by PECVD (plasma enhanced chemical vapour deposition).

For precipitation and complexometric titrations, silver electrodes were introduced. To this end, a silver layer was grown electrochemically on the platinum layer of corresponding devices. The electrodeposition was carried out in a silver cyanide bath (Silver GLO 3K, n° 68000371, purchased by Lea Ronal AG, Switzerland) at a current density of 50 $\mu A/mm^2$, yielding a 3 µm thick Ag layer.

The sample channel was created with a ring of polysiloxane that was deposited and patterned by a photopolymerization process developed at the IMT Neuchâtel [35].

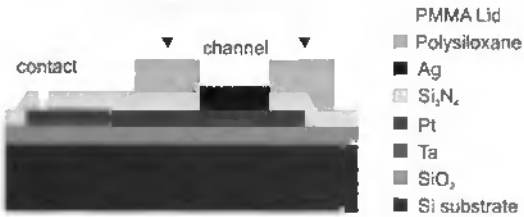


*Fig.2.6. Cross-section of the coulometric nanotitrator, showing the fabrication steps.*

The original height of the polysiloxane layer was 120 µm. A PMMA lid with both an inlet and an outlet was then fixed on the top of the device, so that the polysiloxane layer was squeezed between the lid and the silicon substrate. The resulting height of the channel was about 80 µm. The whole chip was then glued onto a printed circuit board, on which electrical contacts were bonded (fig.2.7).

*Fig.2.7. Photograph of the coulometric nanotitrator equipped with a polysiloxane ring.*

### 2.5.3. Problems encountered with polysiloxane

Polysiloxane is undoubtedly an interesting material for sensors and microsystems, since it can be structured, is very flexible, and presents good sealing properties. In addition, its permeability to oxygen and other gases [35] makes it a valuable polymer as a gas-permeable membrane. Nevertheless, the permeability to oxygen, the softness of the polysiloxane and the problems related with carry over effects are drawbacks in view of an application of this polymer for the coulometric nanotitrator. In fact, lifetime measurements revealed the high sensitivity of the polysiloxane ring towards near environment vibrations (see §2.7.2). Moreover, due to the poorly controllable pressure of the PMMA lid on the polysiloxane ring, the geometry of the reaction chamber was badly defined. This would ultimately lead to the need for a higher number of calibrations in order to assess the geometrical constants of the system. The fragility of the polysiloxane ring was also observed after several manipulations, and showed that it would eventually tear off the substrate. Finally, the permeability to oxygen of the polysiloxane ring may be responsible for a partial oxidation of sensitive sample solutions, such as redox couples.

The use of a polymer harder than polysiloxane could have resolved some of the problems. The negative photoresist SU-8, for example, which forms a solid epoxy product after polymerization, may adequately replace the polysiloxane. However, so far, only a few papers reported on applications of this [36, 37] and other new photosensitive polymers [38].

In a second design of the coulometric nanotitrator, a channel etched in Pyrex therefore replaced the polysiloxane ring, so as to prevent the above-mentioned problems.

### 2.5.4. Fabrication process of the nanotitrator equipped with a glass channel

The new design feature chosen was a chemically etched Pyrex channel with both inlet and outlet drilled holes. This solution has the advantages of a fully integrated nanotitrator and of a very robust and well-defined titration chamber. Indeed, unlike polysiloxane, glass can be structured precisely; this is why the geometry of the microchannel becomes highly reproducible. In addition, glass is not permeable to oxygen and thus offers a high chemical stability.

The coulometric nanotitrator of the second generation consists of two parts: a silicon substrate on which platinum planar electrodes are deposited, just as in the first design, and a glass cover in which a microchannel is etched. The two parts are anodically bonded. Figure 2.8 shows a cross section of the complete device.

An additional step was required for the second generation of coulometric nanotitrators. It consisted of levelling the Ta/Pt layer with the silicon surface to allow a good bonding between the substrate and the lid. Therefore, the 500nm thick thermal oxide was partially etched in buffered HF, so that a thin cavity (160nm) was created for the uptake of the Ta/Pt layer [39].


*Fig.2.8. Cross-section of the coulometric nanotitrator equipped with a glass channel*

The microchannel was etched in a 1.5mm thick Dow Corning #7740 Pyrex wafer with a 50% HF solution. The etching rate was about 10μm/min, depending on the age of the solution. A LPCVD (low-pressure chemical vapour deposition) polysilicon mask (200nm) defined by plasma etching was used to protect the glass surface [40]. Channels with heights from 9 to 100μm were fabricated. The inlet and outlet of the channel were made either of two ultrasonically drilled holes (fig.2.9), or they were made by conventional diamond drilled holes (1mm in diameter). Prior to the bonding step, the polysilicon layer was removed in a 60°C KOH bath.

The anodic bonding of the silicon substrate, coated with a nitride layer, with the glass cover lid was performed at 450°C by applying a voltage of 1.2kV. The anodic bonding mechanism has not yet been completely understood. It is commonly suggested that due to the combined action of the temperature and of the high electric field – created by applying a high negative voltage to the glass with respect to the silicon – positive and negative ions move in the glass towards the electrodes. The cations are in most cases $Na^+$ ions. They leave the interface region, and they are

displaced towards the cathode. There, the reaction with the atmospheric humidity leads to the formation of NaOH, which accumulates on the glass surface. The negative ions are displaced towards the anode, and chemical reactions take place at the glass-silicon interface, resulting in the silicon oxidation and thus, in permanent bonds between the two wafers [33, 41]. If a nitride layer is placed at the glass-silicon interface, the oxygen from the top wafer reaches the interface and, during the bonding process, the oxygen seems to diffuse into the nitride, where a layer of about 10nm oxide is developed [42]. The whole process results in strong bonds.


*Fig.2.9. SEM picture of a halved cover lid, with the etched channel and a drilled hole.*


*Fig.2.10. Photograph of the coulometric nanotitrator equipped with a glass cover plate.*

## 2.6. Experimental Section

### 2.6.1. Reagents

KCl p.a. was used for precipitation titrations, $Na_2S_2O_3 \cdot 5H_2O$, 99.5% for complexometric titrations and $FeSO_4$ for redox titrations. An excess of 20mM cerium (III) chloride heptahydrate was added to the iron sulphate. These salts were dissolved in deionised water. A saturated quinhydrone 97% solution was used as a redox couple to carry out acid-base titrations with nitric and acetic acids as sample solution ($HNO_3$ and acetic acid: Titrisol 0.1M, Merck). A background electrolyte of 0.1M $KNO_3$ p.a. was used for precipitation, complexometric and acid-base titrations. Redox titrations were carried out with a background electrolyte of 1M $H_2SO_4$. All the reagents were purchased from Aldrich, except if specified otherwise.

### 2.6.2. Procedures

The experimental procedure was completely automated so that all measurements could be performed under the same conditions. In addition, automation of the experiment led to a better reproducibility of the measurements.

A peristaltic pump was used to inject the sample solution into the nanotitrator. A pinch valve was placed between the nanotitrator and the peristaltic pump to increase the non-flow stability of the solution in the microchannel. Constant current sources were home made. The detection circuit, galvanically separated from the coulometric circuit was realized using an instrumentation amplifier AMP01, in combination with a high impedance stage. A RC low-pass filter was placed after the amplification stage (cut-off frequency: 10 Hz).

The measuring cycle consisted of a pumping period (2 seconds), a stabilization time to get a steady state (4 seconds), and a titration period during which the current was switched on. The titration always proceeded with a fresh sample aliquot. Unless otherwise specified, titrations were repeated twelve times for each analyte concentration. During the first two titrations the electrodes were preconditioned. During the following ten titrations, results were sampled and averaged, and the standard deviation was calculated.

## 2.7. Results and Discussion

### 2.7.1. Applicability of the device

Precipitation, complexometric, redox and acid-base nanotitrations were carried out on the basis of the same device. Titration curves as shown in figure 2.11a were obtained for all types of titrations. The titration end-point was determined as the time difference between the starting point where the current was switched on and the point where the derivative of the titration curve reached the maximum (fig. 2.11a). A linear relationship between the titration end-point and the concentration of the titrated species was observed in a given range (fig. 2.11b).

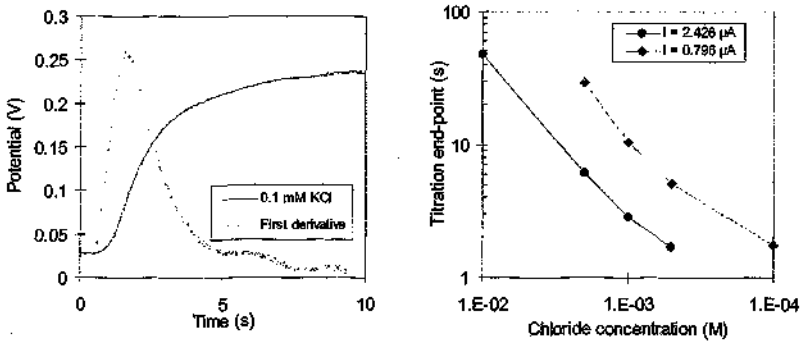


*Fig.2.11. a) Precipitation titration curve with its first derivative for a solution of 0.1 mM KCl. b) KCl concentration vs titration end-point for two currents. A nanotitrator equipped with a polysiloxane channel was used.*

Potassium chloride titrations were based on the precipitation of chloride with electrolytically generated $Ag^+$ ions. In the case of the titration of sodium thiosulphate, complex ions were formed with the silver ions released at the electrodes (fig.2.12). It should be pointed out here that the titration of 0.1mM sample solution in a few nanoliters corresponds to less than a nanogramm of analyte.

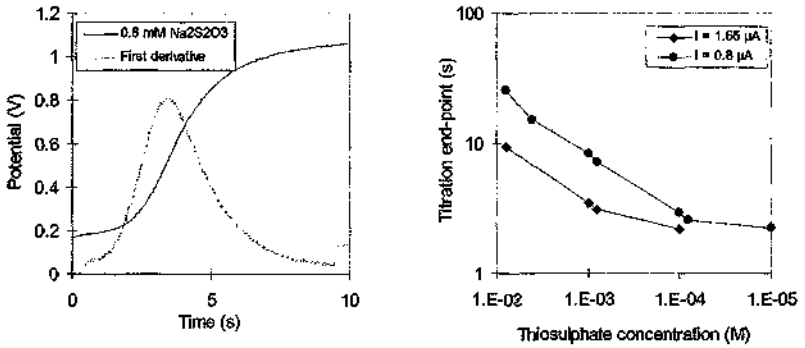


*Fig.2.12. a) Complexometric titration curve with its first derivative for a 0.8 mM $Na_2S_2O_3$ sample. b) Thiosulphate concentration vs titration end-point for two currents. A nanotitrator equipped with a polysiloxane channel was used.*

Platinum electrodes were used for redox titrations. The redox couple Fe(II) / Fe(III) was considered as a typical example suited for redox titrations. Figure 2.13 shows redox titrations for different sample concentrations. A back titration was first carried out for a few seconds, using a negative current. Then a positive current was applied and the potential was monitored. The titration end-point was defined as the time difference between the two maxima of the first derivative.

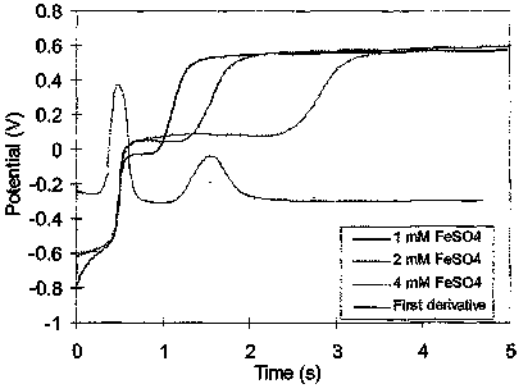


*Fig.2.13. Redox titration curves for different concentrations of Fe(II). A back titration was carried out at -2.2 µA for a few seconds, then a positive current of 2.3 µA was applied and the potential was monitored. A nanotitrator equipped with a Pyrex channel was used.*

The reproducibility of these measurements was not as good as for the other type of titrations. This effect may be due to the oxidation of the platinum electrodes by the cerium [26].

In view of a simple device, it was not intended to integrate a pH electrode into the microchannel. Therefore, acid-base titrations were carried out using the indirect method, based on the measurement of the redox potential of quinhydrone (see §2.2.2). Acetic and nitric acid solutions were titrated by this procedure. In all measurements, a high reproducibility was achieved, the standard deviation being always below 1-2%.

Table 2.1 summarizes the species which were titrated with the nanotitrator. It specifies the titration parameters and the range, where a linear relation between the titration end-point and the concentration of the different species was obtained.

| *Type of titration* | *Species titrated* | *Chemical reactions* | *Background electrolyte* | *Electrodes* | *Linear range (M)* |
|---|---|---|---|---|---|
| *Precipitation*[a] | $Cl^-$ | $Ag \rightarrow Ag^+ + e$<br>$Ag^+ + Cl^- \rightarrow AgCl$ | *0.1M* $KNO_3$ | *Ag* | $10^{-2}$ - $8x10^{-4}$ |
| *Complexo-metric*[a] | $S_2O_3^{2-}$ | $Ag \rightarrow Ag^+ + e$<br>$Ag^+ + 2S_2O_3^{2-} \rightarrow [Ag(S_2O_3)_2]^{3-}$ | *0.1M* $KNO_3$ | *Ag* | $8x10^{-3}$ - $10^{-4}$ |
| *Redox*[b] | $Fe(II)$ | $Ce(III) \rightarrow Ce(IV) + e$<br>$Fe(II)+Ce(IV) \rightarrow Fe(III)+Ce(III)$ | *1M* $H_2SO_4$ | *Pt* | $10^{-2}$ - $10^{-3}$ |
| *Acid-base*[b] | $H^+$ | $2H^+ + 2e \rightarrow H_2$<br>$C_6H_4O_2 + 2H^+ + 2e \rightarrow C_6H_4(OH)_2$ | *0.1M* $KNO_3$ | *Pt* | $10^{-2}$ - $2x10^{-4}$ |

*Table 2.1. Summary of the titrations carried out with coulometric nanotitrators equipped [a]with a polysiloxane channel, [b]with a Pyrex channel. [c]An excess of 20 mMCe(III) was added to the Fe(II) sample solution.*

## 2.7.2. Comparison of polysiloxane microchannels vs glass microchannels

As reported earlier, nanotitrators were equipped with a microchannel either made from polysiloxane or directly structured in glass. Comparative titrations carried out with nanotitrators based on the two microchannels showed a better reproducibility

of the measurements for the glass structured microchannel. In 180 measurements, a standard deviation of only about 1% was found for the device equipped with the glass channel. For the nanotitrator with the polysiloxane channel, on the other hand the standard deviation for the same series of experiments was in the range of 3 to 8%. Table 2.2 also reveals that, the smaller the height of the microchannel is, the better the reproducibility of the measurements is.

| *Channel material* | *Polysiloxane* | *Polysiloxane* | *Pyrex* | *Pyrex* |
|---|---|---|---|---|
| *Channel height (μm)* | *about 60* [a] | *about 50* [a] | *100* | *25* |
| *Current (μA)* | *5* | *4* | *9* | *2* |
| *Titration end-point (s)* [b] | *2.53* | *2.53* | *2.86* | *2.82* |
| *Standard deviation (%)* | *8* | *2.7* | *1.2* | *0.7* |

*Table 2.2. Parameters and results of titrations of a 2 mM $HNO_3$ sample carried out with nanotitrators equipped with a structural polysiloxane channel and a glass channel, respectively. [a]The height of the polysiloxane channel could not be accurately measured, [b]Average of the titration end-points for 180 measurements.*

### 2.7.3. Linearity of the response

As expected from theory (eq.2.1), a linear relationship between the titration end-point and the concentration of the analyte was found. Figure 2.14 documents these results for nanotitrators with different *channel heights*. The measurements were carried out under the same conditions for both systems, and the same sample solutions were used. The ratio between the channel heights of 1:4 is perfectly reflected by the slopes of the fits. Since the effects of lateral diffusion are only negligible for relatively short periods of time, the titration end-points above 12 seconds were not taken into account for the fits.

Linearity was also observed in experiments performed at different *currents* (fig.2.15). It should be noted that a current variation makes it possible to cover a larger concentration range in the linear regime of titration end-points (i.e. below 12s).

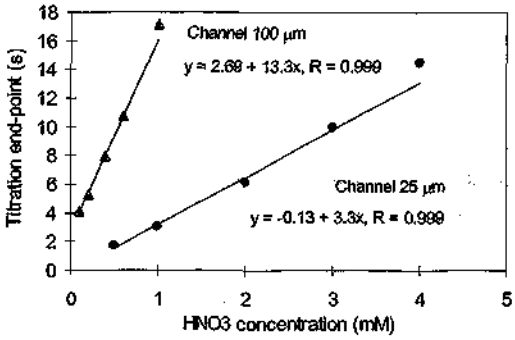


*Fig.2.14. Comparison of results obtained for nanotitrators with two different channel heights of the Pyrex glass channels. $HNO_3$ solutions were titrated at 1 µA. Values above 12 s were not taken into account for the curve fits.*

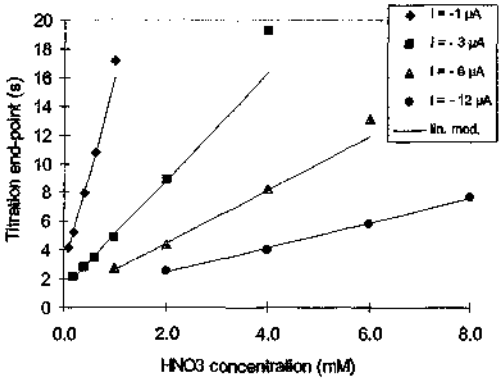


*Fig.2.15. Results of titrations carried out at a current of ♦ 1 µA, ■3 µA, ▲ 6 µA and ● 12 µA, respectively using a nanotitrator equipped with a100 µm Pyrex glass channel.*

### 2.7.4. Mathematical model

It can be seen from figures 2.14 and 2.15 that the curve fits do not cross the time axis at the origin, but at the intercept $t_d$ (delay time). This delay time is partly given by the time of diffusion from the generating electrode to the indicator electrode. It also follows from the experimental results that the total amount of charge needed to

reach the equivalence point is somewhat larger than the theoretical value according to equation (2.1). This effect has also been reported by van der Schoot [10]. Therefore, $t_d$ and an additional empirical factor $a$ are introduced in (eq.2.1):

$$t = czFVa/i + t_d \qquad (2.21)$$

The parameters $a$ and $t_d$ were found to be *1.9* and *0.3 s* for a channel height of 100µm, and *2* and *0.2 s* for a channel height of 25µm, respectively. Surprisingly, these values correspond to the values given by van der Schoot. The factor $a$ is almost independent of the current, but at least a fraction of $t_d$ is inversely proportional to the current, as shown in figure 2.16. Thus, according to these findings, (eq.2.21) may be extended to:

$$t = (czFVa' + \beta)/i + t_d' \qquad (2.22)$$

where $a'$, $\beta$ and $t_d'$ are constant parameters of the system. $\beta$ may be identified with a charge contribution related to interferents, such as dissolved oxygen. Figure 2.15 shows results of measurements that were fitted according to equation (2.22). Values for the basic parameters $a'$, $\beta$ and $t_d'$ were determined from calibration measurements carried out at 6µA and are summarized in table 2.3. For the sake of simplicity, this model was only verified for acid-base titrations of $HNO_3$ samples. However, equation (2.22) is expected to be more generally applicable since linearity could be shown for all types of titrations.

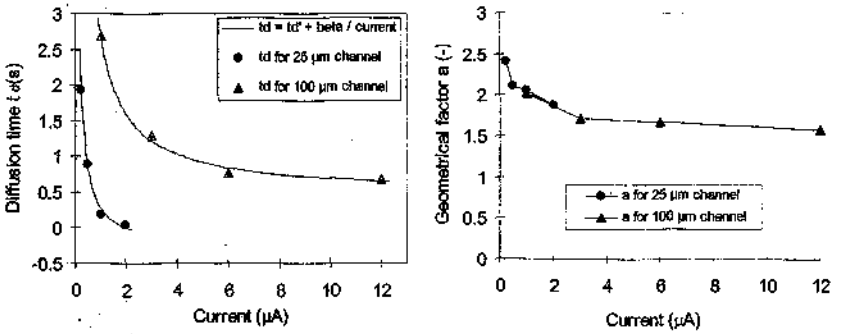


*Fig.2.16. a) Variation of the diffusion time parameter $t_d$ as a function of the applied current for two different channel heights. b) Variation of the geometrical factor a as a function of the current for two channel heights.*

| *Channel height (μm)* | *a'* | *β ($10^6$ As)* | *$t'_d$ (s)* |
|---|---|---|---|
| *25* | *2.14* | *0.27* | *0.26* |
| *100* | *1.69* | *5* | *0.25* |

*Table 2.3. Parameters of the extended model (eq.2.25) for two channel heights.*

### 2.7.5. Design of an intelligent sensor

The concept of an intelligent sensor aims at a device that is able to scan the sample before the real measurement is made, i.e. to perform a fast titration at a high current density. This makes it possible to adjust the current of the subsequent high-precision measurement in order to get a titration end-point of less than 12s. Figure 2.17 shows the $HNO_3$ concentration values detected by the nanotitrator in such a procedure, using equation (2.22) for the evaluation, versus the nominal concentrations of the sample solutions. The resulting errors were within a few per cent, but always below 5%.

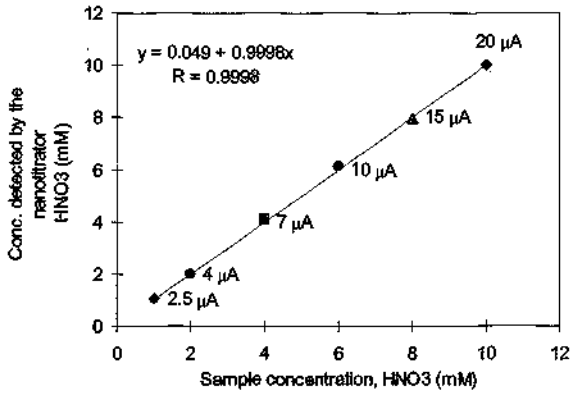


*Fig.2.17. Results obtained for an intelligent sensor adjusting the applied current to yield titration end-points in the optimal range. A unique calibration was made at 20 μA.*

### 2.7.6. Titration of $H_3PO_4$

Titrations of phosphoric acid were carried out in order to demonstrate the linearity of the nanotitrator. Figure 2.18a shows a typical titration curve with two titration end-points, and figure 2.18b illustrates the relation between the first and the second end-point.

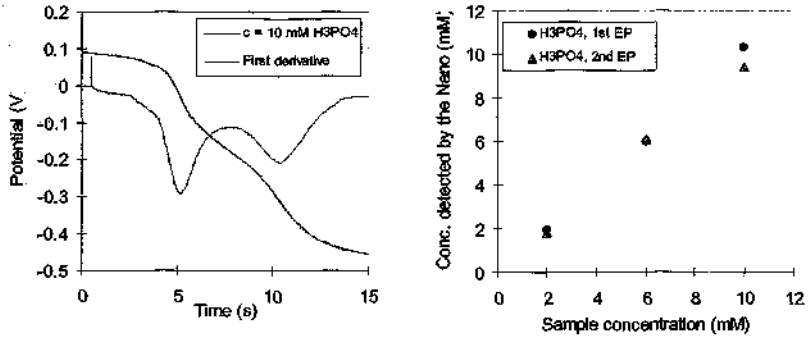


*Fig.2.18. a) Titration of 10 mM $H_3PO_4$ at a current of 19 μA. b) Detected $H_3PO_4$ concentration versus nominal concentration of the sample. The first end-point (EP) at 6 mM was used for calibration.*

### 2.7.7. Titration of weak acids

Acetic acid was considered to be a typical example suited for weak acid titration. Acetic acid samples were titrated in the same nanotitrator and under conditions similar to those used for nitric acid titrations. Figure 2.19 compares results obtained for both acids. The given detected concentrations were again calculated on the basis of equation (2.22). A single calibration of the system with the 100μm channel was performed at 10μA for the 6mM nitric acid sample, and the parameters obtained were used to calculate the resulting concentrations of all the other samples. The same procedure was used to calibrate the device equipped with a channel of 25μm height (calibration measurements on 6mM $HNO_3$ at 3μA). As can be seen in figure 2.19, linearity was observed for acetic acid, in similarity to the results found for strong acids. Nevertheless, for titrations performed under identical current

conditions, the titration times for acetic acid samples were found to be shorter than for nitric acid samples. These results agree with the predictions of the theoretical analysis described in §2.4, and are comparable to the findings by Olthuis et al. [16] for a device without cover lid. It is clear that the presence of a cover lid does not completely eliminate the diffusion effects of the different analytes. Nevertheless, the height of the microchannel does clearly influence the ratio between the titration times for the acetic acid and the nitric acid samples. In this study, the titration time ratio was found to be 0.7 and 0.8, for 100μm and 25μm channel height, respectively, whereas Olthuis observed a ratio of 0.64. These results demonstrate that the diffusion influences decrease with the channel height. The latter parameter can unfortunately not be arbitrarily reduced, when a conventional pumping system (peristaltic or piston pumps) is used to introduce the sample solution in the microchannel, since the hydraulic resistance of the microchannel increases with the reciprocal third power of the channel height (see § 4.4.2).

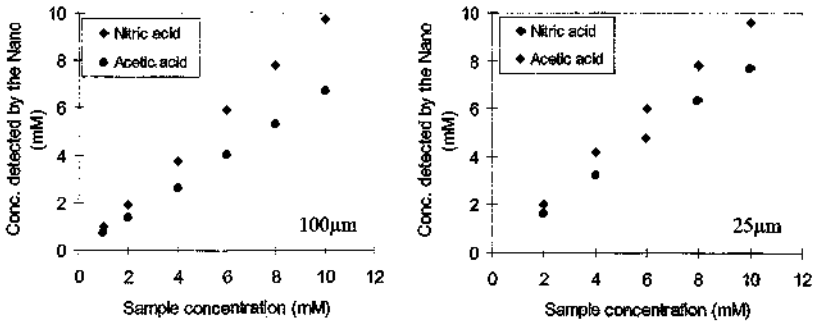


*Fig.2.19. Comparison between titration of nitric and acetic acids. The concentration of both acids were determined for two different channel heights: 100μm and 25μm.(see text for calibration parameters)*

### 2.7.8. Long-term stability of the nanotitrator

The *long-term stability* of the nanotitrator was tested in different respects. Figure 2.20a shows results of two sets of measurements carried out within an interval of three weeks. The sample preparations and the measuring conditions were the same. A

single calibration was made during the first set of measurements using a 10mM solution. The observed errors were within a few per cent for both sets of measurements.

The practical *lifetime* of the nanotitrator was found to be sufficiently long for most applications (fig.2.20b). More than 2000 measurements were carried out with the same device (25 μm channel height). A solution of 2mM $HNO_3$ was titrated at a current of 2 μA. Three measurements were done per minute, which corresponds to about 12h for all measurements. The averaged titration end-point was at 4.84s with a

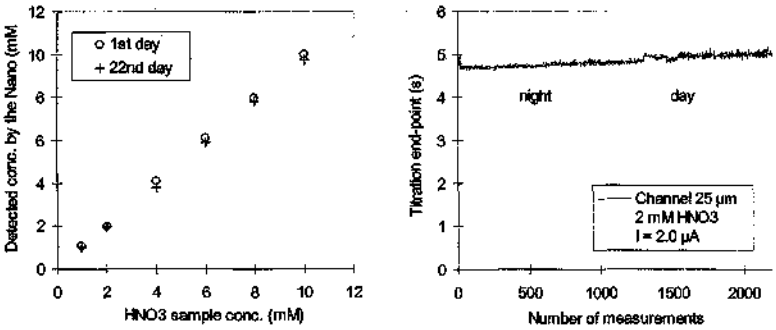


*Fig.2.20. Long-term stability of the nanotitrator: a) Comparison of measurements carried out within a three weeks interval. b) Results of continuous measurements on 2mM $HNO_3$ samples at 2 μA. After 2200 measurements, the device was still working.*

standard deviation of 0.11s or 2.3%. If only the first 1300 measurements (during the night) are considered, one even gets a standard deviation of only 1%. The small drift observed is probably due to the slow oxidation of the quinhydrone solution.

In the case of a device for precipitation titrations, the lifetime mainly depends on the rate of consumption of the active layer of the generator electrodes, and thus on the thickness of this layer. For instance, about $1.5 \times 10^{-7}$ mol of silver is available in a 3μm Ag layer – if we assume an active area of $0.5 mm^2$ –, which will theoretically last for 600 titrations of 10mM KCl sample solution. To prolong the life expectancy of the device, one could obviously increase the silver layer thickness. In practice, however,

silver chloride precipitates are deposited in a coarsely crystalline form (fig.2.21) that can ultimately lead to shortcuts.

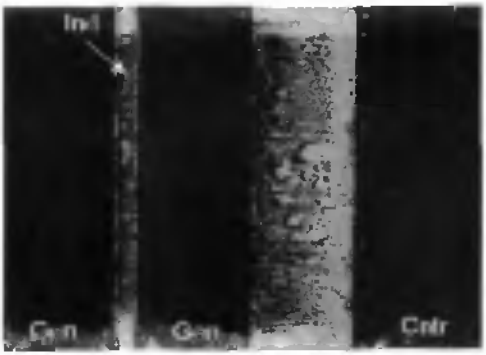


*Fig.2.21. Picture of the coarsely deposited AgCl precipitate between two generator electrodes (Gen) and the counter electrode (Cntr) after about 100 precipitation titrations. The indicator electrode (Ind) is located between the generator electrodes.*

Finally, the *temperature influence* on the response of the nanotitrator was investigated. It can be seen from figure 2.22 that the relative error arising within a temperature range of 20°C is only 2%.

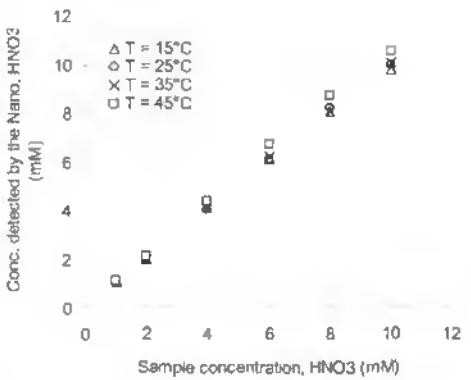


*Fig.2.22. Influence of the temperature on the response of the nanotitrator. Measurements were carried out using a 100µm channel.*

## 2.8. System Optimisation

A large number of parameters, including the dimensions of the microchannel and of the microelectrodes, the titration conditions, such as the pumping speed of the fresh sample aliquot, the stabilisation time, and the concentration of the background electrolyte have a distinct influence on the determined of the titration end-points. Some of the most important parameters are discussed in the following paragraphs. Discussions are based on experimental results obtained in this study, as well as on the conclusions derived from a mathematical model by Kolev et al. [23] for a coulometric titrator without cover lid. This model was founded on three-dimensional diffusion – infinite in x- and y-axis and semi-infinite in z direction – and accounted for all the species interacting in an acid-base titration. The good agreement between theoretical and experimental data allowed Kolev to quantitatively investigate the influence of some geometrical parameters, such as the width of the generator electrode, the distance between the generator electrode and the sensor, the symmetry and the degree of miniaturization of the sensor. Even though the nanotitrator presented in this thesis is significantly different from the one studied by Kolev et al., some of the earlier results are also applicable to the present system.

### 2.8.1. Influence of the geometrical parameters

*Coulometric electrodes*

The width of the generator electrode is one of the main system parameters influencing the titration end-point. According to Kolev's calculations, the wider the generator electrode is, the shorter the equivalence time becomes, finally reaching an asymptotic value that corresponds to infinite width. The titrations of a 4mM strong acid sample, carried out under conditions (i.e. 20A/m$^2$) comparable to those used by Kolev, corresponded well with the model (fig.2.23). As a matter of fact, the end-point times of titrations performed with 250μm wide generator electrodes were almost twice as long as those with 500μm wide electrodes. In both cases, the experimental data were easily reproducible. On the other hand, the results obtained with even wider electrodes were not as reproducible and did not well agree with the model (fig.2.23). This may be due to a limiting diffusion boundary on the z-axis, i.e. the height of the

cover lid, which transforms the semi-infinite diffusion problem into a more complex one.

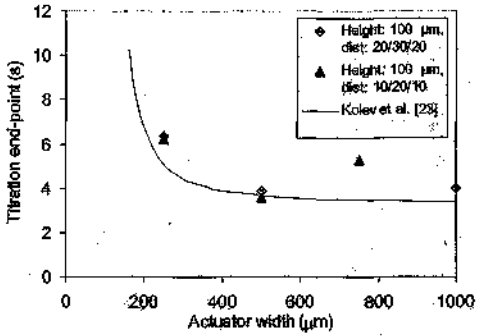


*Fig.2.23. Influence of the width of the generator electrode on the titration end-point for the titration of a 4mM strong acid (channel height: 100µm). The numbers indicated after "dist" correspond to the distance between first generator and indicator electrode/ width of indicator electrode/ distance between indicator and second generator electrode.*

The distance between the generator electrodes and the counter electrode, as well as the size of the latter electrode, also play some role in the determination of the titration end-point. As shown in figure 2.24a, the titration times slightly increase with

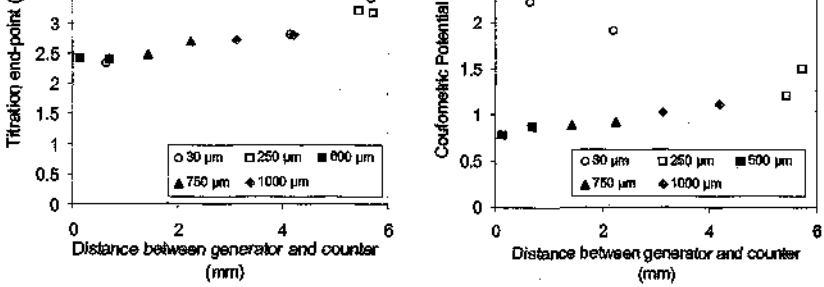


*Fig.2.24. Influence of the distance between the generator and the counter electrode for different values of the counter electrode width (width of the generator electrodes:2x250µm) a) Titration end-points for a 4mM strong acid sample at 20 µA, b) Electrolysis potential measured during the titrations.*

the above-mentioned distance. Since the current remains constant, this must be related to a modification of the propagation of the electric field in the solution. It is well known that planar electrodes suffer from edge effects in the sense that the electric field and the related current density are much more intense at the periphery of the electrodes. Migration may also be a source for such effects, but only if the concentration of the background electrolyte is not high enough [21]. Another aspect related to coulometric actuation is displayed in figure 2.24b, which shows the measured potential drop between the coulometric electrodes during the titration. It seems clear that, when wider counter electrodes are used, the electrolysis potential is essentially limited by the iR drop in the solution, whereas it is mainly determined by an electrode boundary resistance (polarization effect) when the counter electrodes are smaller. In the latter case, the potential is so high that water electrolysis can take place as a side reaction, which leads to less reproducible titration end-points (fig.2.24a).

In conclusion, the best results with regards to reproducibility and titration curve transition were obtained for 250 - 500μm wide generator electrodes. To reduce effects arising from the inhomogeneity of the electric field, the generator electrodes should be placed symmetrically and as near as possible from each other. Moreover, a single generator electrode shaped around the indicator electrode should be preferred in this respect. Finally, by adjusting the area of the counter electrode to that of the generator electrodes, additional geometrical limitations can be avoided.

*Potentiometric electrodes*

According to the former discussion, the sensor should be positioned in the middle of the actuator electrodes and should be as small as possible. As shown in figures 2.23 and 2.25a, the smaller the sensor is and the closer it is to the generator electrodes, the shorter the titration time becomes. The response time, which is partly dictated by the diffusion time, is evidently related to the distance between the actuator and the sensor.

On the other hand, due to the high input impedance of the operational amplifier, the position and the size of the pseudo-reference electrode do not influence the titration end-point, as long as this electrode is sufficiently far from the titrated solution (fig.2.25b).

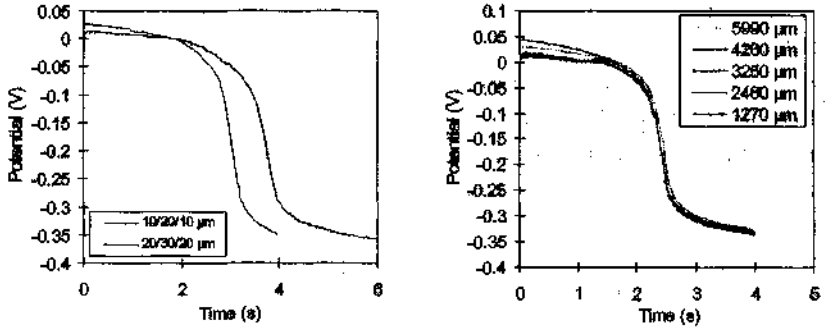


*Fig.2.25. a) Influence of the sensor-actuator distance and of the sensor size; the numbers indicated correspond to the distance between first generator and indicator electrode/ width of indicator electrode/ distance between indicator and second generator electrode. b) Titration curves obtained with five reference electrodes of different widths (30 to 1000 µm) located at the given distance x (µm) from the first generator electrode.*

## 2.8.2. Influence of the titration conditions

*Pumping speed and stabilisation time*

A peristaltic pump was used to inject the sample solution into the nanotitrator. The measurement cycle was modified in order to study the influence of the pumping speed and of the stabilisation time. After each titration, a new solution was pumped into the microchannel at a specified flow rate during 2 seconds. When the pump stopped, a pinch valve was simultaneously closed so as to hinder any further movement of the fluid which could be due to a residual pressure of the pump.

For each individual set of measurements, twelve titrations were carried out. During the first two titrations, the electrodes were preconditioned. Standard deviations were calculated from the following ten titrations and were found to be ±0.01 seconds, that is 0.4% of the averaged titration times. The influence of the stabilisation time was usually found to be in the same order of magnitude (fig.2.26). The influence of the flow rate was somewhat more important, i.e. typically around 1.2%. This can be explained by the regeneration of the stagnant layer near the

electrodes in various degrees. However, the observed effects seem to be non-proportional to the pumping speed (fig.2.26).

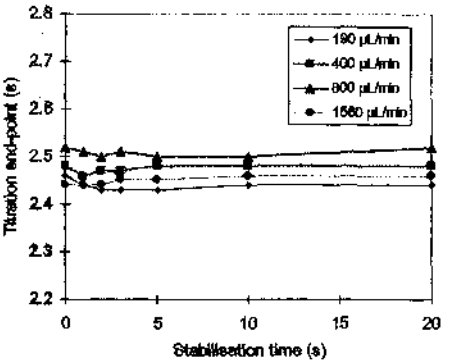


*Fig.2.26. Influence of the stabilisation time and of the pumping speed on the resulting titration time. Experiments were carried out with a 4mM $HNO_3$ sample titrated at 20µA in a 100µm high channel.*

## 2.9. Conclusion

The reported results demonstrate that the novel nanotitrator can be applied for precipitation, complexometric, redox and neutralisation titrations. For all types of titrations, a linear relationship between titration times and analyte concentrations up to $10^{-2}$M of the tested solutions was observed. In all cases, a very short electrolysis time – typically less than 10 seconds – was sufficient for completing the coulometric titration. This corresponds to a gain by a factor of 30 to 60 over conventional batch titrators which require typical titration times in the order of 5 to 10 minutes. In addition, the sample volume needed to carry out the titration is only about 10μL, which is around 10000 times (2500) lower than the usual 100mL (sometimes 25mL) used in conventional laboratory instruments. The comparison is even more impressive when the actual titrated volume of down to 15nL is considered, which permits determinations of a few tenths of nanograms of analyte, about 2.5 million times less than what is being titrated in a conventional apparatus.

In addition, the simple structure and the astonishingly high long-term stability of the system, the excellent reproducibility of the measurements, and their independence from temperature make the new nanotitrator a valuable and universal device.

It could also be demonstrated that the presence of the cover lid, which limits the height of the titration channel, influences the titration end-point. The smaller the height of the channel is, the smaller the titrated volume and the shorter the titration time is. By using a smaller channel, the influence of diffusion coefficients could also be reduced.

**References**


[1] Guenat O.T., Arquint Ph., Weber I., Morf W. E., van der Schoot B. H., de Rooij N. F., *Micro Total Analysis Systems for Nano Titrations of Analytes*, Proc. of the 2nd Int. Symp. on Miniaturized Total Analysis Systems μTAS'96, Basel, Switzerland, 1996, p. 215.

[2] Guenat O. T., Arquint Ph., Morf W. E., van der Schoot B. H., de Rooij N. F., *Coulometric Nanotitrators with Potentiometric Endpoint Detection*, Microreaction Technology, Proc. of the 1st Int. Conf. on Microreaction Technology, W. Ehrfeld (Ed.), Springer, Berlin, 1998, p.340-7.

[3] Guenat O.T., Morf W. E., van der Schoot B. H., de Rooij N. F., *Universal coulometric nanotitrator*, Proc. Transducers'97, Chicago, USA, 1997, p.1375-8.

[4] Guenat O. T., Morf W. E., van der Schoot B. H., de Rooij N. F., *Universal coulometric nanotitrators with potentiometric detection*, Anal. Chim. Acta, 361 (1998), p.261-272.

[5] Valcarcel M., Luque de Castro M.D., *Flow injection analysis*, John Wiley & Sons, New York, 1987, p.275-85.

[6] Ruzicka J., Hansen E.H., *Flow injection analysis*, 2nd ed., John Wiley & Sons, New York, 1988, p.156-66.

[7] Taylor R.H., Ruzicka J., Christian G.D., *Flow injection coulometric titrations*, Talanta, vol. 39, No.3, 1992, p.285-92.

[8] Taylor R.H., Winbo C., Christian G.D., Ruzicka J., *Bromine number determination by coulometric flow-injection titration*, Talanta, vol. 39, No.7, 1992, p.789-94.

[9] Chen R., Ruzicka J., Christian G.D., *Flow injection titration-linear or logarithmic*, Talanta, vol.41, No.6, 1994, p.949-55.

[10] van der Schoot B. H., *Coulometric sensors*, Ph.D. Thesis, Univ. of Twente, Enschede, The Netherlands, 1986.

[11] van der Schoot B. H., Bergveld P., *An ISFET-based microlitre titrator: integration of a chemical sensor-actuator system*, Sensors and Actuators, 8, 1985, p.11-22.

[12] van der Schoot B. H., Bergveld P., *Coulometric sensors, the application of a sensor-actuator system for long-term stability in chemical sensing*, Sensors and Actuators, 13, 1988, p.251-62.

[13] Olthuis W., van der Schoot B.H., Chavez F., Bergveld P., *A dipstick sensor for coulometric acid-base titrations*, Sensors and Actuators, 17, 1989, p.279-83.

[14] Olthuis W., Luo J., van der Schoot B.H., Bomer J.G., Bergveld P., *Dynamic behaviour of ISFET-based sensors-actuators systems*, Sensors and Actuators, B1, 1990, p.416-20.

[15] Olthuis W., van Kerkhof J.C., Bergveld P., Bos M., van der Linden W.E., *Preparation of iridium oxide and its application in sensor-actuator systems,* Sensors and Actuators, B4, 1991, p.151-6.

[16] Olthuis W., Bomer J.G., Bergveld P., Bos M., van der Linden W.E., *Iridium oxide as actuator material for the ISFET-based sensor-actuator system,* Sensors and Actuators, B5, 1991, p.47-52.

[17] Olthuis W., Bergveld P., *Integrated coulometric sensor-actuator devices,* Mikrochim. Acta, 121, 1995, p.191-223.

[18] Olthuis W., Robben M.A.M., Bergveld P., Bos M., van der Linden W.E., *pH sensor properties of electrochemically grown iridium oxide,* Sensors and actuators, B2, 1990, p.247-56.

[19] Luo J., Olthuis W., Bergveld P., Bos M., van der Linden W.E., *A porous actuator for an ISFET-based coulometric sensor-actuator system,* Proc. Transducers'91, 1991, p.229-32.

[20] Olthuis W., Luo J., van der Schoot B.H., Bergveld P., *Modelling of non-steady-state concentration profiles at ISFET-based coulometric sensor-actuator systems,* Anal. Chim. Acta, 229, 1990, p.71-81.

[21] Luo J., Olthuis W., van der Schoot B.H., Bergveld P., Bos M., van der Linden W.E., *Modelling of the migration effect occurring at an ISFET-based coulometric sesnor-actuator system,* Anal. Chim. Acta, 237 (1990), p.71-83.

[22] Luo J., Olthuis W., Bergveld P., Bos M., van der Linden W.E., *Modelling of coulometric sensor-actuator systems based on ISFETs with a porous actuator covering the gate,* Anal. Chim. Acta, 274 (1993), p.7-23.

[23] Kolev S.D., van der Linden W.E., Olthuis W., Bergveld P., *Mathematical modelling and optimisation of a coulometric sensor-actuator system based on three-dimensional diffusion,* Anal. Chim. Acta, 285, 1994, p.247-63.

[24] Skoog D. A., Leary J. J., *Principles of Instrumental Analysis*, Saunders College Publishing, New York, 1992.

[25] Fiaccabrino G.C., *Thin-film microelectrodes arrays: materials and designs,* Ph.D. Thesis, Univ. of Neuchâtel, IMT, Neuchâtel, Switzerland, 1996.

[26] Lingane J. J., *Electroanalytical Chemistry*, Interscience, New York, 1958, p.129-39, p.598-603.

[27] Bishop E., *Comprehensive analytical chemistry, volume IID, Coulometric analysis*, ed. Wilson & Wilson, Elsevier, Amsterdam, 1975.

[28] Clark Westcott C., *pH Measurements*, Academic Press, New York, 1978, chap. 6, pp. 136-7.

[29] Kortüm G., *Lehrbuch der Elektrochemie,* Verlag Chemie GmbH, Weinheim, Bergstr., Germany, 1962, p.582.

[30] Manz A., Graber N., Widmer H., *Miniaturized total chemical analysis systems: a novel concept for chemical sensing,* Sensors and Actuators, B1, 1990, p.244-8.

[31] Bard A. J., Faulkner L. R., *Electrochemical Methods, Fundamentals and Applications,* Wiley, New York, 1980.

[32] Crank J., *The Mathematics of Diffusion,* 2nd ed., Clarendon Press, Oxford, 1975.

[33] Madou M., *Fundamentals of Microfabrication*, CRC Press LLC, Boca Raton - New York, 1997.

[34] Kovacs G. T.A., *Micromachined Transducers Sourcebook*, McGraw-Hill, New York, 1998.

[35] Arquint Ph., *Integrated blood gas sensor for $pO_2$, $pCO_2$ and pH based on Silicon Technology*, PhD Dissertation, IMT, Univ. of Neuchâtel, Switzerland, 1994.

[36] Lee K.Y., LaBianca N., Rishton S.A., Zolgharnain S., Gelorme J.D., Shaw J., Chang T.H.P., *Micromachining applications of a high resolution ultrathick photoresist*, J. of Vac. Sci. Technol. B13, 1995, pp. 3012-6.

[37] Lorenz H., Despont M., Fahrni N., LaBianca N., Renaud P., Vettiger P., *Epon SU-8: A low-cost negative resist for MEMS*, Proc. MME 1996, Barcelona, Spain, pp. 32-35.

[38] Bratov A., *Photocurable polymers applied to chemical sensor development*, Proc. Eurosensors XI, Warsaw, Poland, 1997, p.883-8.

[39] Reimer K., Köhler C., Lisec T., Schnakenberg U., Fuhr G., Hintsche R., Wagner B., *Fabrication of electrode arrays in the quarter micron regime for biotechnological applications*, Sensors and Actuators, A 46-47 (1995), p. 66-70.

[40] Grétillat M.-A., Paoletti F., Thiébaud P., Roth S., Koudelka-Hep M., de Rooij N. F., Proc. Eurosensors X, Leuven, Belgium, 1996, p. 259.

[41] Nitzsche P., Lange K., Schmidt B., Grigull S., Kreissig U., Thomas B., Herzog K., *Ion drift process in Pyrex-type alkali-borosilicate glass during anodic bonding*, J. Electrochem. Soc., Vol.145, No.5, 1998, p.1365-8.

[42] Berthold A., Nicola L., Sarro P.M., Vellekoop M.J., *A novel technological process for glass-to-glass anodic bonding*, Proc. Transducers'99, Sendai, Japan, 1999, p. 1324-7.

# 3. Continuous flow coulometric nanotitrations

Coulometric nanotitrations were realized in a microchannel system using a continuous flow titration technique with a triangle current-time profile. Redox and acid-base titrations were carried out on Fe(II), nitric and acetic acid samples, respectively, with the same nanotitrator device. A linear relation between the concentration and the coulometric current transferred to the solution was found. The advantages of this universally applicable nanotitrator are fast response, low sample volume, high sensitivity, high reproducibility and the convenience of the handling of an automated analyzer of the flow-through type. Parts of this chapter have been published in [1, 2].

---

## 3.1. Introduction

Titrations carried out in continuous flow mode present some advantages with regards to stopped-flow titrations, such as the continuous regeneration of the stagnant layer above the electrodes, which may lead to even more reproducible results. This feature is also especially interesting for substances which may produce gas at the coulometric electrodes. In addition, the presence of a second source of mass transport in the system, i.e. convection, may reduce the diffusion contribution to the velocity of the solution. This may lead to a diffusion independent system that does only require a single calibration.

Since the flow is continuous and in order to observe a physical change at the indicator electrode, the concentration of electrogenerated ions needs to fluctuate in function of the time. In the early seventies Pungor et al [3-5] introduced the so-called triangle-programmed titration technique. This method, based on a linearly increasing and decreasing current, was applied in a macroscopic system. The streaming sample solution was gradually titrated, and, before reaching the sensor, a homogenization of

the titrated solution was performed in a mixing chamber. Pardue and Fields [6] pointed out that, since the titrant and the analyte react in non-stochiometric proportions, this method has to be classified as a variable-time kinetic method.

Numerous types of titrants were electrogenerated by this technique: silver [7], hydroxide [8], mercury [9], hypobromite [10] ions, and also bromine [11] and iodine [12] were used for carrying out argentimetric, acid-base, mercurimetric, bromimetric and iodimetric titrations. Although the triangle-programmed technique could widely be applied, the titration times reported were never below a few minutes. Several detection methods have been investigated in relation to the triangle-programmed titration technique. Depending on the domain of application, voltammetric [7], potentiometric [7, 8], biamperometric [10-12], photometric [8] and spectrophotometric [13] methods were used.

The present chapter deals with coulometric titrations carried out under continuous flow conditions, using nanotitrator devices similar to those described in chapter 2. Again, a direct potentiometric method is used to detect the titration end-points.

Due to the large-scale miniaturization, the volume of the sample solution participating in the reaction is reduced to only a few microliters. In addition, the present microdevice also differs from the macroscopic systems proposed by Pungor in that it needs no mixing unit. Furthermore, the sensor is placed next to the chemical actuator, which leads to a very short response time.

## 3.2. Coulometry in Continuous Flow

### 3.2.1. Variable-time kinetic method

If a continuously flowing analyte solution and a coulometrically generated reagent (titrant) are mixed in a certain section of a microchannel, the degree of titration in the flowing solution depends on the respective rates of molar input of the two educts. By changing these rates, the degree of titration can be altered and monitored by an appropriate sensor placed in a flow-through detector cell. When a triangle current-time profile is applied to the coulometric electrodes, the flowing sample solution becomes gradually titrated by coulometrically generated ions. The evolution of the reaction is monitored by the indicator electrode. During the first half-period (the leading edge) of the current-time profile, the usual titration curve is recorded, whereas, during the second half-period (the trailing edge), the reverse titration curve is monitored. End-points of the titration appear in both directions. The first titration end-point is situated on the leading edge, the second on the trailing edge

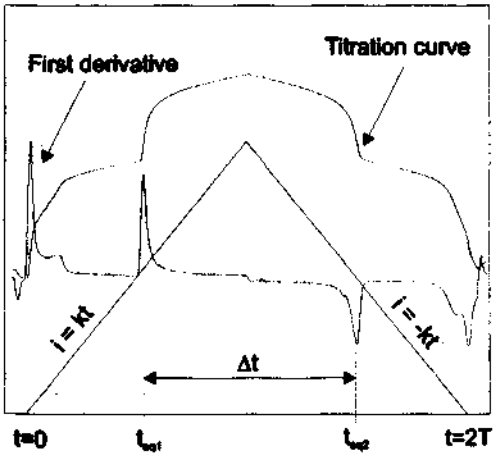


*Fig.3.1. Triangle-programmed current-time profile and titration curve for continuous titrations of a flowing sample. The potentiometric titration curve and its first derivative were obtained for a 10 mM Fe(II) sample solution.*

of the titration curve. The effective peak width of the titration curve, denoted as time span ($\Delta t$) in the following, is determined by the time elapsed between the minimum and the maximum of the first derivative (fig.3.1).

### 3.2.2. Simple Model

A simple description of the equivalence point can be obtained from a balance of the flows of the species participating in the chemical reaction. For a redox titration, the reaction is the following:

$$\nu_A A_{red} + \nu_B B_{ox} \Leftrightarrow \nu_A A_{ox} + \nu_B B_{red} \qquad (3.1)$$

where $\nu_A$ and $\nu_B$ are the stoichiometric coefficients. The mass flow rate $R_{A,red}$ of the coulometrically generated educt is determined by the current-time profile ($i$ vs. $t$), and depends on the respective proportionality factor $k$ [A/s]:

$$R_{A,red} = \frac{i}{nF} = \frac{\nu_A}{\nu_B}\frac{kt}{F} \qquad [mol/s] \qquad (3.2)$$

where $n$ is the number of electrons transferred per ion, and $F$ is the Faraday constant. The mass flow rate $R_{B,ox}$ of the analyte species to the titration cell is given by the product of the initial concentration $c_o$ [M] of the sample solution and the volumetric flow velocity $Q$ [L/s]:

$$R_{B,ox} = Q\, c_o \qquad [mol/s] \qquad (3.3)$$

Equation (3.2) holds for the leading edge of the titration curve. At the corresponding equivalence point after the time $t_{eq,1}$, the two reagent mass flows are balanced:

$$\nu_B R_{A,red} = \nu_A R_{B,ox} \qquad (3.4)$$

Accordingly, the first equivalence time $t_{eq,1}$ becomes:

$$t_{eq,1} = \frac{Q}{k} F c_o \qquad [s] \qquad (3.5)$$

Equations (3.4) and (3.5) hold for the idealized case, where the mixing between the two reagent flows is complete (see, however the extended model described below). In

analogy, the second equivalence time $t_{eq,2}$, as found for the trailing edge of the titration process, can be described as:

$$t_{eq,2} = 2T - \frac{Q}{k} Fc_o \qquad [s] \quad (3.6)$$

where $2T$ is the period of the titration cycle. Finally, the time span $\Delta t$ is given by:

$$\Delta t = t_{eq,2} - t_{eq,1} = 2T - 2\frac{Q}{k} Fc_o \qquad [s] \quad (3.7)$$

### 3.2.3. Extended Model

The simple model leading to equation (3.7) does not account for physico-chemical effects arising in the microchannel, namely the actual hydrodynamics of flow and the diffusion of ions.

For the present system, a Reynolds number of about 2 is calculated for the highest flow rate used in this study (120µL/min). This indicates that the flow is strictly laminar, i.e. a parabolic flow profile is built up in the microchannel. The near proximity of the chemical actuator and of the sensor implies that the titration occurs mainly in the boundary zone of the channel (see fig.3.2). Therefore, the effective volume of the titrated sample solution moves with an average velocity $v_{sam}$, which is related to the maximum rate $v_{max}$ by a reduction factor $\alpha$. The value of $\alpha$ must be

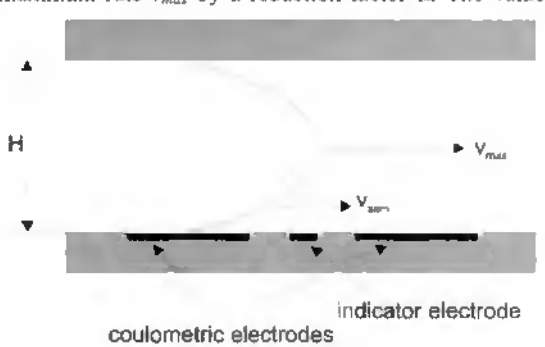


*Fig.3.2. Parabolic flow profile in the microchannel. The effective volume of sample solution titrated moves with an average velocity of $v_{sam} = \alpha v_{max}$.*

experimentally determined from a calibration curve, since the effective volume titrated is not known.

In addition, the response time asymmetry $t_r$ of the potentiometric sensor [14], revealed by the asymmetry of the titration curve, can also be accounted for in equation (3.7), which finally yields the relationship:

$$c_O = (T - \frac{\Delta t}{2} - t_r)\frac{k}{\alpha FHWv_{max}} \qquad (3.8)$$

where $H$ is the channel height, $W$ is the channel width and $v_{max}$ is the maximum velocity at the center of the parabolic flow profile.

### 3.2.4. Direct Potentiometric Detection

The end-points detection method used in continuous flow titration is similar to that used in the stopped-flow procedure. The potential is measured between the indicator electrode, located where the titration takes place, and the reference electrode, placed 7mm upstream in the microchannel. The reference electrode was located far from the titration cell, in order to prevent interference from the redox reactions. Both electrodes were made from platinum. The platinum reference electrode can be considered as a pseudo-reference electrode, since its potential depends on the composition of the native sample solution. As a relative signal arising between the potentiometric electrodes is sufficient for the determination of the titration end-point, this simple reference electrode is adequate for the present measurement.

In continuous flow analysis, the measuring rates and the detection limits are generally comparable to those found in batch titrations. For certain types of reaction and especially near the detection limit, the behaviour of the sensor can even be improved due to the short contact time of the sample with the indicator electrode. In other words, adsorption, desorption and dissolution processes may play a minor role in continuous flow analysis [15]. Accordingly, the emf $E$ of the electrode cell still follows the Nernst equation [16] in such measurements as for stopped-flow titrations.

## 3.3. Experimental Section

### 3.3.1. Design of the Nanotitrator

An array of platinum planar electrodes of different sizes are deposited on a silicon substrate, within a microchannel etched in a glass cover plate. This cover plate is anodically bonded on the silicon substrate. The whole process of the microfabrication of the coulometric nanotitrator was reported earlier in § 2.5. Figure 3.3 shows a schematic view of the nanotitrator. The coulometric titration method applied in this study makes use of two coulometric electrodes (a generator and a counter electrode) and of two potentiometric electrodes (an indicator and a 250μm wide reference electrode). The width of the generator and the counter electrode, respectively, is 250μm. Both coulometric electrodes are separated from the 5 μm wide indicator electrode by a distance of 5μm. Length and width of the microchannel are 20mm and 1mm, respectively. The height of the channel used in this study is either 30 or 50μm. Thus, the total volume of the whole channel is 0,6 and 1μL, respectively.

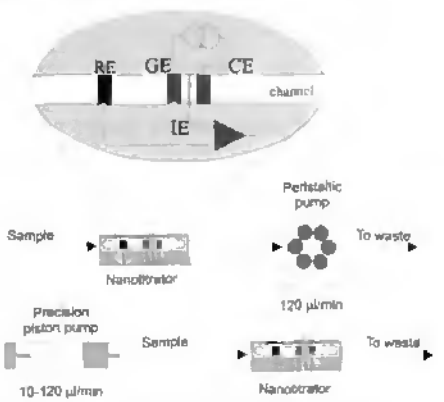


*Fig.3.3. Experimental set-up and schematic view of the μTAS for coulometric nanotitrations. IE, RE, GE, CE denotes indicator, reference, generator and counter electrode, respectively.*

### 3.3.2. Equipment and set-up

All the experiments were automated, so that the triangle-programmed coulometric titrations could be well reproduced. Either a piston-pump (700 Dosino-2 mL, Metrohm) or a peristaltic pump (MV CA-4, Ismatec) were used to continuously and precisely inject the sample solution into the microchannel. Pulses of the Dosino have a resolution of 0.2 μL. The triangle current-time profiles were provided by a Galvanostat Model 273A (EG&G Princeton Applied Research). The data acquisition was made using a home made acquisition circuit, driven by a National Instruments (Lab-PC+) acquisition board.

Each measuring cycle consisted of a 20 seconds titration period, during which the triangle current-time profile was applied and the potential response was recorded. The next cycle started five seconds later, in order to replace the sample solution in the microchannel. Cross-contamination between the sample solutions was inhibited by pumping the new sample solution in the nanotitrator for about 5 seconds, before the beginning of the titration cycle. The titrations were repeated seven times for each concentration. The electrodes were preconditioned during the first two titrations. Results obtained during the following five titrations were averaged, and the standard deviation was calculated.

### 3.3.3. Materials

All reagents were purchased from Aldrich except when specified otherwise. $FeSO_4$ was used as analyte for redox titrations. An excess of 20mM cerium(III) chloride was added to the iron(II) solution. The salts were dissolved in deionised water. A background electrolyte of 1M $H_2SO_4$ was used for redox titrations. A 97% quinhydrone solution was used as a redox couple to carry out acid-base titrations with nitric acid as a sample solution ($HNO_3$ Titrisol 0.1M, Merck). A background electrolyte of 0.1M $KNO_3$ p.a. was used for acid-base titrations.

## 3.4. Results and Discussion

### 3.4.1. Redox titrations

The redox couple Fe(II) / Fe(III) was chosen as a typical example suited for redox titrations. To prevent that hydrolysis of water occurs, an excess of Ce(III) was added to the solution as an electron-transferring reagent [17, 18]. This ion is oxidized at a lower potential than that for water.

$$Ce(III) \rightarrow Ce(IV) + e \qquad (3.9)$$

The cerium (IV) produced diffuses rapidly from the electrode surface and oxidizes an equivalent amount of iron (II).

$$Fe(II) + Ce(IV) \rightarrow Fe(III) + Ce(III) \qquad (3.10)$$

The overall reaction is finally given by:

$$Fe(II) \rightarrow Fe(III) + e \qquad (3.11)$$

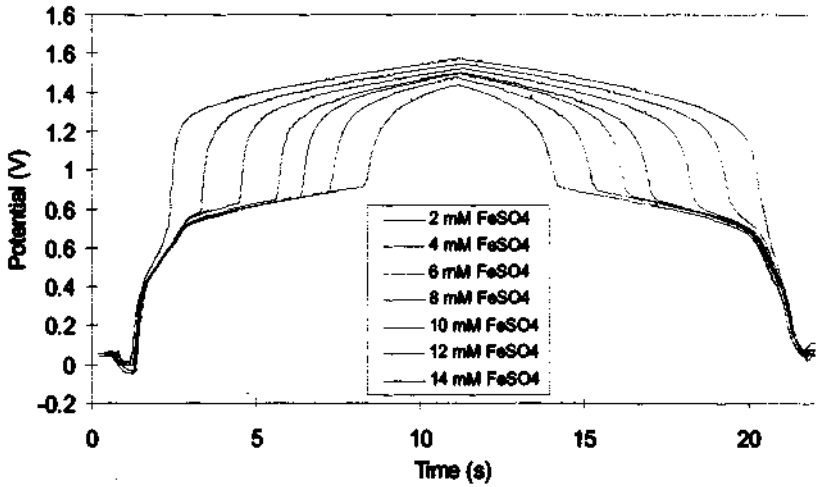


*Fig.3.4. Triangle-programmed coulometric titrations of Fe(II). The sample solutions with concentrations ranging from 2 to 14mM (curves from top to bottom) were titrated using a current-time slope of 8μA/s and a flow rate of 120μL/min (peristaltic pump).*

Figure 3.4 shows redox titrations for different sample concentrations, carried out in a 30μm high channel. A cycle *2T* of 20 seconds was chosen for the triangle current-time profile; this cycle could of course be shorter. The titration rate was found to be sufficiently high for sample concentrations ranging between 2 and 14mM and for a current scan of 8μA/s. The excellent symmetry of the curves in figure 3.4 indicates that the titration conditions are extremely stable in the microchannel. Accordingly, a high reproducibility was achieved for all measurements, the standard deviation being always below 1%, except for titration end-point larger than 17 seconds (up to 4%). In comparison with earlier redox titrations carried out at a constant current in static sample solutions (see chapter 2), the present measurements showed a slightly better reproducibility. This may be due to the establishment of a well-defined stagnant layer at the indicator electrode.

Figure 3.5 exhibits the linear relationship between the titration end-point and the sample concentration for different current-time slopes. The titration end-point is defined as the difference between the period of a cycle and the time span. Equation (3.8) was used to fit the data obtained for 8μA/s. The reduction factor $\alpha$ was found to

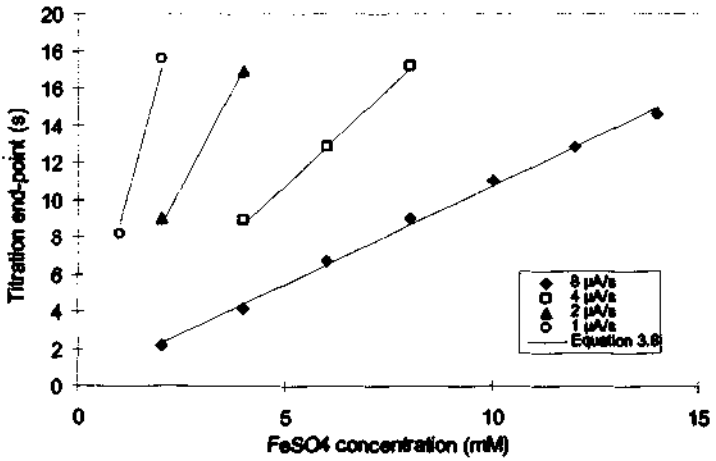


*Fig.3.5. Linear relation between the Fe(II) concentration and the titration end-point, 2T-Δt, for different current–time slopes. Equation (3.8) was used to fit the experimental data ($\alpha$=0.022 and $t_r$=0.09s).*

be 0.022 and the response time asymmetry $t_r$ of the sensor was 0.09s. All the other data were fitted on the basis of the same parameters, using the respective current-time slopes. The observed reduction factor $\alpha$ indicates that only 2% (about 400nL for a half-period of 10 seconds) of the sample solution is titrated above the sensor at a flow rate of 120µL/min. The average speed of the titrated sample, $v_{sam}$, is calculated from these results as 0.04mm/s.

### 3.4.2. Influences of the current-time slope and the flow rate

As expected, the current-time slope and the flow rate are decisive for the titration efficiency. A higher current-time slope is expected to increase the speed of the titration. Figure 3.6a shows the response curves obtained for the titration of a 8mM Fe(II) sample at different current-time slopes. The variation of the current intensities allows the coverage of a wide concentration range. According to equation (3.8), the time span $\Delta t$ is related to the reciprocal of the current-time parameter $k$. These predictions are confirmed by experimental results in figure 3.6b. The same coefficients $\alpha$ and $t_r$ were used as in figure 3.5.

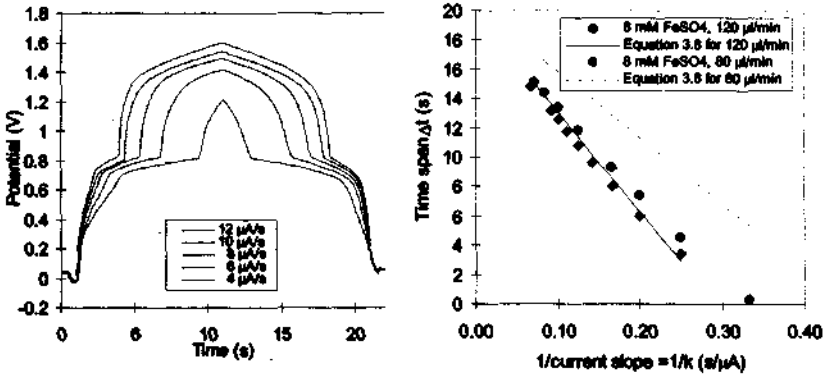


*Fig.3.6. a) Triangle-programmed coulometric titrations of a 8 mM Fe(II) sample, using current-time slopes of 12µA/s to 4µA/s (curves from top to bottom). A flow rate of 100µL/min was chosen (piston pump). b) Relationship between the time spans Δt and the reciprocal of the applied current-time slopes. Theoretical curves according to equation (3.8) using the same parameters α and $t_r$ as in figure 3.5.*

Figure 3.6b also reveals that equation (3.8) fits well the experimental data obtained for a flow of 120μL/min, but only qualitatively for 80μL/min. Two opposite effects can explain this discrepancy. At smaller flows, the maximum velocity of the stream is obviously smaller, and the diffusion effects become more important, which means that the effective volume of titrated sample is larger at 80μL/min than at 120μL/min (at 80μL/min the coefficient $\alpha$ becomes larger: 0.028). A more systematic study of the influence of the sample flow rate on the titration behaviour is presented in figures 3.7a and 3.7b. Evidently, a tenfold increase of the flow rate leads to a reduction of the time-span between the titration endpoints by a factor of about 3-4.

The pulsations of the piston-pump used can clearly be seen in figure 3.7a, especially for low flow rates. At a flow rate of 10μL/min, 200nL are pumped every 1.2 seconds.

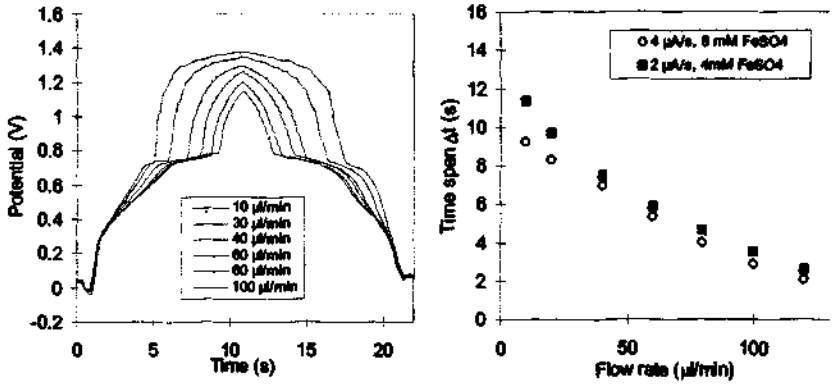


*Fig.3.7. a) Triangle-programmed coulometric titrations of a 4mM Fe(II) sample at a current scan of 2μA/s for different flow rates (10 to 100μL/min, from top to bottom). b) Relationship between the time spans Δt and the sample flow rates. Results from two different series of experiments are given.*

### 3.4.3. Acid-base titrations

Acid-base titrations were carried out using an indirect detection method. The pH determination was based on the measurement of the redox potential of quinhydrone

[19]. By saturation of the sample with quinhydrone, an equimolar mixture of quinone and hydroquinone was established. The basic equilibrium for the hydroquinone couple is:

$$C_6H_4O_2 + 2H^+ + 2e^- \rightarrow C_6H_4(OH)_2 \quad (3.12)$$

This is a reversible redox reaction in which hydrogen ions participate.

*Titration of strong acids*

Nitric acid solutions were titrated by this procedure in a 50μm high microchannel. Figure 3.8 illustrates typical titration curves obtained for different sample concentrations. For this titration type, a linear relationship between the titration end-point and the sample concentration was found for almost two orders of magnitude (0.2mM to 8mM) when using the appropriate current scan. In all measurements, a high reproducibility was achieved, the standard deviation being always below 1%, except for end-point times larger than 14 seconds (standard deviation up to 10%).

Equation (3.8) was used to fit the data obtained for 2μA/s. In this case, the reduction factor found was 0.042, and the response time asymmetry $t_r$ of the indicator

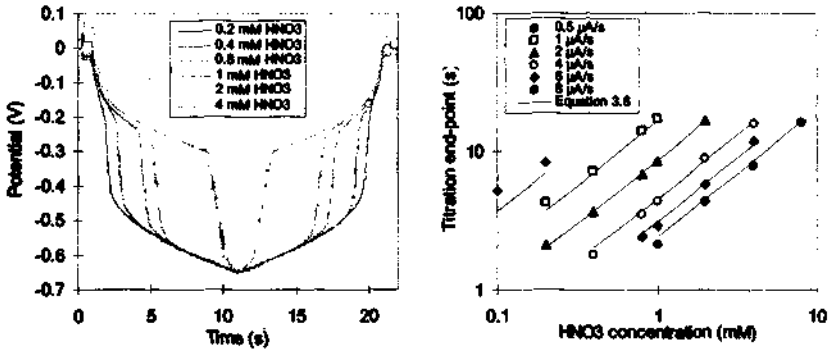


*Fig.3.8. a) Titrations of nitric acid sample solutions with concentrations ranging from 0.2 to 4mM (curves from bottom to top) using a current-time slope of 2μA/s and a flow rate of 120μL/min. b) Linear relation between the $HNO_3$ concentration and the titration end-point, $2T-\Delta t$, for different current–time slopes. Slopes of the fits were: 32.91, 16.07, 8.03, 4.01, 2.67 and 2mM$^{-1}$, for 0.5, 1, 2, 4, 6 and 8μA/s, respectively.*

electrode 0.19s. All the other data were fitted on the basis of the same parameters, using the respective current-time slopes. It should be pointed out that, except for the smallest current-time slope applied, the simple model developed here gives an excellent agreement with the data obtained for different current-time slopes.

The difference observed between the reduction factors $\alpha$ for the titrations of Fe(II) ($\alpha = 0.022$) and the titrations of nitric acid ($\alpha = 0.042$) may be explained by the height difference of the microchannel used for both experiments: 30μm for Fe(II) titrations and 50μm for $HNO_3$ titrations, respectively. In both cases, the response time asymmetry is very small, which is due to the proximity of the indicator electrode to the coulometric electrodes.

*Titration of weak acids*

Acetic acid solutions were titrated in the same nanotitrator as the one used for the precedent titrations. Figure 3.9a displays titration curves obtained for sample solutions with concentrations ranging from 0.2 to 4mM. The titrations were carried out at a current density of 1μA/s and a flow rate of 120μL/min. As expected for a weak acid due to the low dissociation constant (pKa=4.76) in comparison with

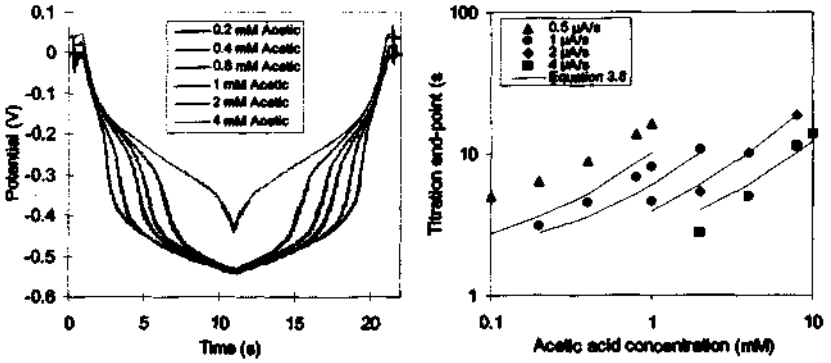


*Fig.3.9. a) Titrations of acetic acid sample solutions with concentrations ranging from 0.2 to 4mM (curves from bottom to top) using a current-time slope of 1μA/s and a flow rate of 120μL/min. b) Linear relation between the acetic acid concentration and the titration end-point, 2T-Δt, for different current-time slopes.*

a fully dissociated strong acid, the titration curves in figure 3.9a are less pronounced than for a strong acid (fig.3.8a).

Figure 3.9b shows the relationship between the titration end-points and the acetic acid sample concentrations. Equation (3.8) was used to fit the data obtained at a current density of 2μA/s. The reduction factor was found to be 0.01, and the response time asymmetry $t_r$ of the indicator electrode was 0.94s. Evidently, this simple theoretical model does only roughly correspond with the experimental data found for other current-time slopes. Nevertheless, the relation between the measured data is linear. It should be mentioned that nearly perfect curve fits were achieved, even for current-time slopes of 0.5 and 1μA/s and in the lowest concentration range (from 0.1 to 1mM acetic acid: $R^2$ values higher than 0.999).

Figure 3.9b also illustrates the difference of the titration speeds between acetic and nitric acids (fig.3.8b). This discrepancy may again be explained by the difference of the diffusion coefficients of the two acids, similarly than for the stopped-flow titrations. As a matter of fact, despite convection, diffusion still seems to play a predominant role in the determination of the titration end-points. The disparity between the titration of the two acids can clearly be distinguished for higher concentrated samples (fig.3.10). According to Nagy et al. [8], who also reported this effect, acetic acid in diluted sample is dissociated to such a degree that the titration can be regarded as virtually a titration of a strong acid. Indeed, the titration end-points found for 0.1mM nitric and acetic acid samples were almost identical with the same current (fig.3.10a), whereas the titration end-points found for 2mM were dissimilar. The concentration of hydrogen ions can be calculated from the protolysis equilibrium of a weak acid dissolved in water.

$$HA + H_2O \leftrightarrow H_3O^+ + A^- \qquad (3.13)$$

Assuming that the contribution by the autoprotolysis of water is negligible, one $H_3O^+$ is formed for each $A^-$ ion. Furthermore, the sum of molar concentrations of the weak acid and its conjugate base equals the total concentration of the acid $c_{HA}$. By substituting these relationships in the equation for the dissociation constant $K_a$, the amount of hydrogen ions is given by [20]:

$$\left[H_3O^+\right] = \frac{-K_a + \sqrt{K_a^2 + 4K_a c_{HA}}}{2} \qquad (3.14)$$

Thus, the percentages of dissociation for 10, 1, and 0.1mM acetic acid are 4, 12 and 34%, respectively. Regarding these results, one may conclude that, even if the most diluted acetic acid sample is not fully dissociated, the value of the respective titration rate may be compared to the one observed for a strong acid.

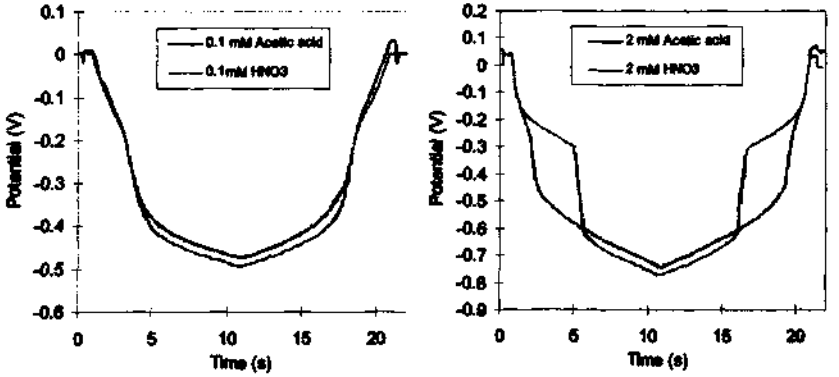


*Fig.3.10. Comparison between titration curves of acetic and nitric acid samples a) c=0.1mM, i=0.5μA/s, Q=120μL/s, b) c=2mM, i=4μA/s, Q=120μL/s.*

## 3.5. Conclusion

The present results show that the reported nanotitrator was successfully applied for triangle-programmed coulometric titrations. As compared with earlier studies by Pungor and co-workers on a macroscopic device, the titration time could significantly be reduced in the present case. The reproducibility of the measurements was very good, and redox titrations in particular were even more reproducible than those carried out by the stopped-flow titration method. This can be due to the continuously renewed boundary layer near the electrodes that creates well specified titration conditions. It should also be noted that more than 1000 measurements were performed using the same device in the same configuration, without noticeable deterioration of the device and of the titration curves.

In contrast to macroscopic systems, an excellent symmetry of the titration curves was achieved, due to the absence of a mixing unit, which permits to place the coulometric and the indicator electrodes very closely. The small dimensions of the microfabricated device and the close arrangement of the electrodes not only eliminates the tailing effect, but also allows an excellent determination of the absolute starting point of the titration. Therefore, by knowing the starting point, a reduction of the measurement time by a factor of at least two can be envisaged, because only a half-cycle of the titration is then necessary for the determination of the sample concentration. This modification would eliminate the need for a bi-directional current ramp.

Because the flowing solution sample is titrated only in a small zone near the electrodes, a calibration of the nanotitrator is required for quantitative analyses. The high precision found in the present studies documents that the titration volumes were well reproducible in all experiments. Nevertheless, titrations of weak acids revealed the necessity of an extended model which would take the dissociation effects into account.

Finally, as in the case of the stopped-flow titration mode, the comparison between the titrations of strong and weak acids shows that diffusion still plays an important role in determining the titration end-point. It seems that the convection contribution to the propagation of the titrated volume is not sufficient to fully eliminate diffusion influences. In fact, the flow velocity of the titrated volume is

0.04mm/s at 120µL/min, whereas the diffusion contribution to the total transport rate is only about twenty times smaller, that is 0.002mm/s, calculated with a diffusion coefficient of $10^{-3}$mm$^2$/s. These values are of course only mean values; since the flow velocity near the microchannel edges is even much slower, the diffusion effect may even be more significant. A possibility for reducing the diffusion influences would be achieved by an arrangement of the electrodes in the middle of the channel, in order to benefit from the maximum convection speed that is 2mm/s in the present case, i.e. 1000 times faster than diffusion.

**References**


[1] Guenat O.T., Morf W.E., van der Schoot B., de Rooij N.F., *Continuous flow injection coulometric nanotitrations*, Proc. 2nd Int. Conf. On Microreaction Technology, New Orleans, 1998, p.230-4.

[2] Guenat O.T., Morf W.E., van der Schoot B., de Rooij N.F., *Triangle-programmed coulometric nanotitrations completed by continuous flow with potentiometric detection*, Anal.Chem., 72, 2000, p.1585-90.

[3] Pungor E., Toth K., Nagy G., *Some aspects of the application of ion selective electrodes in flowing systems*, Ion and enzime electrodes in biology and medicine, Int. Workshop at Schloss Reisensburg near Ulm, Urban & Schwarzenberg, München, 1976, p.56-76.

[4] Pungor E., Toth K., Nagy G., Feher Zs., *Methods for automatic analysis with ion-selective electrodes*, 2nd Symp. on Ion-selective electrodes, Matrafured, Hungary, 1976, p.67-91.

[5] Nagy G., Fehér Zs., Tóth K., Pungor E., *A novel titration technique for the analysis of streamed samples – the triangle-programmed titration technique. Part I. General Considerations*, Anal. Chim. Acta 91, (1977) 87-96.

[6] Pardue H.L., Fields B., *Kinetic treatment of unsegmented flow systems, Part 1. Subjective and semiquantitative evaluations of flow-injection systems with gradient chamber*, Anal. Chim. Acta, 124, 1981, p.39-63.

[7] Nagy G., Fehér Zs., Tóth K., Pungor E., *A novel titration technique for the analysis of streamed samples – the triangle-programmed titration technique Part II. Argentimetric titrations*, Anal. Chim. Acta 91, (1977) 97-106.

[8] Nagy G., Fehér Zs., Tóth K., Pungor E., *Evaluation of acid-base titration curves obtained by the triangle–programmed titration technique in flowing solutions*, Talanta, 26, 1979, p.1143-53.

[9] Nagy G., Fehér Zs., Tóth K., Pungor E., *Analysis based on complete coulometric titration in flowing solutions*, Hung. Sci. Instrum., 46, 1979, p.5-15.

[10] Fehér Zs., Kolbe I., Pungor E., *Determination of the drug content of pharmaceuticals containing phenothiazine compounds by triangle-programmed flow titration*, Fresenius Z. Anal. Chem., 332, 1988, p.345-50.

[11] Nagy G., Fehér Zs., Tóth K., Pungor E., *A novel titration technique for the analysis of streamed samples – the triangle-programmed titration technique Part III. Titrations with electrically generated bromine*, Anal. Chim. Acta 100, (1978) 181-91.

[12] Fehér Zs., Kolbe I., Pungor E., *Iodimetric determination of penicillins by a triangle programmed flow-through titration technique*, Analyst, 113, 1988, p.881-4.

[13] Fehér Zs., Kolbe I., Pungor E., *Application of flow-trough techniques to drug dissolution studies*, Analyst, 116, 1991, p.483-7.

[14] Morf W.E., *The principles of ions-selective electrodes and of membrane transport*; Elsevier: Amsterdam, 1981, p. 379-398.
[15] Tóth K., Fucskó J., Lindner E., Fehér Zs., Pungor E., *Potentiometric detection in flow analysis*, Anal. Chim. Acta, 179, 1986, p.359-70.
[16] Skoog D.A., West D.M., Holler F.J., *An Introduction to Analytical Chemistry*; Saunders College Publishing: Philadelphia, 1994, p.272.
[17] Lingane, J. J.; *Electroanalytical Chemistry*; Interscience: New York, 1958, p.139, 559-560.
[18] [16] p.374.
[19] Clark Westcott, C. *pH Measurements*; Academic Press: New York, 1978, p. 136-7.
[20] [16] p.44.

# 4. Electroosmotic Nanopump

The objective of the present work is to develop a pump able to generate a pulsation free flow in the range of nL/min to a couple of µL/min. The integration of this pump and of other components such as a micromixer (chapter 5) and a reactor-sensor unit (chapter 6) on the same chip will lead to the reduction of the sample contamination, the sample volume and thus the analysis time.

In the first part of the chapter, a simple nanopump dedicated to coulometric nanotitrations is presented. It is followed by the study of a mathematical model, which describes the behaviour of electroosmosis in a rectangular capillary. On the basis of this model, an improved nanopump designed for volumetric nanotitrations is investigated. Parts of this chapter have been published in [1-3].

---

## 4.1. Introduction

The fluid propulsion device is one of the most important components in micro total analysis systems. Constant low flow rates and especially pulsation free flows are often the primary requirements for flow injection analysis (FIA) systems and for microfluidic systems, which need a constant and small supply of solutions.

Among available types of fluid delivery systems, peristaltic pumps and piston-pumps are the most commonly used means of propelling carrier and reagents streams in fluidic systems. Different volumetric pumping rates may be obtained by varying individual tube diameters of peristaltic pumps, and this even for several channels in parallel. Although these pumps present several other advantages, such as bidirectionality and constant flow rates, some major drawbacks hinder their use for the above-mentioned applications. Firstly, they generate pulsating flows, particularly visible at low flow rates, and in addition, their tubes must be frequently replaced to maintain constant flow rates. Moreover, at the sub µL/min domain, peristaltic pumps will simply not operate reliably in this scale. On the other hand, piston pumps can precisely deliver solutions at stable flow rates. Even pumps for low flow rates are

available, but these are very expensive and generally unidirectional. Finally, flow pulsations can only be avoided with additional complexity.

Pressurized fluid systems could be a suitable and inexpensive approach, but the accurate adjustment of uniform flow rates might be difficult.

Within the last ten years, most pumping principles, with and without moving parts have been successfully scaled down. Numerous papers focusing on the development of micropumps have been published. Some review articles comment on this progress and particularly on mechanical micropumps [4-6]. Most mechanical micropumps make use of a membrane that can be actuated in different ways: piezoelectrically [7-9], pneumatically [10,11], electrostatically [12] and electromagnetically [13]. In all cases, high voltages are needed to actuate these membranes, which produce pulse flow in channels. One of the advantages of all these different types of membrane pumps is their ability to pump almost any kind of liquids within a typical flow range of 1-100 µL/min.

Non-mechanical micropumps, on the other hand, are of special interests, because they do not have any moving parts and are therefore able to create a pulsation free flow. In this case, the fluid driving force can be generated by thermal [14], chemical (osmotic pumps) [15], acoustical [16], magnetical [17], or electrical actuation. The latter actuation type can be subdivided in several interesting pumping principles. Firstly, electrohydrodynamic pumps [18-20] can pump dielectric liquids, secondly, electrochemical pumps [21] produce air bubbles by electrolysis to expulse the solution from a close reaction chamber, and finally electrokinetic pumps make use of electrophoretic and electroosmotic effects [22,23]. For more than ten years, a significant research base has been built up in the area of capillary electrophoresis system on chip using electroosmotic flow (EOF) as pumping mechanism. The development of this domain can be attributed to key research carried out by several groups, some of them belonging to the pioneers [24-27]. In their systems, the voltage is applied across the entire solution conduit. In a capillary, EOF has fundamentally a flat profile, which limits the dispersion despite long reaction times and continuous flow. It is also able to create high pressures in small capillaries, unlike newtonian systems. However, despite the attractive features described above, EOF has unfortunately a very important practical limitation. Indeed, the composition of the pumping fluid is directly responsible for EOF characteristics. This means that when

the carrier solution has a very high or very low pH, is a highly conductive saline, or a non-conducting organic medium, the current levels are either excessive or inadequate to support significant EOF.

In order to utilize EOF pumping in microreactor systems, it is necessary to separate the pumping device from the chemical reaction system while maintaining hydraulic connectivity between them. It would also be desirable to eliminate all electric fields in the reaction zone to simplify system considerations. This idea was developed by Dasgupta and Liu [25,28-32] who demonstrated for conventional capillaries, that by using these techniques, it was possible to pump almost any kind of liquids. Their system was made of one or several 40cm long capillaries (75 µm i.d.), linked to a 3m long reagent holding coil (250 µm i.d.) via a small Nafion tube used as a conductive membrane. They reported an output flow rate of 700 nL/min when 15kV were applied across the first capillary [29].

In the present research work, it was decided to use electroosmotic flow as the pumping mechanism, not only for the above-mentioned reasons, but also for the simplicity of the technology required to build such a pump. This simplicity fits well with the overall fabrication goals set within this thesis (see § 2.5) and will lead to a mechanically robust device.

The idea was to benefit from the advantages of the microfabrication techniques and to scale down the size of the system described by Dasgupta and Liu on a single chip. This miniaturization will make possible a higher degree of complexity of the entire analytical system, and will ultimately lead to a lab-on-a-chip. Furthermore, the proximity between the pump and the other microfluidic components will end in lower sample consumption, and will thus lead to higher analysis rates.

## 4.2. Electrokinetic Effects

Navier–Stokes equations are the basic equations, which describe the fluid motion with appropriate electromigratory flux terms. They represent the effect which the applied electric field has on the carrier and/or the charged species. The effect of the applied field can be divided into two fundamental components: electrophoretic and electroosmotic effects, which are closely related. Note however that, since no ion separations will be performed within this work, electrophoretic effect will only play a minor role. Excellent books [33-35] and several papers [22,23,36,37] comment on these phenomena.

### 4.2.1. Electrophoresis

The basis for electrophoresis is the differential migration of the charged species ions relative to the carrier molecules under the influence of an externally applied electric field E (fig.4.1).

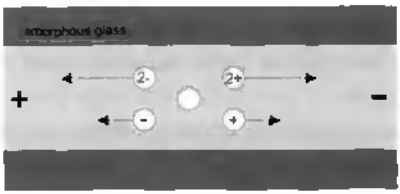


*Fig.4.1. Schematic illustrating electrophoresis in a capillary. The circles indicate molecules (ions) of the indicated charges, as well as their migration speed vector.*

The differential migration is primarily an effect of the difference in the net charge between the solvent and the sample ions. The migration velocity, $v_{ep}$, of an ion relative to the solvent can be expressed in terms of the applied field strength $E$ as

$$v_{ep} = \mu_{ep} E \qquad (4.1)$$

where $\mu_{ep}$ is the electrophoretic mobility of the ion in the carrier solvent. This mobility is determined by the electric force that the molecule experiences, balanced by its frictional drag through the medium.

4.2.2. Electroosmosis

In contrast to electrophoresis, electroosmosis is a more macroscopic phenomenon, which involves the pumping of fluid through a capillary tube by an externally applied electric field (fig.4.2). A prerequisite for electroosmosis is the presence of immobilized surface charges at the capillary wall (typically $SiO^-$) in contact with an electrolyte solution. The surface charge density might either be due to ionizable groups (e.g. deprotonation of silanols groups in the case of glass or fused silica capillaries) or caused by strong adsorption of charged species, which are present in the buffer solution. This surface charge leads to the formation of an electric double layer by attracting oppositely charged ions from the buffer (e.g. alkali ions), and therefore leads to concentration and charge density gradients in the immediate vicinity of the wall.

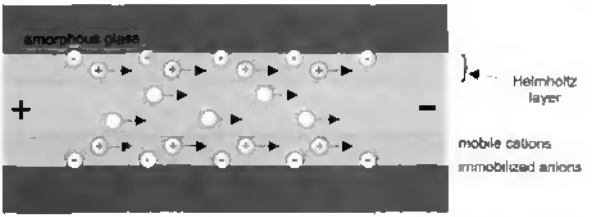


*Fig.4.2. Schematic illustrating electroosmosis in a capillary. The circles indicate molecules and ions of the indicated charges, as well as their migration speed vector.*

This diffuse double layer is sometimes referred to as the Gouy-Chapman or Helmholz layer. The double layer acts as a parallel-plate electric capacitor whose potential difference between the plates is called zeta potential ($\zeta$):

$$\zeta = \sigma d / \varepsilon_r \varepsilon_0 \qquad (4.2)$$

where $\sigma$ is the electric charge per unit area, $d$ is the distance between the plates, $\varepsilon_r$ is the relative permittivity of the medium (dielectric constant), and $\varepsilon_0$ is the permittivity of free space.

The application of the electric field exerts a force on the fluid, which initially affects the charged zone of the double layer. As a result, the fluid in the near vicinity of the wall starts to move. Due to the viscous forces, the fluid in the center of the channel is also accelerated until the net velocity gradient in the radial direction is zero

and the whole fluid in the channel moves at a constant velocity. Numerical simulations have shown that this process takes place within a few hundred microseconds [38].

The velocity of the electroosmotic flow can be found out by combining the Poisson-Boltzmann equation with the equation of motion [36]. In general, the double layer thickness is extremely small in comparison with the channel width. For example, the double layer thickness calculated from the Gouy-Chapman theory equals about 10nm for a buffer concentration of 1mM [39], which is in fact negligible for a typical channel height of 50μm.

If we assume that the buffer viscosity $\eta$ and the dielectric constant $\varepsilon_r$ are the same in the double layer and in free solution, the Smoluchowski equation becomes valid.

$$v_{eo} = \mu_{eo} E \qquad (4.3)$$

with

$$\mu_{eo} = \varepsilon_r \varepsilon_0 \zeta / \eta \qquad (4.4)$$

where $\zeta$ is the zeta potential. Both phenomena, the electrophoretic microscopic migration of ions and the macroscopic electroosmotic flow velocity, $v_{eo}$, are linearly dependent on the axial electric field strength applied. In the case of pressure driven flow, the external force is applied across the whole cross section of the tube, leading to a parabolic flow profile. In contrast, in electroosmosis the external force is only exerted to a thin layer of fluid close to the wall, thus resulting in a plug-flow profile. The electroosmotic effect and the electrophoretic effect combine for ionic species to give the total velocity (combination of equations (4.1) and (4.3)):

$$v_{tot} = (\mu_{ep} + \mu_{eo}) E \qquad (4.5)$$

## 4.3. Electroosmotic Nanopump for Coulometric Nanotitrations

A single-channel electroosmotic pump coupled with a sensor and a coulometric actuator cell is designed and studied. The primary goals of this work are to solve the technological problems and to check the functionality of the new pump and of the sensor and the actuator cell, in order to perform coulometric titrations.

### 4.3.1. Principle and design

*Nanopump design*

Figure 4.3 shows a schematic view of the entire system, which consists of a nanopump and a sensor and actuator cell. A high voltage is applied between electrodes E1 and E2, which creates an EOF in the second part of the channel.

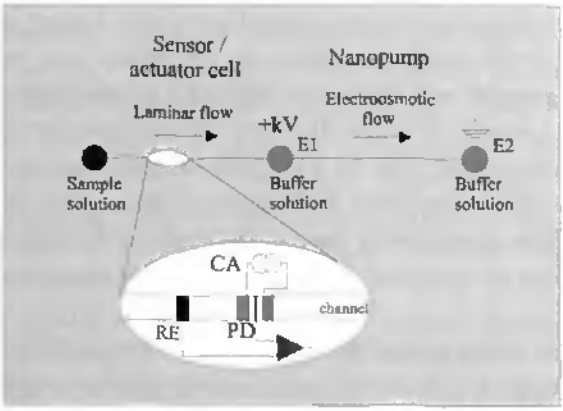


*Fig.4.3. Schematic view of the μTAS for coulometric nanotitrations: CA stands for coulometric actuation, PD for potentiometric detection, RE for reference electrode.*

Changing the polarity of the electrodes E1 and E2 can easily reverse the pumping direction. When a positive voltage (relative to the potential of E1) is applied to E2, the buffer solution is driven through the sensor and actuator cell, thus pushing out the sample solution. In the other operation mode, as illustrated in figure 4.3, the

EOF causes a pressure reduction near E1; and the sample solution is drawn in and driven through the sensor and actuator cell. In this case the EOF is expected to change only when the sample solution reaches the nanopump and replaces the buffer solution. Accordingly, a sufficiently long interval is guaranteed for performing at least one titration cycle. The typical trapezoidal flow profile of EOF changes after E2 into a parabolic flow profile.

The dimensions of the channel etched in Pyrex are defined as follows: 92 mm long, 28 μm deep and 66 μm wide.

*Sensor and actuator cell*

In the first part of the microchannel, the flow profile is laminar for both of the above-mentioned operation modes. The sensor and actuator cell consists of an array of platinum planar microelectrodes of different sizes embedded in the Pyrex substrate, which forms the ceiling of the microchannel.

The coulometric titration method applied in this study is based on the triangular current-time profile described in chapter 3; this method uses two coulometric electrodes (a generator and a counter electrode) and two potentiometric electrodes (an indicator and a reference electrode). The width of the generator electrodes used is 250 μm. These are separated from the 4 μm wide indicator electrode by 4 μm. The reference electrode is situated at the beginning of the channel, so as to prevent interference from the coulometric reaction. The length and height of the first part of the microchannel are 50 mm and 28 μm, respectively. The channel width is either 66 μm or 126 μm.

When the leading edge of the triangular current-time profile is applied to the coulometric electrodes, the flowing sample solution becomes gradually titrated by coulometrically generated ions. The reverse titration curve is measured on the trailing edge of the current-time profile. The indicator electrode monitors the evolution of the reaction. Equivalence points of the titration appear in both directions. The first equivalence point is situated on the leading edge of the titration curve, while the second is situated on its trailing edge. The peak width of the titration curve is determined by the time elapsed between the minimum and the maximum of the first derivative (see theory §3.2).

### 4.3.2. Fabrication

The same technology processes as those described to etch the cover lid of the coulometric nanotitrator (see §2.5.4) were used to etch the 28 µm deep channels in the Pyrex wafer. Ta/Pt (thickness: 10nm/140nm) electrodes were deposited by standard evaporation processes on a second wafer. Just as for the coulometric nanotitrator, the metallic layers had to be embedded to ensure a good bonding of the two wafers. However, an important parameter differed from the former device. The electrical insulation characteristics of $SiO_2$ deposited on silicon were not sufficient to hinder the electrical breakdown caused by the application of a high voltage across the microchannels. Therefore, a Pyrex wafer, used as a substrate for the electrodes, was preferred.

*Bonding process*

Although some new findings [40] demonstrate that anodic bonding between two Pyrex wafers is possible, a conventional fusion bonding process was chosen to bond the wafers together. Prior to the thermal cycle, wafers were cleaned thoroughly, as follows: washing of the wafers with liquid soap, in order to remove the dust and the particles mechanically, cleansing of the organic compounds with acetone and isopropanol, rinsing in deionized water before dipping in $HNO_3$ 100% for 10 minutes to remove any residual organics, and finally rinsing again in deionized water.

The thermal cycle used was based on a cycle developed at the Univ. of Alberta [41] and was modified by K. Fluri at the IMT. The temperature program started with a ramp of 10°C/min to 470°C, it remained stationary for 30 minutes, then continued with a second ramp of 2°C/min to 600°C, remained stationary again for 30 minutes and finally increased to 650°C in 25 minutes. This temperature was maintained during 6 hours, and was followed by natural cooling of the furnace to room temperature (about 8 hours).

The bonded devices were then glued onto a printed circuit board, which was electrically bonded, and the reservoirs were formed with 1cm long tubes, which were glued onto the device. The Nafion (Nafion 117, 0.18 mm thick, purchased from Aldrich) membrane was glued onto the wafer over which a reservoir was placed. Figure 4.4 presents a photograph of the ready-to-use nanopump.

*Fig.4.4. Photograph of the electroosmotic nanopump with glued reservoirs.*

4.3.3. Experimental part

*Nanopump: flow rate characterization*

A 10mM borax solution (pH 9) was used as a buffer solution. Polymeric beads (2.5µm diameter) were added to this solution in order to show the movement of the fluid in the microchannel as a function of the applied voltage. The velocity of the flow was measured in the "non-electroosmotic" part of the microchannel by recording video sequences and by measuring the travel time of the beads over a distance of 250 µm. It was mandatory to calculate the average of the bead velocities, since the movements of the beads followed the parabolic flow profile. Before each measurement, the solution levels of each reservoir were adjusted to ensure that the fluid was stationary.

Figure 4.5a shows the current-voltage characteristic of an electroosmotic flow between the electrodes E1 and E2, and across the whole system. The linearity of the response of this latter measurement reveals that there is no leakage, neither in the system nor around the glued Nafion membrane. Figure 4.5b presents the flow rate as

a function of the applied potential. The results show the capacity of the nanopump to push out, or draw in, a sample solution with flow rates in the range of nanoliters per minute.

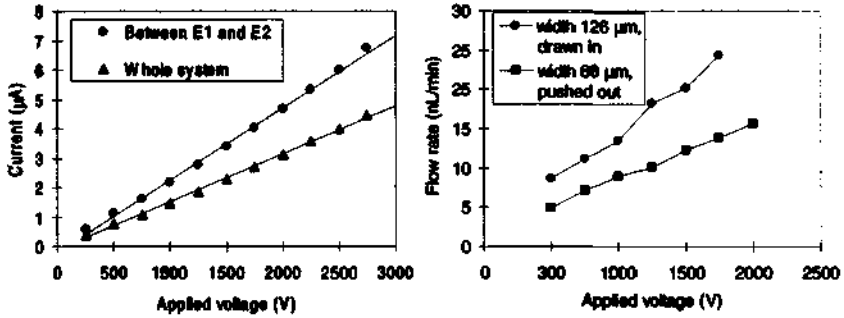


*Fig.4.5. a)Current-voltage characteristics across the whole system and from E1 to E2, b)flow rates as a function of the applied voltage for the two pumping directions. The width of the channel of the sensor and actuator cell is indicated in the legend.*

*Coulometric nanotitrations: first results*

The titration measurements were carried out using a 6mM iron(II) sulphate solution with an excess of 20 mM Ce(III). A background electrolyte of 1M sulphuric acid was used. First results of continuous flow injection titrations were obtained in

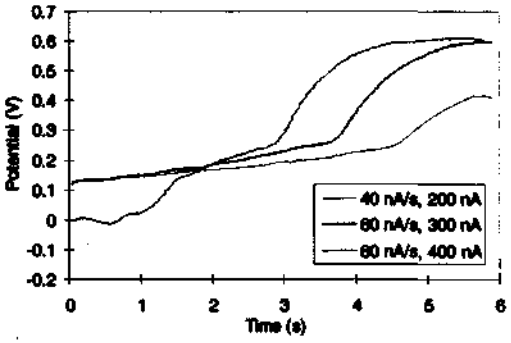


*Fig.4.6. Titration curves of a 6 mM $FeSO_4$ solution, obtained with different current densities.*

the sensor and actuator cell with a pressurized sample solution for three different current densities (fig.4.6). The first half of each titration cycle - having a total duration of 6 seconds - was recorded. During these preliminary measurements, a few problems arose. Air bubbles, probably generated on the coulometric electrodes, were stacked on the surface of the electrodes and interfered with the detection, until they stopped the flow. Coulometric titrations carried out with the electroosmotic nanopump were therefore not reliable enough for practical applications.

### 4.3.4. Discussion and conclusion about nanopump I

The technological unknowns could be solved and an electroosmotic nanopump could be fabricated. Essential functions of the pump have been tested. The current-voltage characteristics showed that the glued Nafion membrane behaved as expected. The linearity of the measured functions also revealed the tightness of the fusion bonding, despite the presence of the metallic layers of the electrodes. The flow rate was measured in the sensor cell of the device and found to be in the order of 80 to 400pL/s. The detection part of the device could also be tested. Despite the undesired thermal treatment of the Pt electrodes during the fusion bonding, no damage occurred and they responded as desired.

However, in order to get a valuable device able to be easily adapted to other microfluidic components, some improvements are still needed. Valves or even microvalves should be implemented to make it possible to separate neatly the buffer solution from the pumped solution. Pneumatically actuated microvalves made of a thin rubber sheet could be a suitable solution [42]. A larger internal reservoir for the sample solution should also be considered, so as to reduce contamination of sample and buffer solutions, and to increase the achievable number of titrations per measuring series.

Next, the measurement of the flow rate should be done by using a different method. In fact, since the velocity of the polymeric beads was observed in the parabolic area of the flow, reliable statistics of the bead velocity should be made [43]. Furthermore, this solution has other drawbacks, notably the presence of the beads themselves, which can ultimately influence the flow rate. A current-monitoring method [44] is sometimes used to determine the electroosmotic flow in CE; yet, since the capillary without electroosmotic flow behaves as a hydraulic resistance, a reliable

calibration would be needed. An adequate solution could be a coulometric flow sensor made out of the existing electrodes.

Finally, a fixture containing the reservoirs and the HV electrodes would be useful in order to facilitate the manipulation and to increase the safety.

Although measurements were not pursued with this first nanopump, this part was very informative and allowed a tailored design of the 2$^{nd}$ generation nanopump.

## 4.4. Models for the Electroosmotic Nanopump

### 4.4.1. Capillary with partial electroosmosis

If an electric field is applied to a defined segment of a capillary (fig.4.7), electroosmosis takes place only in this particular segment. The rest of the capillary serves as hydraulic resistance. The typical plug flow profile of the EOF changes at the pseudo-interface between the two sections into a parabolic flow profile.

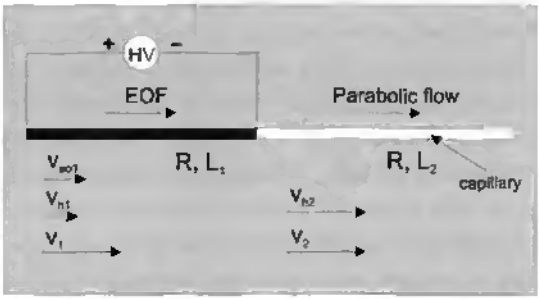


*Fig.4.7. Schematic of a capillary with partial electroosmosis. Labels of the different velocities and their corresponding vectors are indicated.*

The averaged velocity of the flow in the different parts of the microchannel can be expressed in the following way:

$$\bar{v}_1 = \bar{v}_{h1} + \bar{v}_{eo1} = \bar{v}_2 = \bar{v}_{h2} \qquad (4.6)$$

where $v_1$ is the averaged total velocity in segment 1, composed of the hydraulic velocity, $v_{h1}$, and of the electroosmotic velocity, $v_{eo}$, and where $v_2$ is the averaged total velocity in segment 2. As seen before, electroosmotic velocity is given by Smoluchowski's equation (equation (4.3)) and hydraulic velocity is derived from Poiseuille's equation for a circular capillary (equation (4.7)):

$$\bar{v}_{h1} = \frac{R^2}{8\eta L_1}\Delta p_1 \qquad (4.7a) \qquad\qquad \bar{v}_{h2} = \frac{R^2}{8\eta L_2}\Delta p_2 \qquad (4.7b)$$

where $\Delta p_1$ and $\Delta p_2$ are the pressure differences in the two segments, $R$ is the radius, $L_1$ and $L_2$ are the lengths of the capillary segments, and $\eta$ is the dynamic viscosity. The pressure difference is identical in each capillary part, but oppositely directed so as to obey the energy conservation law:

$$\Delta p_1 = -\Delta p_2 \qquad (4.8)$$

The hydraulic velocity for the first segment can be rewritten by substituting $\Delta p_1$ in equation (4.7a), and by then combining the result with equations (4.7b) and (4.6). This procedure yields:

$$\bar{v}_{h1} = -\bar{v}_{eo1}\frac{L_2}{L_1+L_2} \qquad (4.9a) \qquad\qquad \bar{v}_{h2} = \bar{v}_{eo1}\frac{L_1}{L_1+L_2} \qquad (4.9b)$$

Finally, the total velocity as a function of the applied voltage $\Delta\phi_1 = -EL_1$ is:

$$\bar{v} = \bar{v}_{hy2} = -\frac{\mu_{eo}}{L_1+L_2}\Delta\phi_1 \qquad (4.10)$$

This result shows that the velocity of a fluid in a capillary with partial electroosmosis is equivalent to the velocity in a capillary where the full length $L_1+L_2$ is exposed to the same voltage $\Delta\phi_1$. In addition, linear velocity (given in cm/s) is independent of the capillary radius, just as in Smoluchowski's equation. On the other hand, the pressure generated in the capillary (equation (4.11)) strongly depends on the radius.

$$\Delta p_2 = \frac{8\eta L_2}{R^2}\bar{v} = -\frac{8\eta\mu_{eo}L_2}{R^2(L_1+L_2)}\Delta\phi_1 \qquad (4.11)$$

From these results, one can conclude that a high pressure can be created if the capillary radius is very small. However, this configuration results in a low flow rate. In contrast, a larger radius makes possible the formation of a high flow rate, but on the other hand, is expected to limit the pressure. In order to benefit from both, a high pressure and a high flow rate, several small capillaries placed in parallel should be chosen to form the electroosmotic segment. Wider capillaries will be used for the second segment composed of the other microfluidic components.

### 4.4.2. Flow in rectangular channels

The cross-sections of microfabricated microchannels usually have a half-circular shape or, for wider channels, a rounded rectangular shape, which results from the isotropic HF-etch. Therefore, for convenience of a theoretical description, one can assume a rectangular cross-section if the width to height ratio is larger than 3 to 4. Below this limit [45], the approximation of the hydraulic radius $r_h$ will be made (equation (4.12)). Then, if laminar flow is assumed in the whole system, Poiseuille's equation for circular pipes will be used for the calculation of the hydraulic resistance $R_h$ of the channel (equation (4.13)).

$$r_h = 2A/P \qquad (4.12)$$

$$Q = R_h^{-1}\Delta p = \frac{\pi r_h^{\,4}}{8\eta L}\Delta p \qquad (4.13)$$

where $A$, $P$, $L$ are the cross-section, the perimeter and the length of the microchannel, respectively; $\Delta p$ is the pressure difference, $Q$ the flow rate, and $\eta$ the dynamic viscosity. The flow in rectangular pipes, as analyzed by Spurk [46], is characterized by the velocity, $v$, which is derived from Poisson's equation:

$$v = \frac{\Delta p}{\eta L}\left\{\frac{H^2}{8} - \frac{z^2}{2} - \frac{4H^2}{\pi^3}\sum_{n=0}^{\infty}\frac{(-1)^n}{(2n+1)^3}\frac{\cosh(my)\cos(mz)}{\cosh(mW/2)}\right\} \qquad (4.14)$$

$$\text{with} \qquad m = \pi(2n+1)/H \qquad (4.15)$$

where $H$, $W$ and $L$ are the height, the width and the length of the rectangular pipe, respectively. A double integration of the local velocity over the half width and the half height of the channel yields the mean velocity.

$$\bar{v} = \frac{4}{HW}\int_0^{W/2} dy \int_0^{H/2} v\,dz \qquad (4.16)$$

$$\bar{v} = \frac{\Delta p}{\eta L}\left\{\frac{H^2}{12} - \frac{16H^3}{\pi^5 W}\sum_{n=0}^{\infty}\frac{1}{(2n+1)^5}\tanh(mW/2)\right\} \qquad (4.17)$$

The volume flow in the rectangular pipe can then easily be determined, as well as the related hydraulic resistance.

$$Q = R_h^{-1}\Delta p = \frac{HW}{\eta L}\left\{\frac{H^2}{12} - \frac{16H^3}{\pi^5 W}\sum_{n=0}^{\infty}\frac{1}{(2n+1)^5}\tanh(mW/2)\right\}\Delta p \qquad (4.18)$$

4.4.3. Modelling of the flow rate of the complex nanopump

According to the conclusions of §4.4.1, an "electroosmotic" section made of several capillaries in parallel will form the nanopump. The second section is composed of the microfluidic components linked to the nanopump (reservoirs, micromixer, reaction chamber and sensor unit) (fig.4.8).
At steady state, i.e. without any external hydrostatic pressure, the flow conditions in the whole system can be evaluated with the help of Bernoulli's equation for uncompressed flow:

$$\Delta p_{eo} - \Delta p_h = \frac{\rho}{2}\bar{v}_{ex}^{\,2} = \frac{\rho}{2A_{ex}^{\,2}}Q^2 \qquad (4.19)$$

The left side of the equation (4.19) describes the internal pressures involved in the microsystem. $\Delta p_{eo}$ is the electroosmotic pressure produced by the nanopump and $\Delta p_h$ the pressure drop across the whole microsystem. The kinetic energy per unit volume represents the energy leaving the microsystem and is accounted for on the right-hand side of the equation. $\rho$ is the density of the pumped fluid, $v_{ex}$, and $A_{ex}$ are the velocity and the cross-section at the exit of the whole system. The electroosmotic pressure produced in a single channel can be calculated by using the equations of Poiseuille and Smoluchowski, respectively:

$$\Delta p_{eo} = R_{hp} A_p \bar{v}_{eo} = R_{hp} A_p \mu_{eo} E \qquad (4.20)$$

where $E$ is the electric field, and $R_{hp}$ and $A_{hp}$, are the hydraulic resistance and the cross-section of the pump microchannel, respectively. Using the voltage drop $U_p$ across the channel of length $L_p$ instead of the field $E$, we can write equation (4.20) in the form:

$$\Delta p_{eo} = R_{hp} \frac{A_p}{L_p} \mu_{eo} U_p = \frac{R_{hp}}{R_{ep}} \rho_e \mu_{eo} U_p \qquad (4.20a)$$

where $R_{ep}$ is the electric resistance of the pump channel, and $\rho_e$ is the electric resistivity of the buffer solution. If several channels are connected in parallel, their respective electroosmotic pressures will be averaged. In contrast, if some of the segments of the capillary are serially connected, pressures are additive. Surprisingly, a detailed theoretical study of complex pump systems shows that the total electroosmotic pressure can be described in analogy to equation (4.20a):

$$\Delta p_{eo} = \frac{R_{hp(m)}}{R_{ep(n)}} \rho_e \mu_{eo} U_p \qquad (4.21)$$

where $R_{hp(m)}$ is the hydraulic resistance of the whole pump consisting of m channels and $R_{ep(n)}$ is the total electric resistance of the electroosmotically active $n$ channels of the pump. The hydraulic pressure drop across the whole microsystem is given by the following equation:

$$\Delta p_h = \left(R_{hp(m)} + R_{ha}\right) Q \qquad (4.22)$$

where $R_{ha}$ is the hydraulic resistance of additional, non-pumping channels, which is basically given by equation (4.18). An analogy can be made between the hydraulic flow characteristics according to Poiseuille's equation, and the electric current relationship by Ohm's law. Therefore, the hydraulic equivalent resistances $R_{hp}$ and $R_{ha}$ can be calculated in analogy to electrical equivalent resistances. Finally, after introducing equations (4.21) and (4.22) in (4.19), the following relationship can be found for the flow rate:

$$Q = \frac{A_{ex}^{\,2}}{\rho} \left\{ \sqrt{\left(R_{hp} + R_{ha}\right)^2 + \frac{2\rho}{A_{ex}^{\,2}} \frac{R_{hp}}{R_{ep}} \rho_e \mu_{eo} U_p} - \left(R_{hp} + R_{ha}\right) \right\} \qquad (4.23)$$

Except for extremely high voltages $U_p$, equation (4.23) may usually be applied in the reduced form (4.24) which is obtained by expansion of the square-root term into a series:

$$Q \cong \frac{R_{hp}}{(R_{hp} + R_{ha})R_{ep}} \rho_e \mu_{eo} U_p \qquad (4.24)$$

This expression which also follows equations (4.21) and (4.22) with $\Delta p_{eo}=\Delta p_h$ describes the linear regime of the flow vs. voltage characteristic.

## 4.5. Design and Fabrication of the Nanopump of the 2nd Generation

An improved nanopump is presented in this section; it is primarily designed for continuous flow volumetric titrations (see chapter 6), but it can also be linked to other FIA systems. According to the results described above for the first nanopump and based on theoretical models, major elements have been modified. They will be outlined in the following section.

### 4.5.1. Design and principle

Figure 4.8 shows a schematic view of the entire μTAS. It consists of two nanopumps made of six small microchannels, which can be coupled in parallel so as to enable a high flexibility for the adjustment of the flow range. Two large reservoirs with a capacity of 10μl are linked to the pumps. The volume of the sample solution and of the titrant solution contained in the reservoirs is sufficient for several consecutive volumetric nanotitrations. A micromixer, and a sensor cell, which contains a potentiometric detector, are located downstream. Two external electromagnetic valves allow the injection of sample and titrant solutions in the respective reservoirs.

The pumping system is separated from the chemical reaction system, while a hydraulic connection is maintained between them. A conductive Nafion membrane achieves the separation.

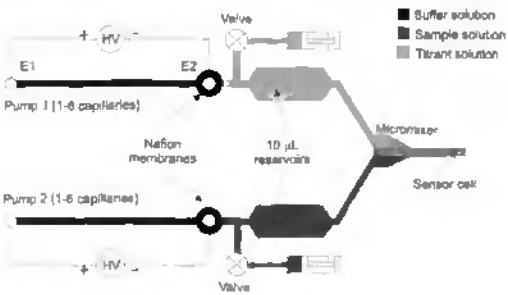


*Fig.4.8. Schematic view of the entire μTAS for volumetric nanotitrations. The capillary-pumps are filled with buffer solutions, which are pushed into the sample and titrant reservoirs.*

*Principle*

The function principle of the 2nd generation nanopump is basically identical to the principle described earlier for the first nanopump. A high voltage is applied across the microchannel located between the electrode E1 and the grounded electrode, E2. The conductive Nafion membrane is located underneath E2.

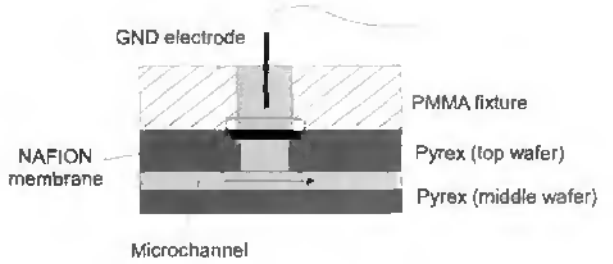


*Fig.4.9. Detailed view of the Nafion membrane squeezed between the fixture and the device. The grounded electrode dips in a buffer solution*

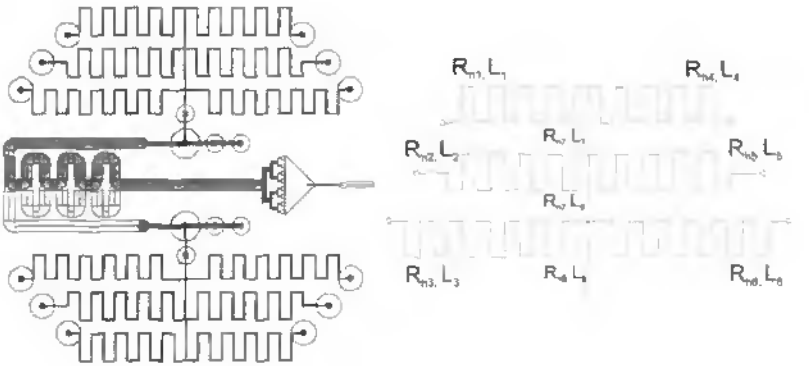


*Fig.4.10. a) Layout of the whole device, the grey channel is the reservoir etched on the top side, the other reservoir is etched on the backside, b) details of one nanopump made of six microchannels with the hydraulic resistances and channel lengths labelled.*

Figure 4.9 shows a detailed schematic of the membrane squeezed between the device and an O-ring located in a fixture. The membrane constrains the flow to follow the microchannel. When a positive voltage (relative to the potential of E2) is applied on E1, a continuous electroosmotic flow is created and the buffer solution is driven towards the reservoir and the mixer, pushing out the sample solution.

*Design considerations*

As described earlier in equation (4.11), a high pressure can be generated if the cross-section of the pump channel is small. On the other hand, a high flow rate would be obtained with a large cross-section of the channels. In order to fulfil both requirements, six 83mm long, 300µm wide and 50µm deep microchannels are connected in parallel. They enable the generation of high pressures, as well as a high

| *Segment (resistance designation)* | *Channel length [mm]* | *Channel width [mm]* | *Cross-section [mm²]* | *Volume [µL]* | *Hydraulic resistance [g/mm⁴s]* | *Reynolds number [-]* |
|---|---|---|---|---|---|---|
| $R_{h1}$ | 62 | 0.3 | 0.015 | 0.93 | 22168.6 | 0.11 |
| $R_{h2}$ | 69 | 0.3 | 0.015 | 1.035 | 24671.5 | 0.11 |
| $R_{h3}$ | 76 | 0.3 | 0.015 | 1.14 | 27174.4 | 0.11 |
| $R_{h4}$ | 62 | 0.3 | 0.015 | 0.93 | 22168.6 | 0.11 |
| $R_{h5}$ | 69 | 0.3 | 0.015 | 1.035 | 24671.5 | 0.11 |
| $R_{h6}$ | 76 | 0.3 | 0.015 | 1.14 | 27174.4 | 0.11 |
| $R_{h7}$ | 7 | 0.3 | 0.015 | 0.105 | 2502.9 | 0.11 |
| $R_{h8}$ | 7 | 0.3 | 0.015 | 0.105 | 2502.9 | 0.11 |
| $R_{h9}$ | 7 | 0.3 | 0.015 | 0.105 | 2502.9 | 0.11 |
| $R_{hp6}$ (6 cap.) | - | 0.3 | 0.015 | 6.525 | 7905.4 | - |
| reservoir | 100 | 2 | 0.1 | 10 | 4876.8 | 0.017 |
| micromixer* | - | - | - | 2.08 | 819.3 | 0.02 |
| sensor cell** | - | - | - | 0.31 | 1943.4 | 0.11 |

*Table 4.1. Values of the hydraulic parameters for the different segments of the microsystem. For details on the micromixer and on the sensor cell, see chapters 5(*) or 6(**). Cap. stands for capillary. Reynolds numbers are calculated on the basis of a 2µL/min flow rate. The channel height is 50 µm.*

flexibility for the adjustment of the flow range. In contrast, the reservoirs are made of 2 mm-wide and 50µm deep microchannels, so as to limit the hydraulic resistance. To save some space on the chip, one of the reservoirs is located on the backside of the wafer, underneath the other reservoir (fig.4.11). This feature simultaneously permits the realization of a three-dimensional micromixer (see chapter 5).

The width to height ratio of all channels, except those of the micromixer, ranges from 6 to 40. Therefore, the hydraulic resistances, $R_h$, of these channels were calculated on the basis of the equation developed for rectangular cross-section (equation (4.18)), and are defined in table 4.1. The equivalent hydraulic resistances for the different pump configurations (one, three or six channels in parallel) were calculated from electrical equivalent resistances. The corresponding Reynolds numbers indicated above were obtained for a maximal theoretical flow rate of 2µl/min. Clearly, the low values of the Reynolds number certify that the flow regime in the whole microsystem is strictly laminar.

### 4.5.2. Fabrication

The present µTAS is composed of three Pyrex wafers attached by fusion bonding. Most of the processes used for the fabrication of this device have been described earlier (see §2.5.4 and §4.3.2).

The bottom wafer contains Pt-planar electrodes buried in the Pyrex as well as an ultrasonically eroded groove, in which a needle has been glued (UV curable glue, UV

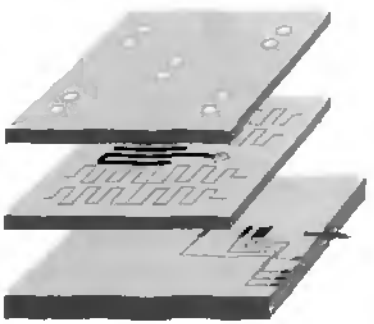


*Fig.4.11. Exploded view of the entire device*

114, Polyscience) at the exit. The 0.5mm thick middle wafer is etched on both sides in order to create the microchannels of the pumps, the reservoirs, the micromixer and the sensor unit. Finally, the 0.5mm thick top wafer is drilled with 1 mm diameter holes for the electrical and hydraulic connections. Electrical connections of the sensor cell are made through a printed circuit board with conductive glue (H20E, Polyscience). Details related to the fabrication of the micromixer are discussed later (see §5.2.3). Figure 4.12 presents a picture of the bonded device.

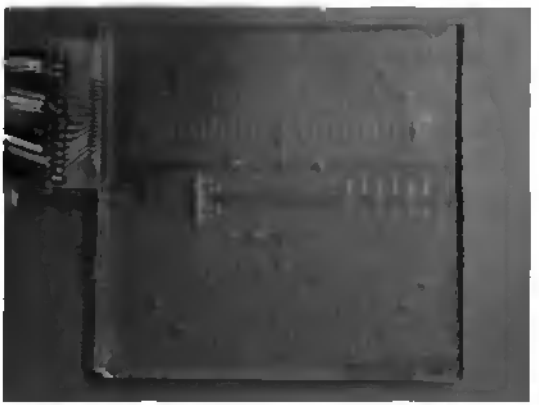

*Fig.4.12. Photograph of a nanopump from the second generation, overall dimensions are 70 x 70 x 2.5 mm.*

## 4.6. Experimental Part

### 4.6.1. Equipment and set-up

The flow rates were measured by gravimetry. This approach was preferred to the beads method used earlier, because it is suited for higher flow rates and does not influence the flow rate.

The set-up of the experiment is displayed in figure 4.13. In order to avoid the influence of backpressure, the nanopump was levelled with the water level of the measurement vessel. The balance used (Mettler-Toledo AE 240) had a precision of 0.01mg (1 digit), which corresponds to a water volume of 10nL. As the lowest flow rates measured were in the range of 5nL/s, an average of the data acquired during the last 20 seconds was calculated using a PC. The acquisition rate was fixed at 1data per second. To avoid evaporation, a paraffin oil layer was put on the top of the water in the measurement vessel. The hydraulic resistance of the measurement tubes had to be taken into account for the determination of the flow rate; it was estimated as 6762g/mm$^4$s.

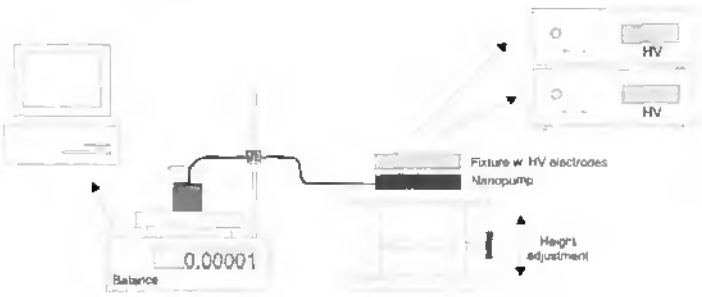


*Fig.4.13. Set-up of the flow rate measurements*

An independent HV power supply was connected with each nanopump. These home-made instruments (HV voltage chip: C40, EMCO, Sutter Creek, CA) can deliver 4kV and have a maximum power of 1W. The electrical grounds of the HV power supplies were galvanically separated to avoid any undesired electric field across the reservoirs.

The device was maintained in a PMMA fixture, in which the buffer solution reservoirs were formed. The HV electrodes, made of standard copper wires, were integrated in another fixture positioned above the reservoirs.

A 10mM borax ($Na_2B_4O_7$) solution, purchased from Aldrich, was used as pump buffer electrolyte solution and as pumped fluid.

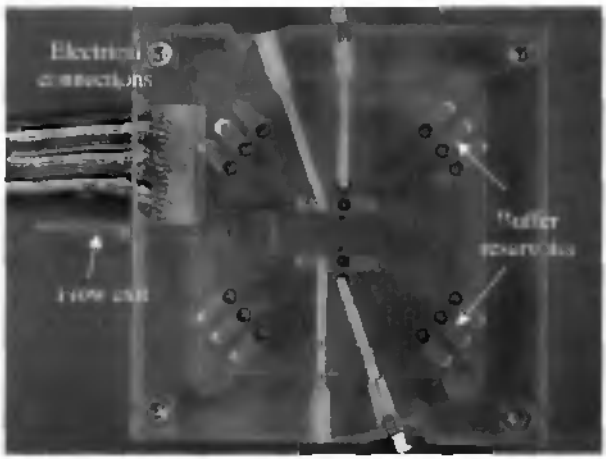


*Fig.4.14. Picture of the set-up with the fixture of the μTAS. Electrical connections seen on the left on the photograph are connections with the potentiometric electrodes.*

4.6.2. Electrical characteristics of the nanopump

The equivalent electrical circuit for one nanopump is displayed in figure 4.15. In principle, the potential of each channel (1-6) can be individually controlled [47]. In the following experiments, three pump configurations are investigated: a) one channel with the voltage (U) applied at 1, b) three channels with U applied at 1-3, c) six channels with U applied at 1-6. For some experiments, the two nanopumps are tested in parallel. Table 4.2 specifies the electrical resistances of all channel segments and the resulting total resistances of the three pump configurations. The resistances were calculated on the basis of the measured resistivity for 10 mM borax solution ($\rho$=6.69k$\Omega$mm). The individual voltage drops for all resistances were calculated by

the well-known Kirchhoff's rules and by Ohm's law; the total applied voltage was taken as 1000V.

| *Segment (resistance designation)* | *Channel length [mm]* | *Electrical resistance [MΩ]* | *Voltage drop 1 capillary [V]* | *Voltage drop 3 capillaries [V]* | *Voltage drop 6 capillaries [V]* | *Electrical field [V/mm]* |
|---|---|---|---|---|---|---|
| $R_1$ | 62 | 27.67 | 747 | 592 | 436 | 7 |
| $R_2$ | 69 | 30.79 | - | 659 | 534 | 8 |
| $R_3$ | 76 | 33.91 | - | 793 | 683 | 9 |
| $R_4$ | 62 | 27.67 | - | - | 436 | 7 |
| $R_5$ | 69 | 30.79 | - | - | 534 | 8 |
| $R_6$ | 76 | 33.91 | - | - | 683 | 9 |
| $R_7$ | 7 | 3.12 | 84 | 67 | 98 | 14 |
| $R_8$ | 7 | 3.12 | 84 | 134 | 149 | 21 |
| $R_9$ | 7 | 3.12 | 84 | 207 | 317 | 45 |
| $R_{ep1}$ (1 cap.) | - | 37.04 | 1000 | - | - | - |
| $R_{ep3}$ (3 cap.) | - | 15.10 | - | 1000 | - | - |
| $R_{ep6}$ (6 cap.) | - | 9.87 | - | - | 1000 | - |

*Table 4.2. Values of the electrical parameters for the channel segments where electroosmosis is taking place. The voltage drops for the resistances were calculated for U=1000V, and the resistances were determined on the basis of a resistivity of 6.7kΩ mm (10 mM borax solution). The electric field indicated corresponds to a pump with six capillaries.*

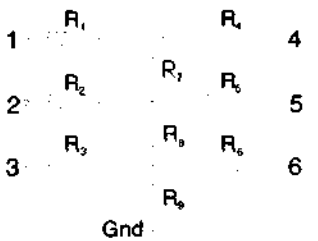


*Fig.4.15. Equivalent electrical circuit for one nanopump.*

### 4.6.3. Characterization of the flow rate

In fig.4.16, the observed flow rates of one and two nanopumps are compared at different applied voltages. When no voltage is applied, a residual flow of about 8nL/s is found due to a small height difference between the measurement vessel and

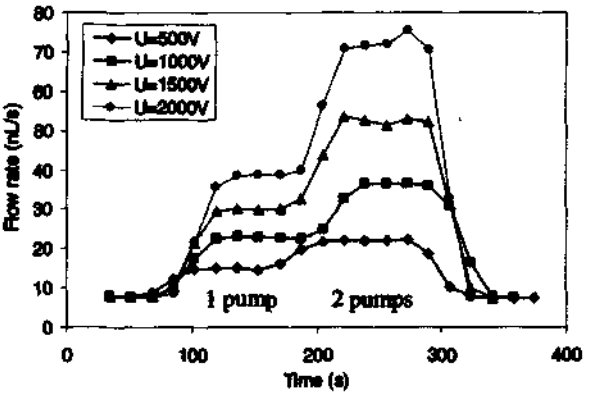


*Fig.4.16. Flow rates as a function of the time and of the applied voltage for one (6 capillaries in parallel) and two (2x 6 capillaries in parallel) nanopumps.*

the nanopump. Then, a voltage is applied to a nanopump with six capillaries connected in parallel. The apparently slow transition between the two states is due to the weight average of the last 20 data acquired, and not to the response time of the electroosmotic effect, which is very short – a few hundred of microseconds [38]. Once the flow rate has been stabilized, the pump is switched on. The flow rate attained with one pump at 2kV almost equals the flow rate obtained with two pumps at 1kV. This linear relationship can be seen clearly in figure 4.17.

Nevertheless, a non-linear effect seems to occur above 2 kV, where the resulting currents and flow rates are higher than expected. Such an effect was reported earlier by Albin et al. [48]. They compared the current-voltage characteristic between rectangular channels (50x500μm) and circular capillaries of an equivalent diameter. In rectangular channels, the linear behaviour ceased around 15V/mm, whereas, in circular capillaries, a perfectly linear behaviour was observed to the range studied (until 40V/mm). The non-ideal characteristics of rectangular channels were explained

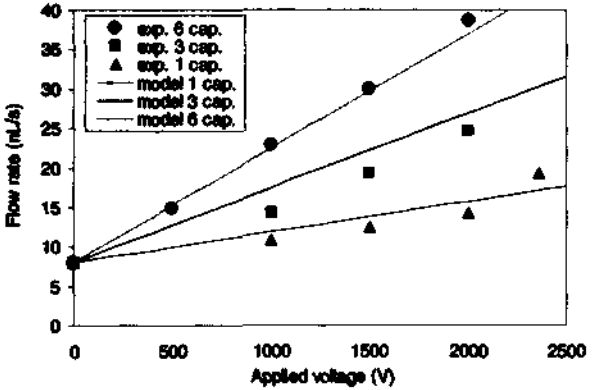


*Fig.4.17. Flow rate as a function of the applied voltage for three pump configurations. Lines represent curve fits according to equation (4.23) with an electroosmotic mobility of 0.06 $mm^2/Vs$ (for details, see text).*

by a greater degree of Joule heating, which is due to a less efficient heat dissipation in comparison with cylindrical capillaries. In the present system, the surface-volume ratio of the rectangular capillaries used (50x300µm) is larger than in the above-mentioned study. Therefore, a higher electric field can be supported, and the non-linear behaviour is observed only above 30V/mm.

The mathematical model for nanopumps (equation (4.23)) was applied to fit the experimental data found for nanopumps with one, three, and six capillaries (fig.4.17). The following parameters were used in the model. The cross-section of the measurement pipe ($A_{ct}$) was calculated on the basis of an inner tube diameter of 0.25mm. The hydraulic resistance $R_{hp6}$ of the pump and the electric resistances $R_{cp1}$, $R_{cp3}$, $R_{cp6}$ were taken from tables 4.1 and 4.2. The density of the borax solution was assumed to be identical to that of water. The total hydraulic resistance $R_h$ is determined by the sum of the partial hydraulic resistances (see table 4.1):

$$R_h = R_{hp6} + R_{ha} = R_{hp6} + R_{reservoir} + R_{mixer} + R_{sensor} + R_{measurement} \qquad (4.25)$$

which yields 22'307 $g/mm^4s$.

The calculated flow rates compare favorably with the experimental data, as shown in figure 4.18. The electroosmotic mobility determined from the model

calculation was found to be 0.06 $mm^2/Vs$. This value fits well with those found in the literature. Dasgupta and Liu [29] reported an electroosmotic mobility of 0.04 $mm^2/Vs$ for a 0.5mM borax buffer solution (pH about 9.2). Manz et al. [22] reported a similar value for a 10 mM borax buffer solution. In addition, estimations on the basis of observed zeta-potential [33] (equation (4.2)) yield comparable data of about 0.04-0.08$mm^2/Vs$. The agreement with the present result nicely validates the model developed above.

It should be pointed out that the square root term in equation (4.23), which follows from the kinetic energy contribution, turns out to be negligible for microscopic systems. As a matter of fact, the typical shape of the square root function would become visible only at a flow rate of about 10 to 100mL/s and a corresponding voltage of 1GV.

The experimental data found for the different pump configurations (1, 3, and 6 capillaries) were fitted using the same electroosmotic mobility value. Figure 4.17 clearly reveals that the fitted lines for all systems are very close to the experimental data. This finally corroborates the applicability of the theoretical model. To simplify the evaluation of flow rates, an easier approach may also be applied. One simply

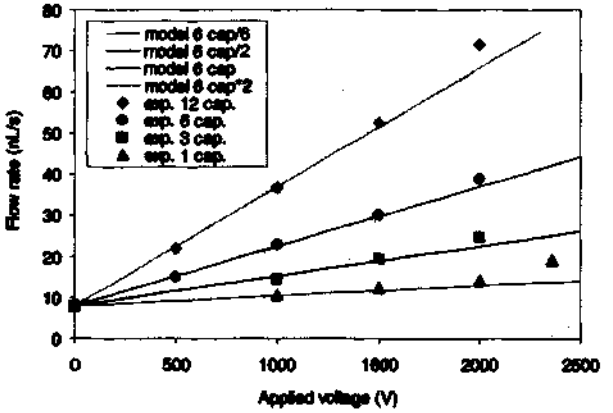


*Fig.4.18. Flow rate as a function of the applied voltage for one and two nanopumps. The lines represent fits from equation (4.23) to the data found for six capillaries and multiplied by the ratio between the respective number of capillaries involved in the pumping.*

takes the slope found in the experiment with 6 capillaries and multiplies it by the ratio between the respective number of capillaries involved in the pumping. This simple method also proves to be remarkably close to the experimental data (fig. 4.18).

The linearity of the flow rate vs. the current can be seen in figure 4.19. As already pointed out, the current sometimes fluctuates quite strongly. This may be the consequence of the non-linear current-voltage relationship mentioned above, or a combined effect of the surface charge modification, influences of the Nafion membrane, and interferences from trapped air bubbles.

Nevertheless, an excellent flow rate reproducibility is usually observed, as shown in figure 4.20. When a voltage of 750V was applied for a longer period of

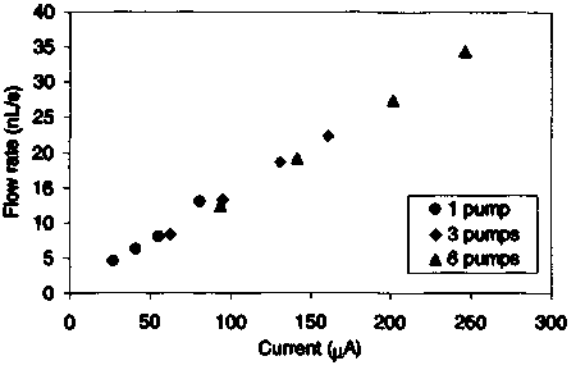


*Fig.4.19. Flow rate vs. current for one, three and six capillaries.*

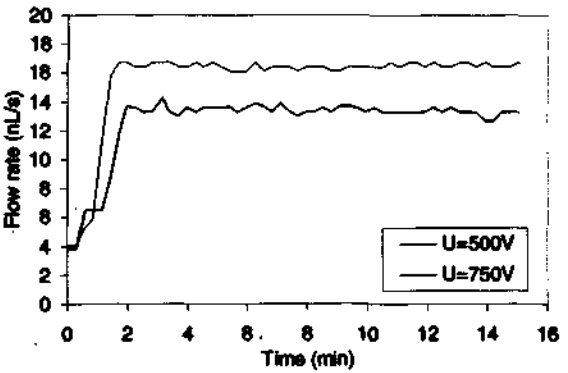


*Fig.4.20. Flow rate stability vs. time for two applied voltages.*

time, a flow rate of 16.4 nL/s was measured with a standard deviation of only ±0.3nL/s. Most of the irregularities observed in figure 4.20 may be attributed to the inertia of the balance and to the movement of the large volume of solution contained in the measurement pipe.

### 4.6.4. Backpressure characteristic

The backpressure is the pressure against which a pump is able to deliver fluid. This feature is fundamental for conventional pumps, since the fluidic components linked to the pump are often not at the same height level. For the nanopump presented here, backpressure is secondary because all the components are located on the same device and are therefore at the same level. Nevertheless, according to theory, electroosmotic pumps should be able to create a large backpressure.

Different voltages were set and the nanopump was vertically displaced until the flow stopped. The two nanopumps – 12 capillaries connected – were working in parallel with the same voltage. Figure 4.21 displays the experimental data of backpressure versus applied voltage. As predicted by theory, this relationship is linear, although the calculated electroosmotic pressures of a single nanopump according to equation (4.21) are somewhat lower than the observed backpressures.

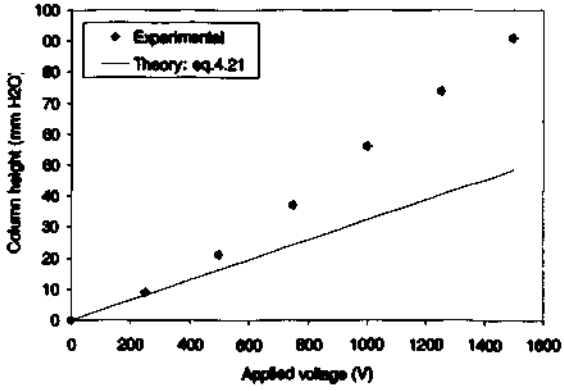


*Fig.4.21. Pressure ($H_2O$ column) to stop flow vs. applied voltage. Continuous line: electroosmotic pressure of one nanopump with 6 capillaries, according to equation (4.21) with an electroosmotic mobility of 0.06 $mm^2/Vs$.*

## 4.7. Conclusion

Two electroosmotic nanopumps were developed and studied. As expected, a pulsation free flow could be generated by means of an electroosmotic flow created in a limited part of a capillary. This feature allowed the pumping of almost any kind of liquids, regardless of their pH or their ionic strength. Flow ranges between 5nL/min to 5µL/min, which corresponds to 3 orders of magnitude, could be attained by an appropriate setting of the voltage and of the number of capillaries involved in the pumping. A theoretical description of the phenomena involved in systems of capillaries with partial electroosmosis led to the development of a physical model. Surprisingly, the latter fitted perfectly with experimental data found for different nanopumps, and revealed a linear relationship between the flow rate and the applied voltage.

There is no doubt that the performance of the system can be further improved. There are still some limitations to an EOF pump regarding flow rate stability and pumping against backpressure. However, this can be largely overcome by an appropriate selection of the microchannel dimensions. A proper design will also enable a more homogeneous repartition of the electric field throughout the nanopump which, in turn, will limit the heating of the solution through the Joule effect.

Nevertheless, for the present designs, the flow rate remained stable at low voltage; and this will enable the connection of the nanopumps with analytical systems working in the continuous flow mode (see chapter 6).

**References**


[1] Guenat O.T., Morf W.E., Verpoorte E, van der Schoot B., de Rooij N.F., *μTAS for volumetric or coulometric titrations of nanomole amounts of analytes in microliter samples*, Proc. μTAS'98, Banff, Canada, p.439-42.

[2] Guenat O.T., Ghiglione D., Pasquier V., van der Schoot B., Morf W.E., de Rooij N.F., *An electro-osmotically driven nanopump for volumetric nanotitration applications*, Proc. Eurosensors XIII, Den Haag, The Netherlands, 1999, p.343.

[3a] Morf W. E., Guenat O. T., de Rooij N. F., *Partial electroosmotic pumping in complex capillary systems, Part 1: Principles and general theoretical approach*, Sensors and Actuators B, submitted for publication.

[3b] Guenat O. T., Ghiglione D., Morf W. E., de Rooij N. F., *Part 2: Fabrication and application of a micro total analysis system suited for volumetric nanotitrations*, Sensors and Actuators B, submitted for publication.

[4] Gravesen P., Branebjerg J., Jensen O.S., *Microfluidics a review*, J. Micromech. Microeng., 3, 1993, p.168-82.

[5] Shoji S., Esashi M., *Microflow devices and systems*, J. Micromech. Microeng., 4, 1994, p.157-71.

[6] Elwenspoek M., Lammerink T.S., Miyake R., Fluitman J.H.J., *Towards integrated microliquid handling systems*, J. Micromech. Microeng., 4, 1994, p.227-45.

[7] van Lintel H.T.G, van de Pol F.C.M., Bouwstra S., *A piezoelectric Micro Pump based on Micromachining of Silicon*, Sensors and Actuators, 15, 1988, p.153-67.

[8] van der Schoot B.H., Jeanneret S., van den Berg A., de Rooij N., *A silicon integrated miniature chemical analysis system*, Sensors and Actuators, B6, 1992, p.57-60.

[9] Zengerle R., Richter M., Brosinger F. Richter A., Sandmaier H., *Performance simulation of microminiaturized membrane pumps*, Proc. Transducers '93, p.106-9.

[10] Branebjerg J., Fabius B., Gravesen P., *Application of miniature analyzers: from microfluidics components to μTAS*, Proc. μTAS '94, Twente, The Netherlands, p.141-151.

[11] Lammerink T.S., Elwenspoek M., Fluitman J.H., *Integrated micro-liquid dosing system*, Proc. MEMS'93, Fort Lauderdale, Florida, p.254-9.

[12] Judy J., Tamagawa T., Polla D.L., *Surface machined micromechanical membrane pump*, Proc. MEMS 91, Nara, Japan, p.182-6.

[13] Zhang W., Ahn C.H., *A bi-directional magnetic micropump on a silicon wafer*, Solid-State Sensor and Actuator Workshop, Hilton Head, South Carolina, 1996, p.94.

[14] Handique K., Burke D.T., Mastrangelo C.H., Burns M.A., *Nanoliter-volume discrete drop injection and pumping in microfabricated chemical analysis*

*systems*, Solid-State Sensor and Actuator Workshop, Hilton Head, South Carolina, 1998, p.346-9.

[15] Nagakura T., Ishihara K., Furukawa T., Masuda K., Tsuda T., *Auto-regulated medical pump without energy supply*, Proc. Transducers'95, Stockholm, Sweden, p.287-90.

[16] Moroney R.M., White R.M., Howe R.T., *Ultrasonic induced microtransport*, Proc. MEMS'91, Nara, Japan, p.277-82.

[17] Lemoff A.V., Lee A.P., Miles R.R., McConaghy F., *An AC magnetohydrodynamic micropump: towards a true integrated microfluidic system*, Proc. Transducers'99, Sendai, Japan, p.1126-9.

[18] Bart S.F., Tavrow L.S., Meregany M., Lang J.H., *Microfabricated electrohydrodynamic pumps*, Sensors and Actuators, A21-A23, 1990, p.193-7.

[19] Richter A., Plettner A., Hoffmann K.A., Sandmaier H., *A micromachined electrohydrodynamic (EHD) pump*, Sensors and Actuators, A29, 1991, p.159-68.

[20] Fuhr G., Schnelle T., Wagner B., *Travelling wave-driven microfabricated electrohydrodynamic pumps for liquids*, J. Micromech. Microeng., 4, 1994, p.217-26.

[21] Böhm S., Olthuis W., Bergveld P., *An electrochemically actuated micropump for use in a 'push-pull' microdialysis based in-vivo monitoring system*, Proc. Transducers'99, Sendai, Japan, p.880-1.

[22] Manz A., Effenhauser C.S., Burggraf N., Harrison D.J., Seiler K., Fluri K., *Electroosmatic pumping and electrophoretic separations for miniaturized chemical analysis systems*, J. Micromech. Microeng., 4, 1994, p.257-65.

[23] Haswell S.J., *Development and operating characteristics of micro flow injection analysis systems based on electroosmotic flow-a review*, Analyst, vol. 122, 1997, p.1R-10R.

[24] Manz A., Harrison D.J., Verpoorte E. M.J., Fettinger J.C., Lüdi H., Widmer H.M., *Miniaturization of chemical analysis systems-A look into next century's technology or just a fashionable craze*, Chimia, 1991, 45, p.103.

[25] Liu S., Dasgupta P.K., *Flow-injection analysis in the capillary format using electroosmotic pumping*, Anal. Chim. Acta, 268, 1992, p.1-6.

[26] Harrison D.J., Glavina P.G., Manz A., *Towards miniaturized electrophoresis and chemical analysis system on silicon*, Sensors and Actuators, B 10, 1993, p.107.

[27] Jacobson S.C., Hergenröder R., Koutny L.B., Ramsey J.M., *Open channel electrochromatography on a microchip*, Anal. Chem., 66, 1994, p.2369.

[28] Liu S., Dasgupta P.K., *Electroosmotically pumped capillary flow-injection analysis*, Anal. Chim. Acta, 283, 1993, p.739-45.

[29] Dasgupta P.K., Liu S., *Electroosmosis: a reliable fluid propulsion system for flow injection analysis*, Anal.Chem., 66, 1994, p.1792-1798.

[30] Liu S., Dasgupta P.K., *Electroosmotically pumped capillary format sequential*

*injection analysis with a membrane sampling interface for gaseous analytes*, Anal. Chim. Acta, 308, 1995, p-281-5.

[31] Dasgupta P.K., Liu S., *Auxiliary electroosmotic pumping in capillary electrophoresis*, Anal.Chem., 66, 1994, p.3060-5.

[32] Liu S., Dasgupta P.K., *Sequential injection analysis in capillary format with an electroosmotic pump*, Talanta, vol. 41, No.11, 1994, p.1903-10.

[33] Kortüm G., *Lehrbuch der Elektrochemie*, Verlag Chemie GmbH, Weinheim/Bergstr., Germany, 1972, p.430-44.

[34] Deen W.M., *Analysis of transport phenomena*, Oxford Univ. Press, 1998, p.461-3.

[35] Koryta J., Dvorák J., *Principles of electrochemistry*, ed. John Wiley & Sons, New York, 1987, chapter 6.

[36] Rice C.L., Whitehead R., *Electrokinetic flow in a narrow cylindrical capillary*, The Journal of Phys. Chemistry, vol. 69, No. 11, 1965, p.4017-24.

[37] Bousse L., Minalla A., Deshpande M., Greiner K.B., Gilbert J.R., *Optimization of sample injection components in electrokinetic microfluidic systems*, Proc. MEMS'99, Orlando, Florida, p.309-14.

[38] Dose E.V., Guiochon G., *Timescales of transient processes in capillary electrophoresis*, J. of Chromatography A, 652, 1993, p.263-75.

[39] Moore W.J., *Physical Chemistry*, Longman 5th ed., London, Great Britain, 1972, p.512.

[40] Berthold A., Nicola L., Sarro P.M., Vellekoop M.J., *A novel technological process for glass-to-glass bonding*, Proc. Transducers'99, Sendai, Japan, p.1324-7.

[41] Fan Zhonghui, Harrison D.J., *Rapid injection and separation of amino acids with capillary electrophoresis systems micromachined on a glass chip*, Anal. Chem. 66, 1994, p.177-84.

[42] Bousse L., Dijkstra E., Guenat O., *High-density arrays of valves and interconnects for liquid switching*, Solid-State Sensor and Actuator Workshop, Hilton Head, South Carolina, 1995, p.272-5.

[43] Taylor J.A., Yeung E.S., *Imaging of hydrodynamic and electrokinetic flow profiles in capillaries*, Anal.Chem. 65, 1993, p.2928-32.

[44] Huang X., Gordon M.J., Zare R.N., *Current-monitoring method for measuring the electroosmotic flow rate in capillary zone electrophoresis*, Anal. Chem. 60, 1988, p.1837-8.

[45] Fox R.W., McDonald A.T., *Introduction to fluid mechanics*, 3rd ed., John Wiley & Sons, New York, 1985, p.389-90.

[46] Spurk J.H., *Strömungslehre*, 4.Auflage, Springer Verlag, Berlin, 1996, p.164-7.

[47] Seiler K., Fan Z.F., Fluri K., Harrison D.J., *Electroosmotic pumping and valveless control of fuid flow within a manifold of capillaries on a glass chip*, Anal.Chem. 66, 1994, p.3485-91.

[48] Albin M., Grossman P.D., Moring S.E., *Sensitivity enhancement for capillary electrophoresis*, Anal. Chem. . 65, 1993, p.489A-497A.

# 5. Static Micromixer

The static micromixer presented here is part of a μTAS dedicated to volumetric nanotitrations. Specifications relative to technology were imposed by the material used for the nanopump described earlier. The purpose of this mixer based on lamination is to provide fast and efficient mixing for flow rates up to 4μL/min. Parts of this chapter have been published in [1, 2].

---

## 5.1. Introduction

Mixing is an important step in analytical chemistry. It is indispensable where reactions between two solutions are desired. In macroscale systems, mixing is usually achieved by stirring; it is based on the creation of turbulent flows followed by inter-diffusion between small domains of differing compositions. In chemical microsystems, on the other hand, turbulence can only be scaled down either when flow rates are high enough [3,4], or when an ultrasonic actuation enhances the mixing [5]. In most of the practically relevant microsystems, however, the mixing is primarily governed by molecular diffusion because of the laminar flow regime fulfilled in such devices.

In recent years, a number of microstructures have been proposed to perform chemical reactions [3-16]. Though all these mixers aim at providing a fast and efficient mixing, it is the field of application which determines the specific requirements as well as the principle and design of the device to be used. Various authors have reported on the use of Y- or T-mixers and other relatively simple channel manifolds [6-9], which seem to work well with either narrow channels or reaction times up to several minutes. A few years ago, a research group reported on a micromixer whose design was based on the idea of increasing the contact area between two liquids by injecting one of the fluids through a matrix of closely spaced tiny nozzles into a flat mixing chamber [10,11]. Other mixers often referred to as Möbius mixers [12-14] operate on a cut-and-slice principle. The layers of the two

liquids are separated perpendicularly to the boundary layer and re-united in such a way as to obtain twice the number of filaments. Repetition of that sequence leads to an increase in the exchange interface area between the different liquids. Besides the Möbius mixer, a number of micromixers based on direct lamination have been developed [9,15,16]. A fluid stream is split into lamellae, which are arranged in such a way as to alternate with lamellae of a second liquid rising through a series of nozzles or small holes.

The goal of this study is to develop a simple micromixer, which, together with the electroosmotic nanopump described in chapter 4 and with a reactor-sensor unit (chapter 6), will be part of a μTAS for volumetric nanotitrations. Just as for the micromixers described above, the aim of the device presented here is to provide fast and efficient mixing for flow rate ranges from 50nL/min up to 4μL/min. Nevertheless, the design of the micromixer is restricted by several features imposed by the concept of the μTAS for volumetric nanotitrations, namely the dimension of the upstream channels, the choice of material and the related technological processes. With regards to this latter aspect, the decision was taken to keep the entire process as simple as possible, for reasons similar as those mentioned for the processing of the nanopump (§ 4.1). All these requirements led to the development of a micromixer based on a direct lamination method.

## 5.2. Design and Fabrication of the Micromixer

Several restrictions regarding technological processes, choice of material and design parameters are directly related to the options taken for the fabrication of the nanopump. As a matter of fact, the integration of the micromixer on the device of the nanopump requires the use of the same material, i.e. Pyrex, and therefore the same microtechnological process, namely HF etching.

In addition, the design of the micromixer is submitted to yet another constraint, imposed by the two reservoirs, both ending with a 2mm wide channel. These are linked to the inputs of the micromixer, one being on the wafer topside, the second on the wafer backside.

Furthermore, the micromixer needs to be designed for a maximum theoretical flow rate of 4 μL/min, which is the resultant flow rate of the two nanopumps working in parallel.

### 5.2.1. Design considerations

As described in the introduction, molecular diffusion is the only one responsible for mixing, provided that the Reynolds number is small. A simple relation between the diffusion time, $t_d$, and the average diffusion length, $x$, can be found from Fick's second law of diffusion:

$$t_d \cong \frac{x^2}{2D} \qquad (5.1)$$

where $D$ is the diffusion coefficient. Typically, $D$ is in the order of $10^{-3}$ mm$^2$/s, leading to a diffusion time of 33 min, if x=2mm. Accordingly, if the two reservoirs mentioned above would simply be linked together by means of a Y-mixer, a mixing of 100% would occur only after 13.3m at a flow rate of 4μL/min (see table 5.1)!

This shows the necessity to increase the active area for diffusion, and to split the incoming flows into smaller channels. Nevertheless, even if theory predicts that the smaller the channel is, the faster the diffusion is, their dimensions are limited by technological considerations. If the same isotropic etching (50μm deep) is used to create both the channels of the nanopumps and those of the mixer, the narrowest channel obtained is 110μm wide – of which 10μm are needed for the mask opening

| Designation | Channel number and width (- x mm) | Max. flow rate (µL/min) | Speed (mm/s) | Diffusion time (s) | Diffusion length (mm) |
|---|---|---|---|---|---|
| Reservoir | 2 | 4 | 0.67 | 2000 | 1333.3 |
| Mixer 1st branch | 2 x 0.88 | 2 | 0.76 | 387.2 | 293.3 |
| Mixer 2nd branch | 4 x 0.44 | 1 | 0.76 | 96.8 | 73.3 |
| Mixer 3rd branch | 8 x 0.22 | 0.5 | 0.76 | 24.2 | 18.3 |
| Mixer 4th branch | 16 x 0.11 | 0.25 | 0.76 | 6.0 | 4.6 |

*Table 5.1. Diffusion times and lengths for different channel widths and for a maximum theoretical flow rate of 4 µL/min.*

and 100µm result from the under etching. Table 5.1 indicates the diffusion times for different channel widths. These values clearly reveal that only the smallest channel is suited for the present purpose. A tree configuration mixer is therefore chosen where the branches are successively subdivided in 2, 4, 8 and 16 branches. The incoming fluids A and B are split into 16 small laminae. Fluid A comes from the wafer topside through small holes, fluid B stays at the bottom side (fig.5.1), and then they are combined in a triangular mixing chamber. Table 5.1 also points out the flow velocity in each channel with the corresponding diffusion length.

In contrast to the mixer presented by Manz et al. [16], the triangular receptacle has two advantages. First, the lateral diffusion of the laminae in two directions is not constrained, which speeds up the diffusion time. Secondly, due to the larger cross-section, which diminishes the diffusion length, the linear flow rate is reduced.

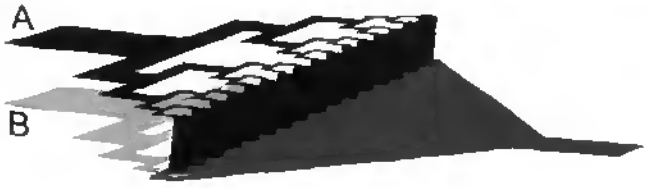


*Fig.5.1. Principle of the micromixer: flows A and B are split in small laminae before they mix in the beginning of the triangle-shaped mixing chamber.*

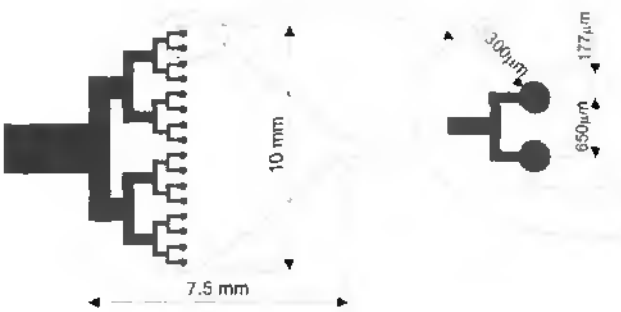


*Fig.5.2. Topside view of the micromixer with the overall dimensions. The distance between two holes is 350µm, hence the maximum lateral diffusion length is 175µm.*

With this device, a nearly complete mixing is achieved after 2mm at 4µL/min, since the maximum lateral diffusion length is only 175 µm (fig.5.2).

5.2.2. Hydraulic characteristics of the micromixer

The values of the Reynolds numbers found for the different segments of the mixer never exceeded 0.05, which certifies the assumption of laminar flow with an exclusive mixing by diffusion. Table 5.2 shows the hydraulic resistances of the different channels calculated with equation (4.18), except for the smallest channel for which the width to height ratio equals 2.2. Therefore, the hydraulic resistance of the latter channel was calculated on the basis of Poiseuille's equation for cylindrical pipes, using the approximation of the hydraulic radius (see §4.4.2). The hydraulic resistance of the triangular mixing chamber was calculated by splitting the triangle into small segments of different widths, for which equation (4.18) was applied, and by adding these increments. The total hydraulic resistance of the mixer was then obtained as:

$$R_{mixer} = \frac{R_{b1}}{2} + \frac{R_{b2}}{4} + \frac{R_{b3}}{8} + \frac{R_{b4} + R_{hole}}{16} + R_{triangle} \qquad (5.2)$$

From this, the hydraulic resistance of the mixer is given by 819.3 g/mm$^4$s.

| Designation | Channel width (mm) | Channel length (mm) | Hydraulic resistance ($g/mm^4 s$) |
|---|---|---|---|
| Mixer 1st branch | 0.88 | 3.6 | 407 |
| Mixer 2nd branch | 0.44 | 2.28 | 536 |
| Mixer 3rd branch | 0.22 | 1.15 | 586 |
| Mixer 4th branch | 0.11 | 0.82 | 1495 |
| Hole | 0.3 | 0.4 | 2 |
| Triangle | from 10 to 0.3 | 5.25 | about 315 |

*Table 5.2. Hydraulic resistances of the different parts of the mixer.*

### 5.2.3. Fabrication of the micromixer

The etching of the channels of the mixer has to be achieved simultaneously with the other μTAS channels (see § 4.5.2). The only mixer-specific process involves the creation of 400μm-deep openings from the wafer topside to the wafer backside. A second HF etching is not a good option since the under etching would form very large holes. Nevertheless, several other techniques can etch or erode Pyrex, for example deep reactive ion etching (DRIE) which is now widespread for the micromachining of silicon. Unfortunately, when applying this technique for Pyrex, only small etching depths have yet been realized [17,18]. Laser ablation could be an alternative method,

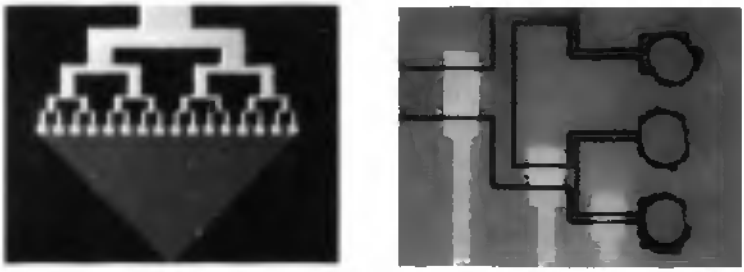

*Fig.5.3. a)Photograph of the whole micromixer after the polysilicon plasma etch; the triangle chamber can be seen in transparency through the polysilicon layer. b) close view of three ultrasonically drilled holes and of some channels etched.*

but some protuberant craters - unacceptable for fusion bonding - are sometimes generated around the holes [19]. Furthermore, most of the research in this field focuses on laser ablation of quartz [20] and not of Pyrex. Micro-electrochemical-discharge machining (μECDM) is less known, but seems to be an interesting technology [21,22] for this kind of task. In spite of this, the process finally chosen is ultrasonic drilling. This is a well-experienced and reliable technique for holes larger than 1mm, and it is available at the IMT! Holes of 0.2 and 0.3mm diameter were drilled in Pyrex, but 0.2mm centre bits broke systematically. Figure 5.3b shows three 0.3mm diameter holes at the end of the small channels of the mixer. The holes were positioned manually, which explains the misalignment. A bonded micromixer with 16 holes can be seen in figure 5.4.

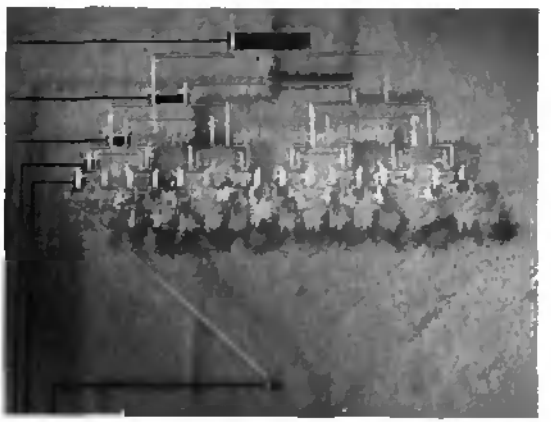

*Fig.5.4. Photograph of the entire micromixer etched and bonded.*

## 5.3. Experimental Results

The micromixer was tested using a Congo red indicator solution (Aldrich) and a 10 mM $HNO_3$ solution. For this purpose, the mixer was linked to two piston-pumps (700 Dosino-2mL, Metrohm) and a flow rate of 200 µL/min was chosen in order to see the mixing process. At lower flow rates, the mixing progression, which was very fast, could hardly be seen. The goal of this experiment was to show the symmetry of the flow in the reaction chamber. Figure 5.4 displays four videoprint sequences at four different times.

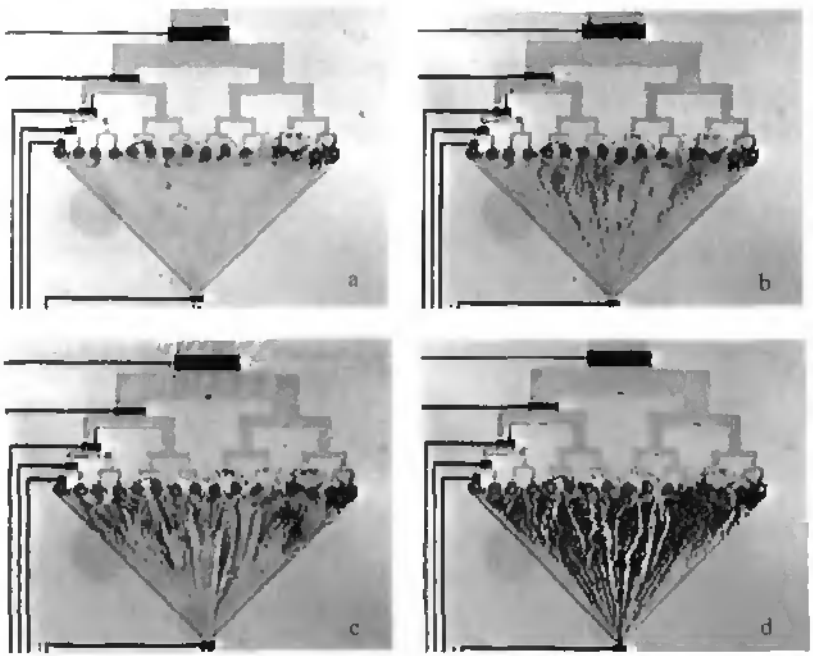


*Fig.5.4. Illustration of the mixing progression at 200 µL/min. a) The Congo red indicator solution is pumped through the mixer. b)-d) Then the acidic solution is added at three different times.*

## 5.4. Discussion and Conclusion

The mixing of two fluids in a micromixer with complicated geometrical shapes is not a simple matter, and a rigorous mathematical description of the hydrodynamic behaviour can be quite arduous. Nevertheless, the simple mathematical relations used were sufficient to roughly describe the behaviour of the fluids in the micromixer and to design the latter. The visual results obtained for different flow rates leads to the conclusion that 100% mixing occurs within the considered flow rates range and within the expected time.

In order to achieve devices with more reproducible holes, the machining step of the holes by ultrasonic drilling should be replaced by DRIE, as soon as technological progress will make it possible.

**References**


[1] Guenat O.T., Ghiglione D., Pasquier V., van der Schoot B., Morf W.E., de Rooij N.F., *An electro-osmotically driven nanopump for volumetric nanotitration applications*, Proc. Eurosensors XIII, Den Haag, The Netherlands, 1999, p.343-4.

[2a] Morf W. E., Guenat O. T., de Rooij N. F., *Partial electroosmotic pumping in complex capillary systems, Part 1: Principles and general theoretical approach*, Sensors and Actuators B, submitted for publication.

[2b] Guenat O. T., Ghiglione D., Morf W. E., de Rooij N. F., *Part 2: Fabrication and application of a micro total analysis system suited for volumetric nanotitrations*, Sensors and Actuators B, submitted for publication.

[3] Scampavia L.D., Blankenstein G., Ruzicka J., Christian G.D., *A coaxial jet mixer for rapid kinetic analysis in flow injection cytometry*, Anal. Chem. 67, 1995, p.2743-9.

[4] Desai A., Bökenkamp D., Yang X., Tai Y.-C., Marzluff E., Mayo S., *Microfluidic sub-millisecond mixers for the study of chemical reaction kinetics*, Proc. Tranducers'97, Chicago, USA, p.167-70.

[5] Yotsumoto A., Nakamura R., Shoji S., Wada T., *Fabrication of an integrated mixing/reaction flow cell for μTAS*, Proc. μTAS'98, Banff, Canada, p.185-8.

[6] Branebjerg J., Fabius B., Gravesen P., *Application of miniature analyzers; from microfluidic components to μTAS*, Proc. μTAS'94, The Netherlands, p.141-51.

[7] Fluri K., Fitzpatrick G., Chiem N., Harrison J., *Integrated capillary electrophoresis devices with an efficient postcolumn reactor in planar quartz and glass chips*, Anal. Chem. 68, 1996, p.4285.

[8] Bökenkamp D., Desai A., Yang X., Tai Y.-C., Marzluff E., Mayo S., *Microfabricated silicon mixers for submillisecond quench-flow analysis*, Anal. Chem. 70, 1998, p.232.

[9] Erbacher C., Bessoth F.G., Busch M., Verpoorte E., Manz A., *Towards integrated continuaus-flow chemical reactors*, Mikrochimica Acta, 131, 1999, p.19-24.

[10] Miyake R., Lammerink T.S.J., Elwenspoek M., Fluitman J.H.J., *Micromixer with fast diffusion*, Proc. MEMS'93, Fort Lauderdale, USA, p.248-53.

[11] Elwenspoek M., Lammerink T.S., Miyake R., Fluitman J.H.J., *Towards integrated microliquid handling systems*, J. Micromech. Microeng., 4, 1994, p.227-45.

[12] Möbius H., Ehrfeld W., Hessel V., Richter Th., *Sensor controlled processes in chemical microreactors*, Proc. Tranducers'95, Stockholm, Sweden, p.775-8.

[13] Mensinger H., Richter Th., Hessel V., Döpper J., Ehrfeld W., *Microreactor with integrated static mixer and analysis system*, Proc. μTAS'94, The Netherlands, p.237-243.

[14] Schwesinger N., Frank T., Wurmus H., *A modular microfluid system with an integrated micromixer*, J. Micromech. Microeng. 6, 1996, p.99-102.

[15] Larsen U.D., Branebjerg J., Blankenstein G., *Fast mixing by parallel multilayer lamination*, Analytical Methods & Instrumentation, Special Issue μTAS'96, Basel, Switzerland, p.228-30.

[16] Manz A., Bessoth F., Kopp M.U., *Continuous flow versus batch process – a few examples*, Proc. μTAS'98, Banff, Canada, p.235-240.

[17] Weibel K., Tests of deep reactive ion etching (DRIE) in Pyrex: depth attained about 10μm with 1μm thick metallic mask, personal communication, IMT, Univ. of Neuchâtel, nov. 1999.

[18] Li X., Abe T., Esashi M., *Deep reactive ion etching of pyrex glass*, Proc. MEMS 2000, Miyazaki, Japan, p.271-6.

[19] Laser Zentrum Hannover e.V., Germany, Dr. P. Lonergan, Tests of micro-holes in Pyrex, personal communication, 2.12.1998.

[20] Varel H., Ashkenasi D., Rosenfeld A., Wähmer M., Campbell E.E.B., *Micromachining of quartz with ultrashort laser pulses*, Applied Physics A 65, 1997, p.367-373.

[21] Shoji S., Esashi M., *Photoetching and electrochemical discharge drilling of Pyrex glass*, Tech. Digest of the 9th Sensor Symposium, 1990, p.27-30.

[22] Langen H., Breguet J.M., Bleuler H., Renaud P., Masuzawa T., *Micro Electrochemical Discharge Machining of Glass*, Int. J. of Electrical Machining, No.3, 1998, p.65-9.

# 6. Continuous Flow Volumetric Nanotitrations

This chapter presents an application of the nanopump and of the micromixer described earlier. The objective of this work is to test the potentiometric detector unit integrated in the microsystem, and to show the ability of the whole μTAS to perform continuous flow nanotitrations of species, which cannot be directly pumped by electroosmosis. The preliminary results of cerimetric nanotitrations illustrate the functioning of the whole microsystem. The experimental results have been presented in part at the Eurosensors'99 conference [1].

## 6.1. Introduction

Due to their almost unlimited field of applications, volumetric titrations are the most widely used techniques among titrimetric methods. In contrast to coulometry, a large number of reagents, able to react selectively with the sample to be determined, can be involved in the titration. Unfortunately, this undeniable advantage is attenuated by the fact that these solutions must be stored and thus often standardized before use.

Most of the commonly employed volumetric titrators are of the batch-type. Nevertheless, over the past few decades, several research groups investigated new methods enabling faster titrations and/or automated techniques. Among these new methods, continuous titrators and FIA titrations have received the most attention. These techniques are based on the creation of a gradient zone, which can result either from a concentration gradient or from a flow rate gradient. In the sixties, Blaedel and Laessig [2] made the first attempts to employ the flow rate changes of the titration reagent to titrate continuously flowing sample solutions. Later, Fleet and Ho [3] and Nagy et al. [4] introduced the generation of linear concentration gradients to perform flow titrations. While Nagy implemented the triangle programmed titration technique

for coulometric titrations (see chapter 3) Fuhrmann and Spohn [5] applied it for volumetric titrations. They created a concentration gradient by diluting the sample solution linearly. Other research groups preferred a flow rate gradient, such as Valcarcel and co-workers, who developed this field by discussing the use of different programmable flow rate gradients [6] and their application to acid-base [7], complexometric and redox titrations [8]. López Garciá et al. [9] used a similar technique to perform automated titrations without calibration. They reported titration cycles of one to three minutes.

By using a FIA titration technique, Ruzicka, Hansen and co-workers [10-13] reported even shorter titration times. This technique is based on the creation of a suitable concentration gradient of a small-injected sample within a carrier stream of titrant. An element of fluid within which equivalence between analyte and titrant is obtained is found both at the front and at the tail of the dispersed sample zone. At constant flow rate, the time difference between these two equivalent points is proportional to the concentration of the injected sample. Several theoretical models describing the relationship of the peak width as a function of the sample concentration have been proposed [14-17].

Other attempts to reduce the titration time have been reported by Gratzl and co-workers [18, 19]. They proposed a system for dispensing the titrant solution by diffusion through a membrane. Their method made use of a titrant filled microburet, positioned in a microscopic sample drop. Litbom et al. [20] proposed a similar device by introducing an automated dosing technique based on the use of piezoelectrically driven pipettes. Nevertheless, the miniaturization of batch volumetric titrations presents some problems, such as the evaporation of the solvents and the lack of accuracy in the dosing of the titrant in the nanoliter or even the picoliter range.

The objectives of this chapter were, first, to test the potentiometric detector and the micromixer of the μTAS presented in the last two chapters, and, second, to perform a few continuous flow volumetric titrations. A simple procedure, similar to FIA titrations, was used to carry out preliminary tests. The experimental part is divided into two sections. First, volumetric titrations were performed with two conventional piston-pumps linked to the μTAS. Second, titrations were carried out by using the integrated electroosmotic nanopumps described earlier.

## 6.2. Continuous Flow Volumetric Titrations

In order to perform preliminary titrations with the above-described μTAS, a simple method was used, which enabled the study of basic features of the device, such as the influence of the flow rate on the sensor response time and the capacity to carry out volumetric titrations. In the following section, the whole titration cycle is explained qualitatively, and a theoretical description of the response time of the sensor is presented.

*Analysis of the titration cycle*

Figure 6.1 depicts the diagram of the continuous flow volumetric titration. The sample and the titrant are continuously pumped in a gradient chamber – the micromixer. At the time $t=0$, the sample stream is stopped, which creates a dispersed sample zone at the trailing edge of the sample plug. The resulting stream is continuously monitored by a flow through detector. The observed titration time, $t_{ep}$, depends on the sensor response time, $t_r$, and on the combined effects of dispersion and chemical reaction at the hypothetical interface between the sample plug and the titrant.

In the flow stream, an analyte species $A$ to be determined reacts with a reactant $B$ to give products, $P$:

$$A + nB \rightarrow P \qquad (6.1)$$

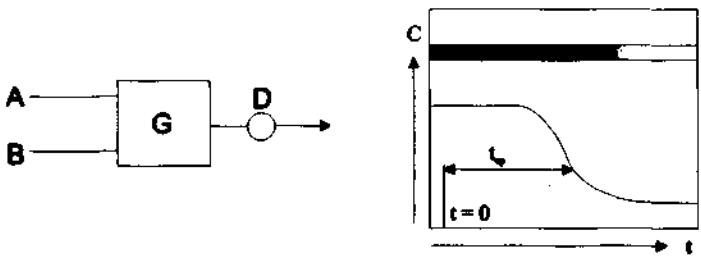


*Fig.6.1. Diagram illustrating the procedure of continuous flow titration. The sample A and the titrant B are pumped continuously in the gradient chamber G. At t=0, the sample stream is stopped and the concentration gradient can be monitored by a flow-through detector D.*

In the present case, the species to be determined is *Fe(II)*, the reactant is *Ce(IV)*, and $n=1$:

$$Fe(II) + Ce(IV) \rightarrow Fe(III) + Ce(III) \qquad (6.2)$$

Three distinct phases can be identified in the measurement cycle, ranging from the time when the sample and the titrant enter in the gradient chamber until they are completely replaced by the titrant. At the time $t<0$, the sample stream with a concentration $C_A$ and the reactant stream with a concentration $C_B$ are introduced in the micromixer with the same flow rate $Q_A=Q_B$. If the concentration of the sample is lower or equal to that of the titrant, this steady state corresponds to the state of complete reaction between the species to be determined and the incoming reactant. However, if $C_A > C_B$, an excess of unreacted sample will be found in the gradient chamber.

Then, at $t=0$, the sample stream is stopped and thus the total flow rate becomes, $Q=Q_B$. At that particular time, the sample volume in the gradient chamber equals that of the reactant, which corresponds to the half of the micromixer volume.

When $t>0$, a gradient zone is created at the trailing edge of the sample plug, which reaches the sensor after a certain time $t_r$. Two different cases can be observed for this gradient zone. If the original sample concentration is smaller or equal to that of the titrant, only a small shift of the reaction equilibrium will occur. On the contrary, if the sample concentration is larger than the titrant concentration, an unreacted part of $A$ is contained in the plug, which reacts with the reactant $B$ contained in the titrant stream.

*Sensor response time*

The total sensor response time $t_r$ is directly related to the flow rate and to the involved volume of the microchannel. In this experiment, it is composed of the time needed by the fluid to cross the micromixer, $t_{rm}$, and of the time taken by the fluid to reach the sensor, $t_{rs}$ (see fig.6.2).

$$t_r = t_{r_m} + t_{r_s} \qquad (6.3)$$

Assuming a constant flow rate $Q$, the response time $t_{rm}$ depends only on the inner volume of the mixing chamber $V_m$:

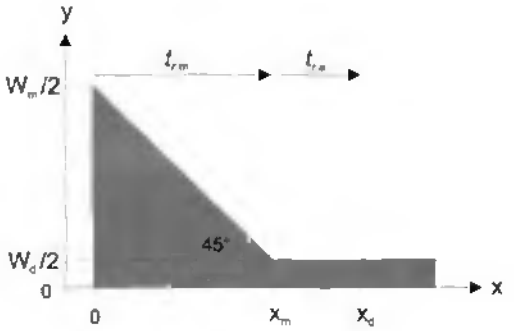


*Fig.6.2. Dimensions of the micromixer (only one half is shown): $W_m$ is the micromixer width, $W_d$ is the width of the channel leading to the detector.*

$$t_{r_m} = \frac{V_m}{Q} = \frac{HA_m}{Q} \qquad (6.4)$$

where $H$ is the channel height, and $A_m$ is the cross-section of the micromixer in the xy-plane. According to figure 6.2 with $x_m = (W_m/2 - W_d/2)$, the volume $V_m$ is given by:

$$V_m = H(W_d x_m + x_m^2) \qquad (6.5)$$

where $W_d$ the width of the channel leading to the detector. Accordingly, the response time $t_{rm}$ becomes:

$$t_{r_m} = \frac{H}{Q}\left(W_d x_m + x_m^2\right) \qquad (6.6)$$

Finally, after adding the time needed to travel through the microchannel from $x_m$ to $x_d$, we obtain the total response time:

$$t_r = \frac{H}{Q}(x_m^2 + W_d x_d) \qquad (6.7)$$

It should be noted that the intrinsic response time of the indicator electrode may give rise to an additional response delay, which, however, was neglected in the present treatment.

## 6.3. Experimental Section

Measurements were carried out in two phases. The capability of the μTAS to perform and detect continuous volumetric titrations was first tested with conventional piston-pumps. Second, the integrated electroosmotic nanopumps (EOP) were used to complete volumetric titrations. In both cases, cerimetric titrations were performed. A 1M $H_2SO_4$ background electrolyte was added to the sample and to the titrant solutions. $FeSO_4$ and $Ce(SO_4)_2$ were used as salts of the analyte and the titrant solution, respectively, and were purchased from Aldrich.

### 6.3.1. Set-up for continuous volumetric titrations carried out with piston-pumps

The set-up for the first experiment is shown in figure 6.3. Two piston-pumps (700 Dosino 2mL, Metrohm) were used to inject the sample and the titrant solutions precisely in the microsystem. A direct potentiometric method was used to detect the titration end-point. A 250μm wide and 1mm long Pt pseudo-reference electrode was located in the part of the micromixer in which the reagent stream is flowing (fig.6.5). An indicator electrode, whose size was 200 x 1000μm, was separated by 11.5mm from the reference electrode and situated downstream, after the micromixer. The potential difference between both electrodes was detected by the acquisition system of the coulometric nanotitrator (see §2.6.2).

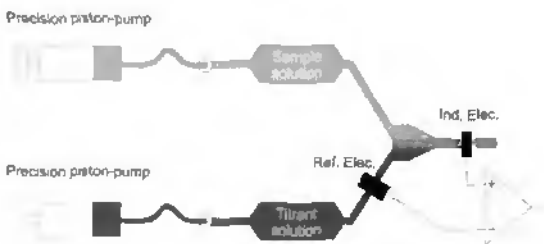


*Fig.6.3. Experimental set-up for the continuous volumetric titrations carried out with piston-pumps.*

6.3.2. Set-up for continuous volumetric titrations carried out with EOP

In the second experimental set-up (fig.6.4), the piston-pumps were replaced by the integrated electroosmotic nanopumps described earlier. A 10mM Borax solution was used as a pump buffer electrolyte. The sample and titrant solutions were introduced in the reservoirs by two external electromagnetic valves. The reference electrode was the same as that used in the previous experiment, but the indicator electrode was located closer, at a distance of 7mm from the reference electrode, in order to reduce the sensor response time at very low flow rates (fig.6.5). Indicator and reference electrodes were connected to an XY recorder (Kipp & Zonen). The X and Y inputs of this instrument were equipped with preamplifiers, which guaranteed two floating inputs with a constantly high impedance of 1MΩ.

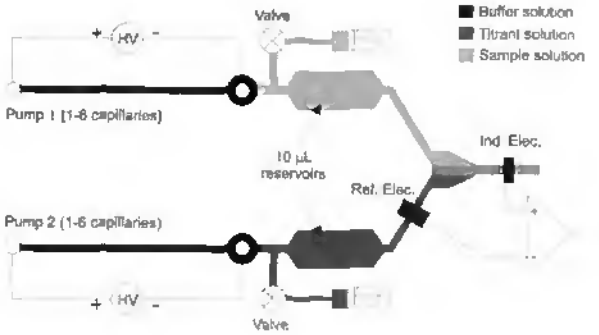


*Fig.6.4. Experimental set-up for the continuous volumetric titrations carried out with electroosmotic nanopumps.*

*Hydraulic resistance of the sensor cell*

As shown in figure 6.5, the channel of the sensor cell is composed of segments with different cross-sections. The planned purpose of this geometry was to test the detection in different configurations, namely at different flow rates. The first part of the channel, located next to the micromixer, is 300µm wide and 4mm long. The second portion is 1mm wide and 5.5mm long, and the last part is a glued needle with

an inner diameter of 0.8mm. The hydraulic resistance of the entire sensor cell was calculated from equation (4.18) and was found to be 1943.4 g/mm$^4$s.

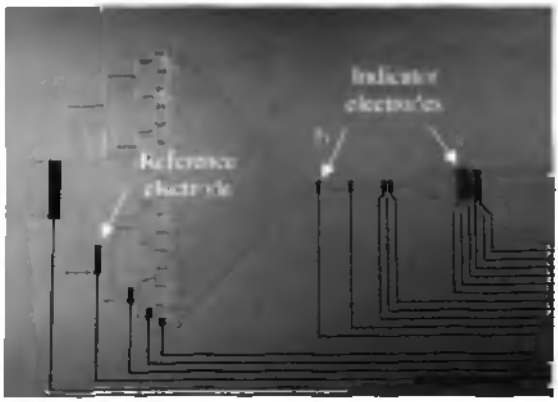


*Fig.6.5. View of the micromixer with the reference electrodes on the left (arrow indicates the electrode used) and indicator electrodes on the right, indicator electrode used a) for experiments with the piston-pumps, b) for experiments with the electroosmotic nanopumps.*

## 6.4. Results and Discussion

### 6.4.1. Results obtained with conventional piston-pumps

*Sensor response time*

Figure 6.6 shows the response time of the sensor as a function of the flow rate. 10mM Fe(II) and 10mM Ce(IV) were pumped during 10 seconds at identical flow rates, before the sample stream was stopped. The potential started to rise when the gradient zone progressively reached the sensor. After a few seconds, the sample solution was pumped again, which provoked an inverse reaction. Then, the potential stabilized again at the same amplitude as that found at the beginning of the experiment. Evidently, the sensor response time stayed below ten seconds for flow rates larger than 10µL/min.

As shown in figure 6.7, the experimental data are in excellent agreement with theoretical values calculated from equation (6.7). This demonstrates that the present device behaves favorably as an integrated flow-sensor. The theoretical values were calculated by using the following dimensions of the micromixer and of the sensor cell: H=50µm, $W_d$=300µm, $W_m$=10mm and $x_d$=5.25mm.

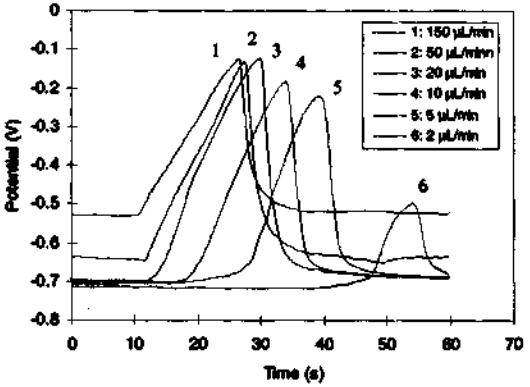


*Fig.6.6. Response time of the sensor as a function of the flow rate. 10mM Fe(II) and 10mM Ce(IV) were first pumped at identical flow rates. After 10 seconds, the sample pump was stopped.*

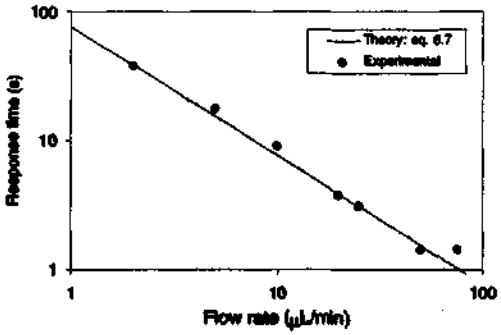


*Fig.6.7. Comparison between theoretical and experimental response times as a function of the flow rate.*

*Cerimetric titrations*

Considering the results obtained for the response time, flow rates of 10 and 20μL/min were chosen to perform volumetric titrations. Higher flow rates were not considered, since the device – pumps, reservoirs and micromixer – was properly designed for relatively low flow rates (≤ 4μL/min). Lower flow rates were avoided here because of the pulsations created by the piston-pumps. The measurement procedure was identical to that used before. The sample concentration varied from 2

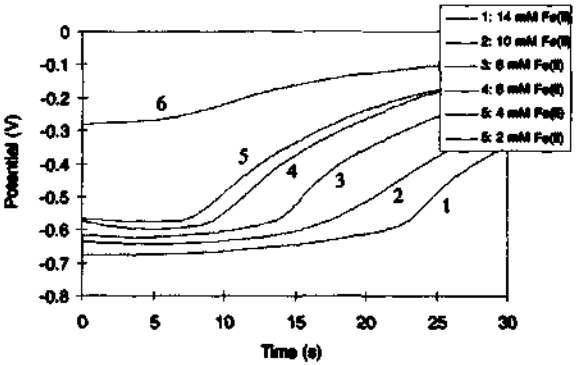


*Fig.6.8. Titration curves for different Fe(II) sample solutions with a titrant stream of 10mM Ce(IV) at 10 μL/min.*

to 14mM Fe(II), whereas the titrant concentration remained identical for all measurements, i.e. 10mM Ce(IV). Measurements were repeated five times and averaged. A standard deviation of about 2 to 8% was found.

Figure 6.9 displays the relationship between the sample concentration and the titration end-point found for two different flow rates. An empirical relationship between sample concentration, flow rate and titration time could be found by fitting the experimental data. As described in equation (6.8), the observed titration times were found to be proportional to the square of the concentration, $c$, and inversely proportional to the flow rate, $Q$:

$$t_{ep} = t_r' + \frac{1}{Q}c^2 \qquad (6.8)$$

The intercept $t_r'$ turned out to be almost identical to the sensor response time $t_r$. As expected, a distinct difference was found between the titration end-points measured for sample concentrations below 10mM and for 14mM, respectively. In paragraph 6.2, this discrepancy was actually explained by an additional titration of excess Fe(II) ions at sample concentrations above 10mM.

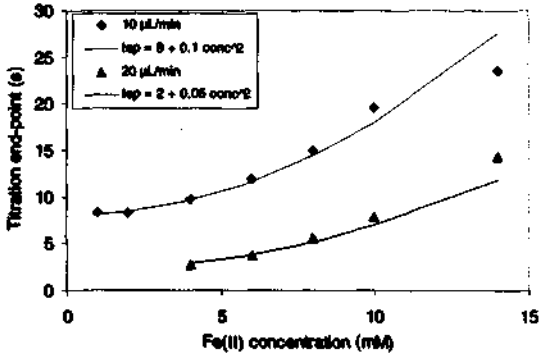


*Fig.6.9. Titration end-point vs. Fe(II) concentration for two different flow rates.*

### 6.4.2. Results obtained with the electroosmotic nanopumps

Final titration measurements were carried out using the complete µTAS with integrated electroosmotic nanopumps. By applying a vacuum at the exit of the µTAS,

the sample and the titrant solutions were first introduced into the reservoirs and the micromixer via external electromagnetic valves. The buffer solution (10mM borax) was introduced in the channels of the nanopumps through the small tanks located in the PMMA fixture. Then, a voltage of 1kV was applied on both nanopumps. After a few seconds, the sample nanopump was switched off (at t=0), whereas the second nanopump continued to push the titrant.

Figure 6.10 shows the first continuous flow volumetric titrations carried out by using electroosmotic nanopumps. Despite the simple titration technique used a clear difference could be seen between the end-points obtained for different sample concentrations, just as for the titrations performed with conventional piston-pumps. It should be pointed out that, because of the low pH value and the high conductivity of $H_2SO_4$ used as background electrolyte, the species involved in the present titrations could not have directly been pumped by electroosmosis.

According to the previous results given in chapter 4, an applied voltage of 1kV corresponds to a flow rate of 1.25μL/min for each nanopump. This roughly conforms to the response time estimated from the titration curves in figure 6.10. In fact, the endpoints for 4mM and 14mM Fe(II) are found at 46 and 62 seconds, respectively, whereas the theoretical response time (equation (6.7)) for 1.25μL/min is calculated as 57.6 seconds.

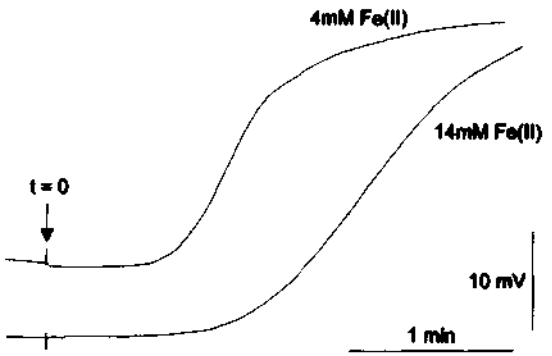


*Fig.6.10. Cerimetric titrations carried out with the electroosmotic nanopumps for two different sample concentrations at a calculated flow rate of 1.25μL/min.*

Figure 6.11 shows that the titration cycle could be repeated several times. However after a few cycles, which corresponded to the sample and titrant reservoir capacity, the pumping buffer solution partly replaced the sample and the titrant solutions, and hence a potential shift was observed. In agreement with the results of figure 6.6, the titration time for the inverse process is shorter for forward titration step.

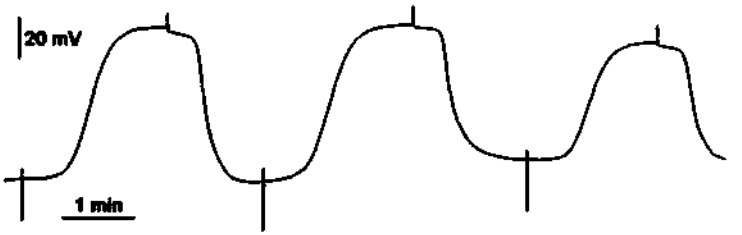


*Fig.6.11. Cycle of three titrations of a 8mM Fe(II) sample solution at 1.25μL/min. The potential peaks indicate the switching of an electroosmotic pump.*

## 6.5. Conclusion

The major result achieved in this last chapter is undoubtedly the successful preliminary tests towards volumetric titrations performed on the integrated volumetric titrator. This result demonstrates the ability of the developed μTAS to indirectly pump liquids that cannot directly be used as pumping buffer solution. It also documents the high stability of the device with regards to the flow rate, and its capacity to detect a potential difference between the pseudo-reference electrode and the indicator electrode – nearly free from the interferences from the electroosmotic nanopumps. In addition, the adequate design of the whole μTAS permitted several titrations cycles to be performed.

The simple measurement cycle applied allowed it to find an empirical relationship between the titration end-point and the sample concentration. It also made it possible to evaluate and analyze the sensor response time. Experimental values obtained for the response time corresponded well with theoretically predicted ones.

Doubtless, the performance of the system can be further improved by applying a more accurate titration technique, such as Pungor's triangle programmed titration technique or Ruzicka's FIA titration technique. The first procedure mentioned could be easily adapted to the μTAS with electroosmotic pumps. To this end, both flow rates would be increased and decreased linearly in opposite phases, in order to keep the total flow rate constant. The advantage of this method would be an improved accuracy of the titration end-point due to a broader gradient zone. FIA titrations could also be performed with a similar device, after changing some of the channels dimensions. They would have the advantage of a higher titration speed due to the extremely small sample plug (down to 200pL), which permits a high sampling rate to be realized.

The actual system could also benefit from the integration of four microvalves located at the inlet of the sample and titrant reservoirs. This would drastically reduce contamination of the sample and titrant solutions by the pump buffer electrolyte and vice-versa.

**References**


[1] Guenat O.T., Ghiglione D., Pasquier V., van der Schoot B., Morf W.E., de Rooij N.F., *An electro-osmotically driven nanopump for volumetric nanotitration applications*, Proc. Eurosensors XIII, Den Haag, The Netherlands, 1999, p.343-4.

[2] Blaedel W.J., Laessig R.H., *Continuous automated buretless titrator with direct read-out*, Anal. Chem., vol.36, No.8, 1964, p.1617-23.

[3] Fleet B., Ho A.Y.W., *Gradient titration – a novel approach to continuous monitoring using ion-selective electrodes*, Anal. Chem., vol.46, No.1, 1974, p.9-11.

[4] Nagy G., Fehér Zs., Tóth K., Pungor E., *A novel titration technique for the analysis of streamed samples – the triangle-programmed titration technique. Part I. General considerations*, Anal. Chim. Acta, 91, 1977, p.87-96.

[5] Fuhrmann B., Spohn U., *Volumetric triangle-programmed flow titrations based on precisely generated concentration gradients*, Anal. Chim. Acta., 282, 1993, p.397-406.

[6] Agudo M., Marcos J., Rios A., Valcarcel M., *Analytical potential of flow gradients in unsegmented flow systems*, Anal. Chim. Acta., 239, 1990, p.211-20.

[7] Marcos J., Rios A., Valcarcel M., *Automatic titrations in unsegmented flow systems based on variable flow-rate patterns: Part1: Principles and applications to acid-base titrations*, Anal. Chim. Acta, 261, 1992, p.489-94.

[8] Marcos J., Rios A., Valcarcel M., *Automatic titrations in unsegmented flow systems based on variable flow-rate patterns: Part2: Complexometric and redox titrations*, Anal. Chim. Acta, 261, 1992, p.495-503.

[9] López García I., Vinas P., Campillo N., Hernández Córdoba, *Linear flow gradients for automatic titrations*, Anal. Chim. Acta., 308, 1995, p.67-76.

[10] Ruzicka J., Hansen E.H., Mosbaek H., *Flow injection analysis: Part IX. A new approach to continuous flow titrations*, Anal. Chim. Acta, 92, 1977, p.235-49.

[11] Ramsing A.U., Ruzicka J., Hansen E.H., *The principles and theory of high-speed titrations by flow injection analysis*, Anal. Chim. Acta, 129, 1981, p.1-17.

[12] Ruzicka J., Hansen E.H., *Peak dimensions and flow injection titrations*, Anal. Chim. Acta, 180, 1986, p.41-5.

[13] Ruzicka J., Hansen E.H., *Flow injection Analysis, 2nd edition*, ed. John Wiley and Sons, New York, 1988, p.54-60, p.229-241.

[14] Pardue H., Fields B., *Kinetic treatment of unsegmented flow systems: Part 1. Subjective and semiquantitative evaluations of flow-injection systems with gradient chamber*, Anal. Chim. Acta, 124, 1981, p.39-63.

[15] Pardue H., Fields B., *Kinetic treatment of unsegmented flow systems: Part 2. Detailed treatment of flow-injection systems with gradient chamber*, Anal. Chim. Acta, 124, 1981, p.65-79.

[16] Pardue H., Fields B., *Kinetic treatment of unsegmented flow systems: Part 3. Flow-injection systems with gradient chamber evaluated with a linearly responding detector*, Anal. Chim. Acta, 179, 1986, p.169-79.

[17] Tyson J.F., *Peak width and reagent dispersion in flow injection analysis*, Anal. Chim. Acta, 179, 1986, p.131-148.

[18] Gratzl M., Yi C., *Diffusional microtitration: acid-base titrations in pico- and femtoliter samples*, Anal. Chem., 65, 1993, p.2085-8.

[19] Yi C., Gratzl M., *Diffusional microtitration: reagent delivery by a diffusional microburet into microscopic samples*, Anal. Chem., 66, 1994, p.1976-82.

[20] Litborn E., Stjernström M., Roeraade J., *Nanoliter titration based on piezoelectric drop-on-demand technology and laser-induced fluorescence detection*, Anal. Chem., 70, 1998, p.4847-52.

# 7. Conclusion and Outlook

The present thesis was devoted to the development and applications of microsystems for titrimetric measurements in analytical chemistry. By using microfabrication technologies, microchannels and microelectrodes could be miniaturized to such an extent that the sample volume normally used in conventional batch titrations was reduced by a factor of up to ten million. This tremendous volume reduction led to a 60 to 100-fold decrease of the analysis time.

The first part of this work focuses on the fabrication and on the characterization of a universal coulometric nanotitrator, which has been tested with two titration techniques, i.e. stopped-flow and continuous flow coulometric titrations. Both methods gave an excellent reproducibility of the titration parameters, which resulted in very small standard deviations for the measured titration end-point times. In addition, the universality of the device allowed it to perform neutralisation, complexometric, redox and precipitation titrations. Besides, and in contrast with the early-developed disposable device concept, the lifetime of the device revealed to be surprisingly long, so that several thousand measurements could be achieved with the same device and with the same electrode configurations.

One limitation of the nanotitrator, related with the need for a specific calibration, was nevertheless established. As a matter of fact, experimental and theoretical results indicated a certain influence of diffusion coefficients on the determined titration end-points. With regards to a potential commercial application of the nanotitrator, this drawback could be eliminated by using an appropriate software or hardware containing a data library of diffusion coefficients and of the geometrical constants of the device. However, prior to this prospect, a few geometrical parameters should be optimized according to the findings of this study. In order to investigate the influence of the sample matrix in more detail, a large number of tests on real sample solutions has to be performed. A mass production of the present nanotitrators would certainly

benefit from the uncomplicated fabrication process, which would keep the production costs per device at a relatively low level.

In the second part of this thesis, a μTAS for volumetric titrations was developed, and was shown to allow the performance of preliminary continuous flow volumetric titrations. The major success of this second part is undoubtedly the realization of electroosmotically driven nanopumps able to indirectly pump liquids, which, due to their high conductivity and/or their pH, could not be directly pumped by electroosmosis. These pumps were able to produce stable flow rates in the nanoliter per second range. Evidently, the optimization of this μTAS would lead to an even higher solution dosing accuracy and, thus, the performance of the volumetric titrator could be improved significantly. Finally, it should be pointed out that, in principle, these electroosmotic nanopumps are not limited to applications for volumetric titrations, but they could be adequately linked to a wide variety of analytical sensors which require pulsation-free flow at very low flow rates for the optimum response behaviour.

# Abbreviations

| | |
|---|---|
| BHF | buffered hydrofluoric acid |
| CE | capillary electrophoresis |
| DRIE | deep reactive ion etching |
| EOF | electroosmotic flow |
| FIA | flow injection analysis |
| HV | high voltage |
| IMT | institute of microtechnology, Univ. of Neuchâtel |
| ISFET | ion selective field effect transistor |
| KOH | potassium hydroxide (40wt.%, 60°C) |
| LPCVD | low power chemical vapor deposition |
| US | ultrasonic (drilling) |
| μECDM | micro-electrochemical-discharge machining |
| μTAS | micro total analysis system |

# Acknowledgements

I have been lucky to have such an amazing group of people help me and support me through the whole period of my PhD, at the Sensors, Actuators and Microsystems Laboratory (SAMLAB) of the Institute of Microtechnology. Among them, I especially would like to express my gratitude to the following people:

I deeply thank Prof. Nico de Rooij for offering me the opportunity to work in such a motivated and multi-disciplinary team. His enthusiasm about this project, his constant encouragement and the freedom of action he gave me allowed me to explore different interesting and challenging areas of the world of microsystems. I truly appreciated his support and his guidance throughout these four years.

Two persons guided me in my daily work and introduced me to the world of analytical chemistry, microfluidics and microsystems. I especially wish to express my gratitude to PD Dr. Werner Morf who spent many, many hours brainstorming, and advising, editing, and correcting our work together. His advice, his continuous and stimulating encouragement, and his helpful suggestions were an immense help and made him an enjoyable person to work with. I am also very much indebted to Dr. Bart van der Schoot, who introduced me to the clean room work and who spent a lot of his time explaining basic aspects of chemistry and electrochemistry. His great expertise in the world of microsystems, his electronics and technological hints, as well as his ideas were an invaluable help, which I greatly appreciated. I really enjoyed working with both of them and I thank them very much for their patience and their assistance.

I also gratefully acknowledge Prof. Milena Koudelka and Dr. Peter Kirschenbühler from Metrohm AG in Herisau, for kindly agreeing to be the co-examiners of my thesis and for their helpful comments about this work.

I am very much indebted to the highly skilled technical team: Sylvain Jeanneret, Bastien Droz, Sabina Jenny, José Vaquera and particularly Sylviane Pochon for dicing and encapsulating the many nanotitrators, and also to Gianni Mondin and Pierre-André Clerc for their invaluable help to solve all kind of technological problems.

Everyone in the lab has helped me in some way. I owe thanks to Philipp Arquint for introducing me to the cleanroom facilities and especially to the photopolymerization of polysiloxane, Peter van der Wal for the many helpful and inspiring discussions about basic chemistry and about everyday life, Sabeth Verpoorte for the many stimulating discussions about electrophoresis and electroosmosis, Karl Fluri for his technical hints about fusion bonding and electroosmosis, Jean-Charles Fiaccabrino for his help and his precious encouragement, Marco Meijerinck for his electronic hints and his extremely sticky drops (...). I recall with pleasure the memorable scientific and less scientific discussions with Cornel Marxer and Pierre Thiébaud with whom it was pleasant to share the same office for four years. Special thanks also go to the students who helped me during their semester and diploma work: Giusi Biundo and Dino Ghiglione. Thanks also go to David Strike, Wilfried Noell, Laurent Dellmann, Claudio Novelli, Christophe Kottelat and Matthias Schulze for their technical and computer support.

I highly appreciated the pleasant atmosphere and working environment in our research group. For that, I also thank Terunobu Akiyama, Vincent Auger, Luca Berdondini, Cynthia Beuret, Marc Boillat, Danick Briand, Laura Ceriotti, Massoud Dadras, Antoine Daridon, Arash Dodge, Philippe Dubois, Sébastien Gautsch, Marc and Florence Grétillat, Beni Guldimann, Lutz Haase, Bas de Heij, Andreas Kuoni, Eva L'Hostis, Mireille Leboeuf, Gian-Luca Lettieri, Jan Lichtenberg, Philippe Luginbuhl, Philippe Michel, Lionel Paratte, Vincent Pasquier, Georges Racine, Sylvain Roth, Margrit Rüegg, Gregor Schürmann, Urs Staufer, Camille Stebler, Bruce Weiler, as well as all the trainees and students without whom the group of Nico de Rooij would not be such a stimulating and friendly team to work with.

I have special memories of a "sledge race" in "La Vue des Alpes" and the communicating enthusiasm (!) of Toru Hirata going downhill on a sledge for the first

time in his life, as well as the challenging project about pneumatic air table we had in common with Marc Grétillat. I also recall with pleasure the famous SAMLAB running team traditionally involved in the *"Tour du Canton de Neuchâtel"*, as well as many other outdoor activities.

I would like to address my special thanks to Sandrine Piaget, who spent many, many hours correcting the English of my thesis. Unfortunately, my style had not much in common with the refinement of English poetry, with which she is much more accustomed to, gadzooks!...

Finally, I also wish to express my gratitude to my parents, who supported me during my studies, and always showed their interest in my research. Special thanks also go to my family and all my friends, for their support and their love.

*I acknowledge the partial financial support of the Swiss Commission for Technology and Innovation (CTI) and of Metrohm AG, Herisau, Switzerland.*

# List of Publications

**Refereed Articles**

*Related to this thesis:*

Guenat O. T., Morf W. E., van der Schoot B. H., de Rooij N. F., *Universal coulometric nanotitrators with potentiometric detection*, Anal. Chim. Acta, 361, 1998, p.261-272.

Guenat O. T., Fiaccabrino G. C., Morf W. E., Koudelka-Hep M., de Rooij N. F., *Microfabricated Chemical Analysis Systems for Environmental Applications*, Chimia 53, 1999, p.87-90.

Guenat O. T., Morf W. E., van der Schoot B. H., de Rooij N. F., *Triangle-programmed coulometric nanotitrations completed by continuous flow with potentiometric detection*, Anal. Chem., 72, 2000, p.1585-1590.

Morf W. E., Guenat O. T., de Rooij N. F., *Partial electroosmotic pumping in complex capillary systems, Part1: Principles and general theoretical approach*, Sensors and Actuators B, submitted for publication, May 2000.

Guenat O. T., Ghiglione D., Morf W. E., de Rooij N. F., *Partial electroosmatic pumping in complex capillary systems, Part2: Fabrication and application of a micro total analysis system suited for volumetric nanotitrations*, Sensors and Actuators B, submitted for publication, May 2000.

*In other areas:*

Guenat O. T., Hirata T., Akashi T., Grétillat M.-A., de Rooij N. F., *A pneumatic air table realised by microelectro-discharge machining*, Journal of Micro-Electro-Mechanical Systems, IEEE, 1998, vol.7, n. 4, p.380-6.

Hirata T., Guenat O. T., Akashi T., de Rooij N. F., *A numerical simulation on a pneumatic air table realized by micro-EDM*, Journal of Micro-Electro-Mechanical Systems, IEEE, 1999, vol.8, n. 4, p.523-8

**Conference and Workshop Papers**

*Related to this thesis:*

Guenat O. T., Arquint Ph., Weber I., Morf W. E., van der Schoot B. H., de Rooij N. F., *μTAS for nanotitrations of analytes*. Proc. of the 2nd International Symposium on Miniaturized Total Analysis Systems μTAS'96, Basel, Switzerland, 1996, p.215-7.

Guenat O. T., Morf W. E., van der Schoot B. H., de Rooij N. F., *A universal coulometric nanotitrator*, Proc. Transducers'97, Chicago, USA, 1997, p.1375-8.

Guenat O. T., Arquint Ph., Morf W. E., van der Schoot B. H., de Rooij N. F., *Coulometric Nanotitrators with Potentiometric Endpoint Detection*, Microreaction Technology, Proc. of the 1st Int. Conf. on Microreaction Technology, W. Ehrfeld (Ed.), Springer, Berlin, 1998, p.340-7.

Guenat O. T., Morf W. E., van der Schoot B. H., de Rooij N. F., *Continuous flow injection coulometric nanotitrations*, 2nd International Conference on Microreaction Technology, New Orleans, USA, 1998, p.230-4.

Guenat O. T., Morf W. E., Verpoorte E., van der Schoot B. H., de Rooij N. F., *μTAS for volumetric or coulometric titrations of nanomole amounts of analytes in microliter samples*, Proc. of the 3rd International Symposium on Miniaturized Total Analysis Systems μTAS'98, Banff, Canada, 1998, p. 439-442.

Guenat O. T., Morf W. E., Verpoorte E., van der Schoot B. H., de Rooij N. F., *Nanotitrators: Highly miniaturized analysis systems for titrimetric determinations of nanomole amounts of analytes in microliter samples*, Proc. of Nanotech'98, Montreux, Switzerland, 1998.

Guenat O. T., Ghiglione D., Pasquier V., van der Schoot B. H., Morf W. E., de Rooij N. F., *An electro-osmotically driven nanopump for volumetric nanotitration applications*, Proc. Eurosensors XIII, The Hague, The Netherlands, 1999, p.343-4.

*In other areas:*

Bousse L., Dijkstra E., Guenat O., *High-density arrays of valves and interconnects for liquid switching*. Solid-State Sensor and Actuator Workshop, Hilton Head, South Carolina, 1996, p. 272-5.

Hirata T., Akashi T., Bertholds A., Gruber H. P., Schmid A., Grétillat M.-A., Guenat O. T., de Rooij N. F., *A novel pneumatic actuator system realised by microelectro-discharge machining*, Proc. MEMS 1998, Heidelberg, Germany, 1998, p.160-5.

Hirata T., Guenat O. T., Akashi T., Grétillat M.-A., de Rooij N. F., *A numerical simulation on the flowfield of the novel pneumatic actuator system realised by micro-EDM*, International Symposium on Mechatronics and Human Science, IEEE, Nagoya, November 1998, p.77-82.

Guenat O. T., Hirata T., Akashi T., Grétillat M.-A., Boillat M., van der Schoot B.H., Fluri K., Verpoorte E., Roulet J.-C., Völkel R., Herzig H.-P., Dändliker R., de Rooij N. F., *Microfactory on a Chip*, Proc. IWMF'98, Tsukuba, Japan, 1998, p.15-20.

Hirata T., Guenat O. T., Akashi T., de Rooij N. F., *Realization of a fluidic switching element and its application to a pneumatic actuator system*, Proc. Transducers'99. Sendai, Japan, 1999, p.1198-1201.

Guenat O.T., Hirata T., Briand D., Clerc P.-A., Mondin G., Kroll U., de Rooij N. F., *Pneumatic conveyance systems for microparts transportation*, Proc. IWMF'2000, Fribourg, Switzerland, 2000.

**Anal. Chem. reports about nanotitrator's results presented at μTAS'96:**

Meyer V.R., Anal. Chem., *News from μTAS'96*, vol.69, n.3, 1997, p.81A.

# Biography

Olivier Thierry Guenat was born on October 4, 1968, in Bienne, Switzerland. In 1990, he received his diploma in microtechnology from the University of Applied Science (HES), Bienne, Switzerland. He then received in 1995 his MSc. degree in Electronics and Physics from the University of Neuchâtel, Switzerland.

He worked in the field of microvalves and micropumps at Molecular Devices Corporation, Sunnyvale, CA. In November 1995, he joined the group of Prof. N. de Rooij at the Institute of Microtechnology (IMT), as a research and teaching assistant. His research interests include micro total analysis systems (μTAS) for chemical analysis and also micro-conveyer systems based on pneumatic actuation.